Structural Analysis and Kinematic Restoration along the Nova Scotia Passive Margin, Atlantic Canada

by

Eren Deniz Berberoglu

A thesis submitted in partial fulfillment of the requirements for the degree of

Master of Science

Department of Earth and Atmospheric Sciences
University of Alberta

Abstract

The Nova Scotia passive continental margin is characterized by longitudinal variation in crustal structure from the volcanic U.S. Atlantic Margin in the southwest to a non-volcanic Newfoundland Margin in the northeast. The objectives of this study include characterizing the tectonic structure of the margin and analyzing the interconnected processes of extension, thermal subsidence, compaction, and isostatic response that contribute to the margin's tectonic evolution. In this study, 2D structural seismic interpretation integrated with published bathymetry, magnetic, and gravity surveys is carried out to characterize the tectonic structure of the margin. The 2D kinematic restorations along NW-SE cross-sections are conducted to quantify the variations in the amount of tectonic extension, subsidence, accommodation, isostatic response and compaction across and along the margin and compare how different crustal structural styles and salt kinematics affect these variations through time.

Structural seismic interpretation reveal five sets of normal faults. (I) NE-SW-striking syn-rift planar normal faults are identified in the acoustic basement (J200) in the continental domain. (II) SE-dipping syn-rift listric normal faults in the basement merge into a flat detachment at ~15 km of depth in the oceanic domain. (IIIa) SE- and NW-dipping post-rift listric faults in the Cretaceous and Jurassic units merge into a basal detachment along the top of autochthonous salt within the northeastern and central shelf and slope. (IIIb) SE-dipping post-rift listric faults in the Cretaceous and Jurassic units merge into a basal detachment along the top of allochthonous extended canopy in the northeastern and central segments. (IV) SE-dipping post-rift normal faults offset the Cretaceous and Tertiary clastic units in the central and northeastern segments of the margin. (V) NE-SW-striking post-rift conjugate planar normal faults are associated with the

deformation of Tertiary deposits above isolated salt diapirs in the southwestern segment of the margin.

The extension amount varies along the margin, gradually increasing from 1.55% in the SW (volcanic) to 3.72% in the NE (non-volcanic). A higher extension of the northeastern segment of the margin in the NW-SE direction results in a higher (~19km) thickness of Mesozoic-Cenozoic sedimentary cover along this segment, while it is 10-12 km in the southwest. Syn-rift faults in the basement accommodate a greater amount of extension (1.17%-2.70%) than the faults formed during the post-rift phases of deformation (0.25%-1.02%) along the margin. The syn-rift listric normal faults in the oceanic domain contributed the most to the extension (56%-86%) compared to the syn-rift planar faults in the continental domain (14%-44%). In the northeastern segment of the margin, both the basement and sedimentary succession exhibit a higher fault intensity with a stretching factor of 1.1-2.2 compared to the southwestern segment, where the lower crustal stretching factor is lower: 1.1-1.4.

The maximum syn-rift subsidence of 1035m - 1200m is reconstructed in the northeastern and central segments of the margin, respectively, at the end of the rifting stage, followed by slow post-rift thermal subsidence. The subsidence rate (m/Ma) for the top of the basement increases basinward along four cross-sections from 1.63 to 13.0. The oceanic domain of the northeastern and central segments of the margin exhibits a maximum subsidence gradient rate (12.15-13) due to crustal thinning with higher stretching factors resulting in greater sediment thickness. In contrast, the southwestern segment of the margin is characterized by the syn-rift subsidence of 775m (J200) with lower maximum subsidence rate (10.11) due to lower crustal thinning and sediment thickness.

The estimated amount of isostatic rebound and decompaction vary along the cross-sections. The highest isostatic rebound of 2610 m is reconstructed for Middle Jurassic (J163) strata in the northeastern shelf and slope of the margin, where the maximum thickness of the unit (6.5km) is observed. Towards the southwest, no visible correlation is observed between high isostatic responses and sediment load in Jurassic units. Instead, the East Coast Magnetic Anomaly associated with the magmatic underplating zone and/or the volcanic layer in the transition zone between continental and oceanic crusts determines the localization of maximum isostatic rebound in the Jurassic units (1055m). For the younger units, sediment load and mini-basin localization accommodated by salt remobilization are the driving mechanisms for higher isostatic responses, similar to the northeastern part of the margin.

Preface

The analysis presented in this study is part of the ongoing project called 'Application of a source to sink sediment model to a petroleum systems analysis of the Scotian Basin from field studies and numerical modelling' and involves the 2D structural interpretation and kinematic restoration along the Nova Scotia passive margin.

The thesis includes six chapters. The first chapter is the introduction that aims to explain the research goal. The second chapter introduces the geologic background, including the geodynamic history, crustal structure, structural elements, and stratigraphic framework of the study area. The third chapter describes an available dataset comprising the confidential 2D seismic profiles in time and depth domains, seismic velocity data, well log suites provided by CNSOPB (Canada-Nova Scotia Offshore Petroleum Board) and NSDRR (Nova Scotia Department of Natural Resources and Renewables), and bathymetry, magnetic and gravity maps downloaded from open-source websites. This chapter also explains the methodology for 2D seismic interpretation through Petrel Slb and 2D sequential modelling through MOVE Petroleum Experts Ltd. The fourth chapter explains the results of the seismic interpretation and kinematic restoration by quantifying the variations in the amount of tectonic extension, subsidence, and isostatic response across and along the margin. Finally, the fifth and sixth chapters cover the discussion and conclusions.

Acknowledgements

I would like to acknowledge my supervisor Dr. Elena Konstantinovskaya for her guidance throughout this research and for expanding my knowledge in structural geology and tectonics.

I would like to thank Professor Nicholas Harris for giving me an opportunity to be a part of this multidisciplinary project that broadens my horizons.

I would like to acknowledge Russell Dmytriw and the OERA (Offshore Energy Research Association), Fraser D. Keppie and Natasha A. Morrison and the NSDRR (Nova Scotia Department of Natural Resources and Renewables) for providing funding and technical support for the project; Slb (former Schlumberger) for providing an academic license of Petrel to University of Alberta; Petroleum Experts for providing the MOVE academic non-commercial license to the University of Alberta and technical support.

I would like to thank Mark Cooper and Marian J. Warren for their contributions to structural geology discussions, from which I have learned much.

I am grateful to Lucia Vivanco, Victoria Chevrot, Guido Garcia Rodriguez, and Hui Li for their friendship and encouragement throughout this journey.

My heartfelt appreciation is to my family and my spouse for their unconditional love and unflagging support from every corner of my life.

Table of Contents

List of Tables

List of Figures

Chapter 1: Introduction

The main goal of this study is to conduct the structural interpretation of geophysical data and numerical modelling of the tectonic evolution of the Nova Scotia passive continental margin. This research is the component of the tectonic and structural analysis of source-to-sink modelling to predict petroleum system elements in the Scotian Basin.

The Nova Scotia margin attracts a special interest in terms of crustal structure and tectonic evolution as it is recognized to involve both volcanic and non-volcanic types of passive continental margins (Holbrook et al., 1994a; Kelemen & Holbrook 1995; Keen & Potter 1995b; PFA, 2011; Louden et al., 2012; Dehler, 2010; Dehler & Welford, 2013). The change from the volcanic margin in the SW to the non-volcanic margin in the NE along the Nova Scotia margin is associated with a strong increase in the thickness of sedimentary cover (from 8-12 km to ~19 km) and crustal extension (stretching factor from 0.2 to ~2.0) established in the same direction (Watts, 1981; Dehler & Welford, 2013). Additionally, the tectonic provinces of different styles of salt kinematics are recognized along the Nova Scotia margin, represented by the salt diapir province in the SW, salt canopy province in the central part and Banquereau detachment wedge zone in the NE of the margin (Parsons, 1975; Shimeld, 2004; Ings & Shimeld, 2006; Albertz et al., 2010; Deptuck, 2011; PFA, 2011; Deptuck & Kendell, 2017). Different styles of salt remobilization contribute to the variation in localization and time of fault emplacement and sedimentary accommodation along the margin.

The Atlantic-type continental margin offshore Nova Scotia passive margin represents the northern part of the 2000-km-long North American-African rifted system that formed during the opening of the Central Atlantic Ocean initiated in the Early Jurassic. The rifting phase was followed by oceanic accretion, subsidence of the margin, and the development of a passive margin that persists to the present day (Jansa & Wade, 1975; Wade & McLean, 1990; Wade et al., 1995). McKenzie (1978) tests an approach for thinning the mantle with same stretching factor as the crust that results in a two-stage subsidence across passive margins during the syn-rift and post-rift deformation phases. First, the lithosphere homogenously is extended and thinned, leading to faulted basin with a rapid subsidence. In the second stage, the cooling increases the density of the lithosphere forcing the lithosphere to subside (thermal subsidence), creating accommodation. The elastic thickness of the lithosphere controls the wavelength of the

lithospheric flexure (Turcotte & Schubert, 1982; Roberts et al., 1998; Watts, 2001; Audet, 2014). Hence, the elastic thickness of the lithosphere controls the magnitude of subsidence and sedimentation associated with lithospheric deflection produced by the load. The presence of uplifts, type and amount of sediment supply influence distribution of load within a passive continental margin, subsidence, and thickness of sedimentary cover. These factors are in turn may trigger salt remobilization and post-rift fault emplacement. The combination of tectonic and paleogeographic factors play a significant role in syn-rift and post-rift deformation of a passive margin.

Previous studies of the Nova Scotia margin established the crustal structure and type of the passive continental margin, interpreted the composition and thickness of sedimentary cover, mapped faults, distinguished salt tectonic provinces, analyzed variations in velocity along selected profiles, gravity and magnetic data, and estimated stretching factor along the margin (Funck et al., 2004; OETR, 2009; Dehler, 2012; Dehler &Welford, 2013). 2D kinematic reconstructions along selected profiles and 1D and locally 3D basin analysis modelling were carried out for the Nova Scotia and Morocco conjugated continental margins (PFA, 2011).

This research aimed to interpret what is the connection between the different rifting styles (volcanic versus non-volcanic) and the nature of the post-rift deformation, whether the effects of the rift type persist into passive margin development or not, what factors contribute to the temporal change from one deformation style to another in different parts of the margin, and how much sediment load is required to mobilize salt.

The objectives of this study are to characterize the tectonic structure of the margin, quantify the variations in the amount of tectonic extension and sediment loading with time during the Atlantic opening, estimate the subsidence, accommodation, isostatic response and compaction across and along the Nova Scotia passive margin, and compare the effect of different crustal structural style (non-volcanic vs volcanic) of the passive margin and salt kinematics on the localization and time of fault emplacement, and the amount of subsidence through time.

For the purpose of structural analysis of deformation along the Nova Scotia passive margin, we interpret geophysical data along the margin integrated with maps of magnetic and gravity surveys through Petrel Slb (former Schlumberger). After that, 2D sequential modelling is conducted along four NW-SE cross-sections located in the SW (line 1100), central (lines 1400A

and 1600) and NE (line 2000) segments of the margin in MOVE Petroleum Experts Ltd., integrating the stratigraphic framework of the basin. Then, we estimate the amount of tectonic extension and quantify the variations in subsidence, isostatic response and decompaction along the four NW-SW-striking cross-sections.

This study adds new knowledge to the previous results by conducting 2D kinematic restoration modelling along four NW-SE cross-sections to simulate interconnected processes of extension, thermal subsidence, compaction and isostatic response that contribute to the tectonic evolution of the Nova Scotia continental margin. A sensitivity study of the parameters of compaction curves, crustal stretching factor (uniform vs non-uniform), and elastic thickness of lithosphere is carried out.

Chapter 2: Geologic Background

2.1. The Tectonic Setting and Geodynamic History of the Nova Scotia Margin

The Nova Scotia continental passive margin represents the northern part of the North American-African rifted system. It is underlain by the basement of the Meguma terrain (Fig. 2.1), which is separated from the Avalonia block by the dextral strike-slip Cobequid-Chedabucto Fault (CCF) emplaced during the Late Devonian – Early Carboniferous (Jansa & Wade, 1975; Pe-Piper & Jansa, 1999; van Staal & Barr, 2012; Waldron et al., 2022).

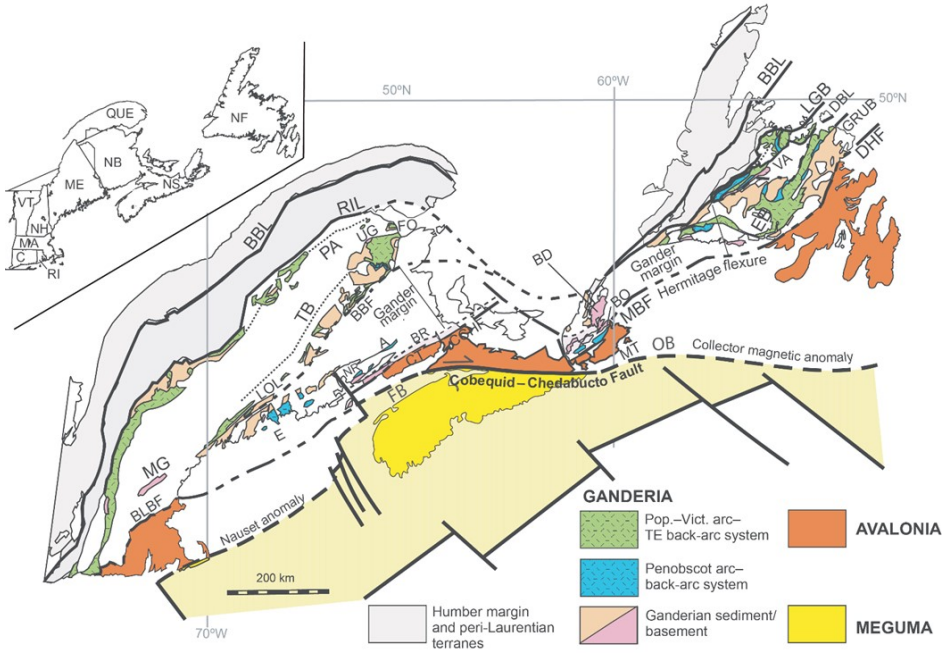

Figure 2.1: Map of tectonic settings of the Nova Scotia passive margin, after van Staal & Barr (2012). The onshore and offshore extent of Ganderia, Avalonia, and Meguma terrains are shown. FB: Fundy Basin and OB: Orpheus Basin. See the original article for other abbreviations.

The onset of rifting during the Mesozoic opening of the Atlantic (Fig. 2.2) occurred in the Late Triassic, simultaneously along eastern North America from Florida to the Canadian Grand Banks (Withjack & Schlische, 2005). The cessation of rifting, breakup, and the onset of drifting (i.e., the stage of intraplate separation and seafloor spreading) occurred first in the latest Triassic in the southern United States and then in Early Jurassic in the northern United States and southeastern Canada. A series of Early Mesozoic rift basins were formed along the passive margin of eastern North America (Withjack & Schlische, 2005). The Fundy and Orpheus pull-

apart basins were formed along the reactivated Cobequid-Chedabucto Fault (van Staal et al., 2009; Withjack & Schlische, 2005). The short-duration Central Atlantic Magmatic Province (CAMP) magmatic activity occurred in the earliest Jurassic at ~200 Ma (Fig. 2.2), simultaneously along the eastern United States up to southern Nova Scotia (Olsen et al., 1996; Hames et al., 2000; Schlische et al., 2003; Withjack & Schlische, 2005). The underplating of CAMP magmatic bodies along the volcanic passive margin is recognized by seaward-dipping reflectors near the continent-ocean boundary. The northern Nova Scotia margin is characterized by the exhumation of a serpentinized mantle (Funck et al., 2004), typical for the non-volcanic continental passive margins.

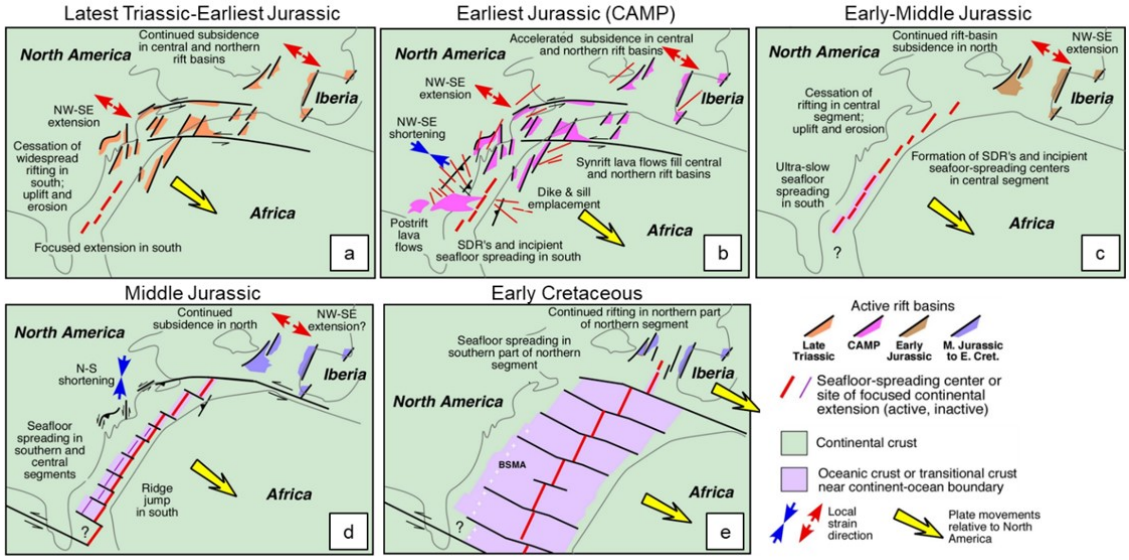

Figure 2.2: Mesozoic tectonic evolution of the eastern North American rift system, after (Withjack & Schlische, 2005). NFZ: Newfoundland Fracture Zone.

The breakup unconformity (J200) marked the rift-drift transition, i.e., the separation of lithospheric plates and the onset of seafloor spreading, and the beginning of the accumulation of Upper Triassic-Lower Jurassic deposits in the northeast-trending rift basins, including Fundy and Orpheus Basins and in the Scotian Basin (Figs. 2.2) (Withjack & Schlische, 2005).

The post-rift passive margin deposits continued to accumulate in the Middle Jurassic-Cretaceous (Figs. 2.2) (Sibuet et al., 2012). The breakup of North America from Iberia at the Late Jurassic – Cretaceous caused the Avalon Uplift (Fig. 2.7). The uplift resulted in erosion and sediment oversupply in the eastern part of the Scotian Basin (Grist et al., 1992) during the Late

Jurassic-Early Cretaceous. The Early Cretaceous breakup stage between the Grand Banks and Iberia (Fig. 2.2) was marked by the Strombolian type eruptions and formation of Hauterivian-Barremian volcanic rocks on the SW Grand Banks and Aptian–Albian volcanic rocks in the Orpheus Graben and SE Scotian Shelf (Bowman et al., 2012). During the Oligocene, tilting of the Scotian Shelf resulted in erosion and reworking of Cretaceous inner shelf sediments and deposition of deep water sediments beneath the outer shelf.

2.2. Crustal Structure of the Nova Scotia Margin

The Nova Scotia passive continental margin is characterized by longitudinal variations in crustal structure and composition, width, and nature of the continent-ocean transition zone (Keen & Potter, 1995b). Magnetic and gravity data integrated with the P-wave velocities of deep seismic refraction profiles (Figs. 2.3, 2.4) have been used to interpret these variations across and along the margin (Funck et al., 2004; PFA, 2011; Dehler, 2012; Dehler & Welford, 2013).

The continental crust across the northeastern non-volcanic segment of the Nova Scotia passive margin is strongly stretched and thinned, extending in the NW-SE direction over a distance of ~200 km (Fig. 2.3). The Mesozoic-Cenozoic sedimentary cover along this segment has ~19 km of the maximum thickness (Figs. 2.3c, 2.9). Based on the velocity data (Fig. 2.3b), it was interpreted that the continent-ocean transition zone is composed of a serpentinized mantle and it is ~100 km wide across the NE segment of the margin (Funck et al., 2004; Wu et al., 2006; Dehler & Welford, 2013). The prolongation of the northernmost East Coast Magnetic Anomaly (ECMA) is not well developed (Fig. 2.6) but is narrow and diffuse and gently disperses into negative values.

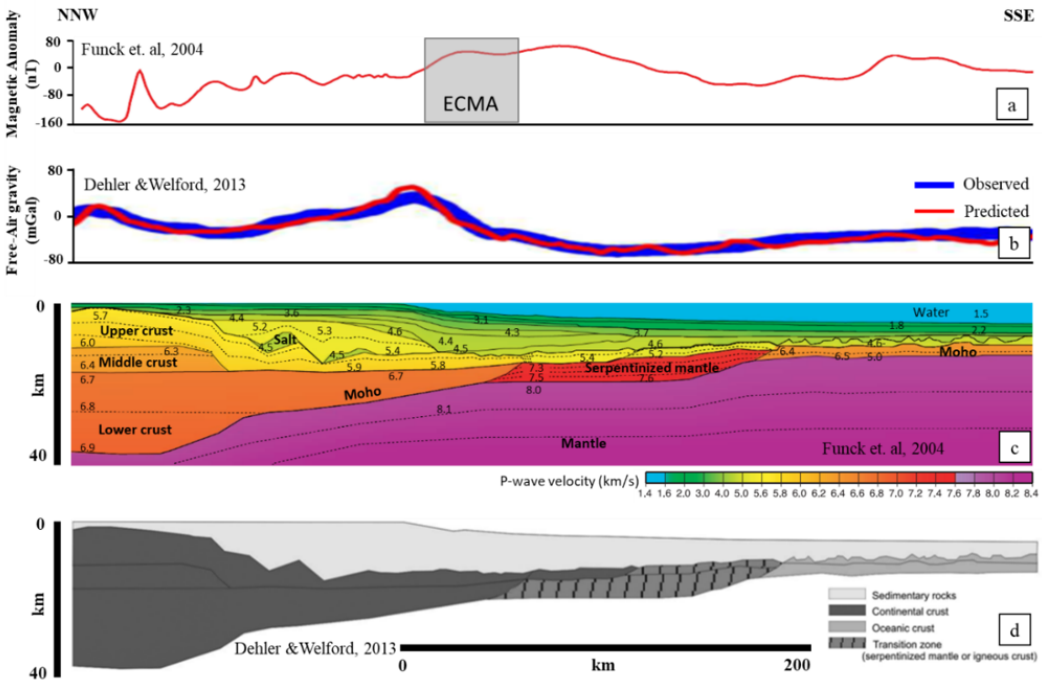

Figure 2.3: The crustal structure of SMART 1 (Lithoprobe 891_mrg) located in the northeastern segment of the margin; a: Magnetic anomaly profile (Funck et al., 2004); b: The observed and predicted gravity anomaly (Dehler & Welford, 2013); c: P-wave velocity model derived seismic from refraction data (Funck et al., 2004); d: Crustal structure denotes the interpreted types of the crust across the margin (Dehler & Welford, 2013). See Figures 2.5-2.6 for the line location.

The continental crust across the southwestern volcanic segment of the Nova Scotia passive margin is about 120-130 km wide in the NW-SE direction (Fig. 2.4) and is narrower than the NE segment. The Mesozoic-Cenozoic sedimentary cover has ~12 km of the maximum thickness (Figs. 2.4c, 2.9). The continent-ocean transition of ~100 km wide is recognized along the SW segment of the margin interpreted within the location of a prominent positive ECMA (~200 nT) (Figs. 2.4a, 2.6). Based on the presence of ECMA, CAMP volcanics, and seaward dipping reflectors (SDRs) described above, the continent-ocean transition zone in the SW segment is interpreted to involve magmatic underplating zone at the Moho and lower crustal level and volcanic flows at the breakup unconformity (Dehler & Welford, 2013). According to Dehler (2012), the magmatic underplating could have been triggered by the upper mantle decompression melting at the seaward edge of the continental crust at the initial rifting stage. ECMA (Fig. 2.4a) can be associated with the zone of magmatic underplating and/or the volcanic layer above the high-velocity body (Fig. 2.4c) (Dehler, 2010). Earlier, Klitgord and Schouten

(1986) proposed that ECMA can be caused by a buried basement ridge or an edge effect of different magnetic properties of rock bodies at the ocean-continent boundary. Alsop and Talwani (1984) postulates that the presence of listric faults between continental and volcanic blocks controls the shape of the ECMA.

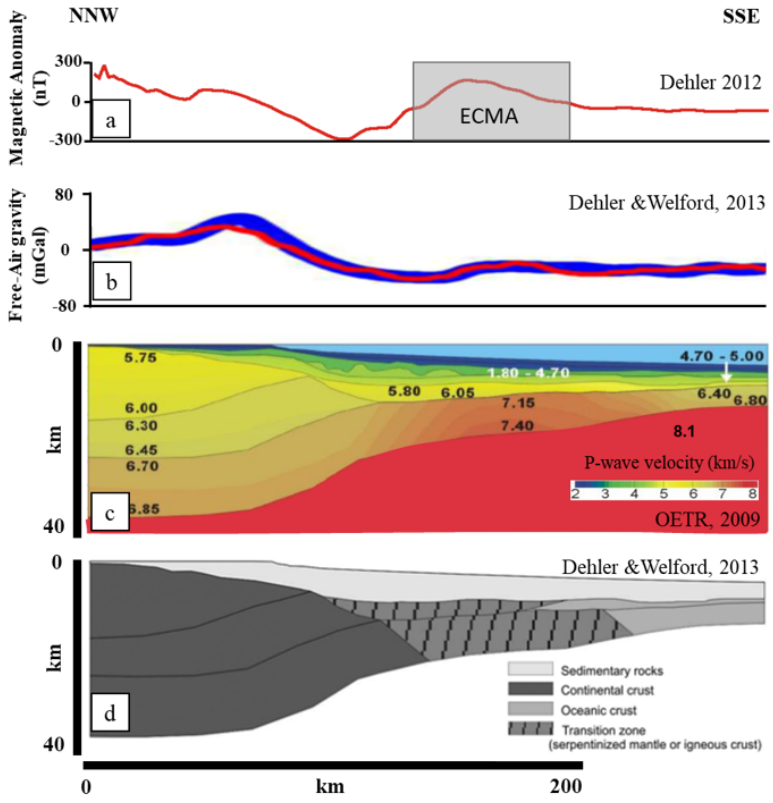

Figure 2.4: The crustal structure of SMART 3 (Line 1100) located in the southwestern segment of the margin; a: Magnetic anomaly profile (Dehler, 2012) of the SMART 3 (Scotian Margin Transects); b: The observed and predicted gravity anomaly (Dehler & Welford, 2013); c: P-wave velocity model derived from seismic refraction data (PFA, 2011); d: Crustal profile denotes the interpreted types of the crust across the margin (Dehler & Welford, 2013). See Figures 2.5-6 for the line location.

Factor β represents stretching of the crust that is defined as a ratio of the thickness of the crust before extension t_c to the thickness of the crust after extension t_f: $\beta = t_c/t_f$ and equivalently the same ratio for the subcrustal lithosphere (McKenzie, 1978). The model predictions assuming a two-layered lithospheric stretching model (Hellinger & Sclater, 1983) were conducted for the Nova Scotia margin (Royden & Keen, 1980; Dehler and Keen, 1993; Keen and Dehler, 1993). In Keen and Dehler (1993), β is defined as the amount of stretching of the crust and δ represents

stretching of the subcrustal lithosphere. The predicted crustal stretching β increases seaward to values exceeding 2.5 that corresponds to the crustal thinning to less than 40% of the original 35 km thickness near the continent-ocean boundary (Dehler and Keen, 1993). The predicted subcrustal lithosphere thinning also increases seaward with δ values up to 5.0 and greater along the continent-ocean boundary (Dehler and Keen, 1993). The stretching factors β and δ predicted in these models can be normalized as 1-1/ β and 1-1/ δ (Keen and Dehler, 1993) to be in a range of values from 0 (no stretching) to 1 (infinite stretching). The study of Dehler and Wellford (2013) aimed the inversion of gravity data, in which the model, constrained by water and sediment thickness, was allowed to solve for crustal thickness based on starting constraints such as reference density, thickness of unstretched crust (40 km), and grid cell size. The Moho depth estimated in the model was used to predict crustal thickness and stretching factor β (Fig. 2.5). Best fit was determined by comparing the predictions with constraints provided by seismic refraction profiles, and predicted Free Air gravity with observed gravity measurements (Figs 2.3, 2.4). The predicted crustal stretching factor β is lower in the SW segment of the Nova Scotia margin (Fig. 2.5b) than it is in the NE segment (Dehler and Keen, 1993; Dehler &Welford, 2013). Regions of increased crustal thinning are also predicted under the subbasins (Fig. 2.5).

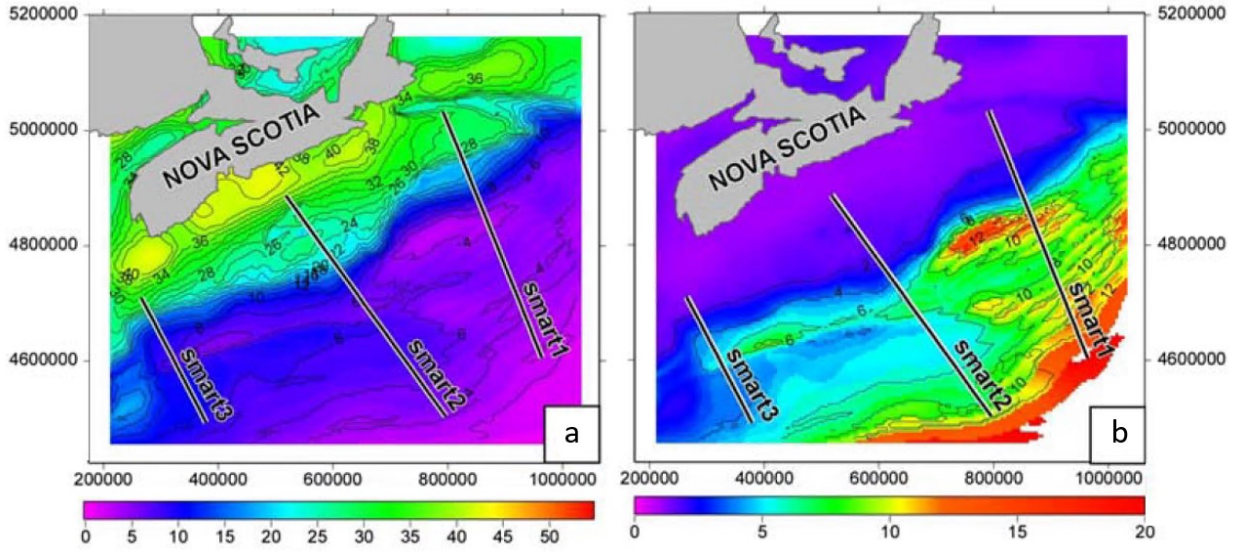

Figure 2.5: Predicted crustal thickness, km (a) and stretching factor β (b), after (Dehler & Welford, 2013). Predicted crustal thickness decreases and stretching factor increases from the SW to the NE along the Nova Scotia margin. The location of lines SMART 1 (Lithoprobe 891_mrg), SMART 2 (Lithoprobe 881a_m), and SMART 3 (Line 1100) are shown.

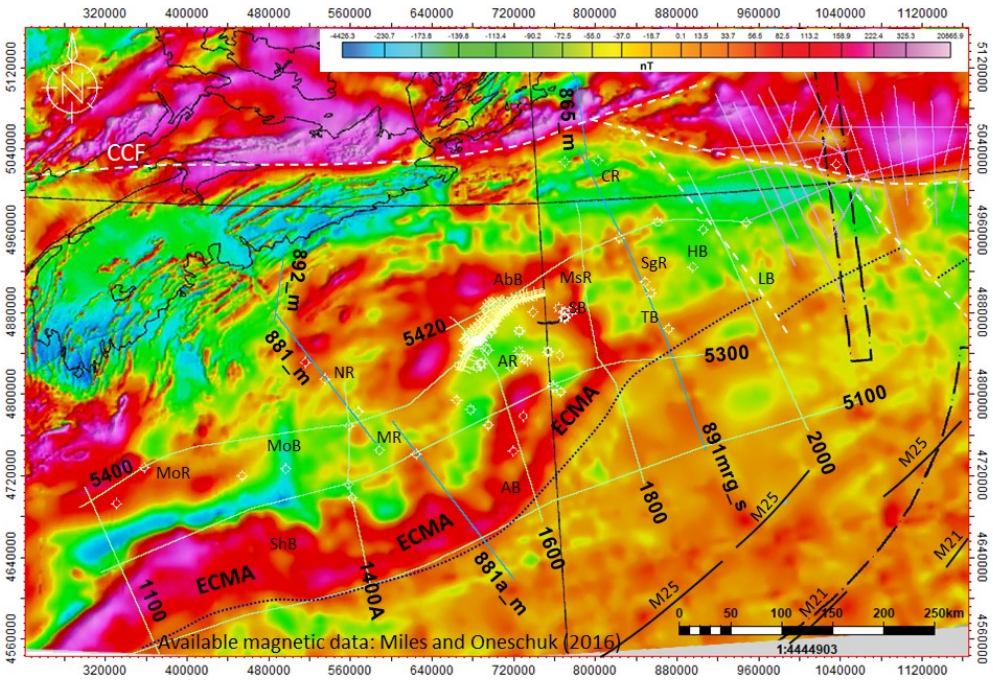

Figure 2.6: The magnetic anomaly map along the Nova Scotia margin (Miles & Oneschuk, 2016). Solid black lines annotated by M25 and M21 indicate the location of magnetic anomalies in the oceanic crust, after (Funck et al., 2004). The dotted black line corresponds to the SE limit of COB. See Figure 2.8 for the explanation of abbreviations.

The Free-Air gravity anomaly map (Fig. 2.7) compiled in this study was built using the open-source dataset (https://topex.ucsd.edu/cgi-bin/get_data.cgi). The present-day shelf edge is characterized by a strong linear positive anomaly (mean ~90 mGal) extended along the Nova Scotia margin. The positive anomaly decreases to 70 mGal in the northeast and to 50 mGal in the southwest along the margin (Fig. 2.7). The highest gravity anomaly (~98 mGal) is observed around Alma Ridge. The high positive anomaly is likely linked to the basement highs located at 9.5 km (TVDSS) and formed during the syn-rifting extension phase of the margin. The presence of low-density salt bodies within the Salt Canopy Province and Banquereau Synkinematic Wedge contributes to low gravity values (-20 – -80mGal).

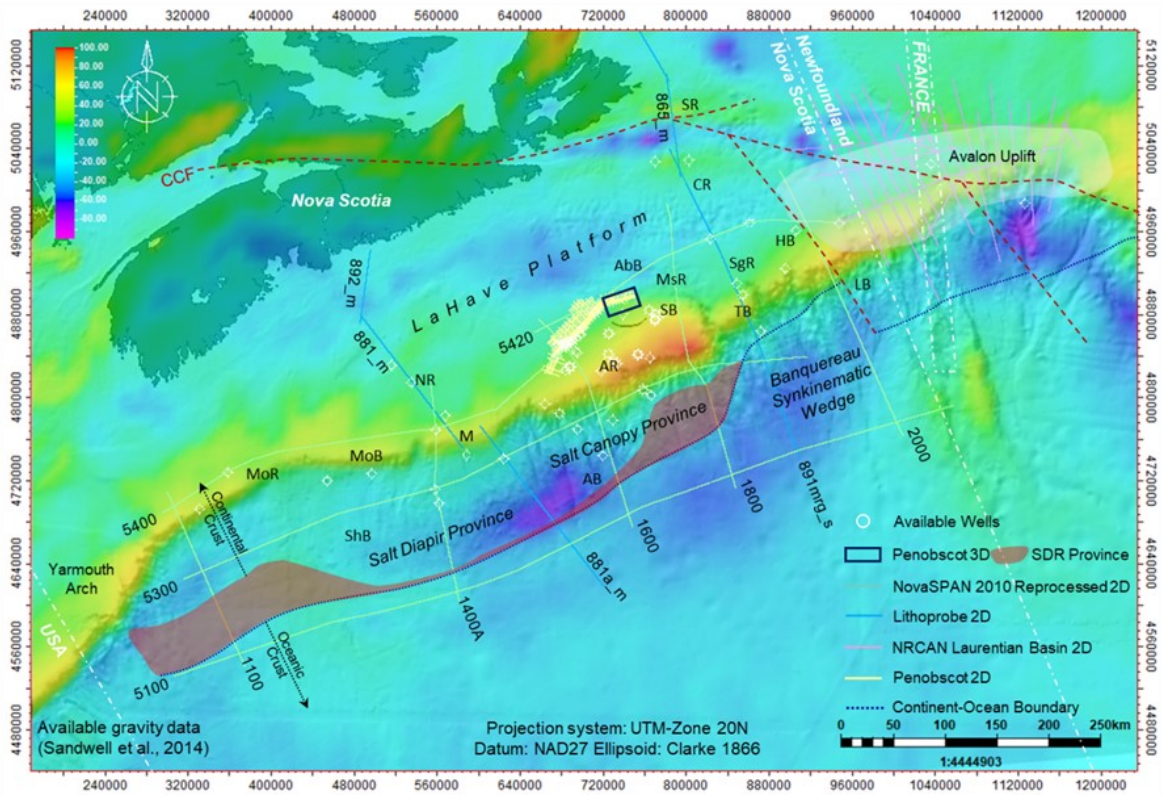

Figure 2.7: The Free-Air gravity map along the Nova Scotia margin displaying a linear high positive anomaly along the present-day shelf edge (Sandwell et al., 2014). See Figure 2.8 for the explanation of abbreviations.

2.3. Structural Elements of the Nova Scotia Margin

The Scotian Basin is subdivided into four post-rift structural zones based on the timing, distribution, and style of salt-related deformation: (1) LaHave Platform Province, (2) Salt Diapir Province, (3) Salt Canopy Province, and (4) Banquereau Synkinematic Wedge Province (Fig. 2.7) (Shimeld, 2004; Ings & Shimeld, 2006; Albertz et al., 2010; Deptuck, 2011; PFA, 2011; Deptuck & Kendell, 2017).

2.3.1. LaHave Platform Province

LaHave Platform (Fig. 2.8) comprises the continental shelf of the Nova Scotia margin and is bounded to the west by the Northeast channel and to the east by the Laurentian channel (Shaw et al., 2006). The province is characterized by a series of elevated structural blocks (i.e. Baccaro Bank, Emerald Bank, Canso Bank) and basins (i.e. LaHave Basin, Emerald Basin).

Within the LaHave Platform, the acoustic basement is overlain by syn-rift deposits. The basement and syn-rift deposits are faulted by a series of syn-rift faults.

2.3.2. Salt Diapir Province

The Salt Diapir Province, first defined in Shimeld (2004), is recognized in the SW segment of the NS margin. It extends for 350 km below the present-day continental slope from the Shelburne Subbasin in the southwest to the Annapolis Subbasin in the northeast (Fig. 2.8). It is mainly characterized by the presence of 2 km to 12-km-wide rooted allochthonous salt diapirs and walls that separate 5 km to 20-km wide mini-basins (Albertz et al., 2010; Deptuck & Kendell, 2017). From the NE to the SW across the margin, the shape of salt body changes from salt pillows to isolated salt diapirs and walls.

2.3.3. Salt Canopy Province

The Salt Canopy Province (Fig. 2.8) includes the Abenaki, Annapolis, and Sable Subbasins and their distal extents in the NE segment of the NS margin and comprises amalgamated salt canopies and salt-cored detachment folds (Shimeld, 2004; Albertz et al., 2010; Deptuck & Kendell, 2017). The canopy domain covering an area of ~13,000 km^2 overlies the Lower Cretaceous (K130) and older units and is underlain overlain by the Upper Cretaceous (K101) and younger units. The multi-tiered salt bodies beneath today's continental shelf turn into amalgamated basinward-leaning salt tongues expelled ~80 km from the primary salt basin below the continental shelf and deep basin (Deptuck & Kendell, 2017).

2.3.4. Banquereau Synkinematic Wedge

The 150-km long (NE-SW) and 130-km wide (NW-SE) Banquereau Synkinematic Wedge province, first described in Parsons (1975), extends from the Huron and easternmost Laurentian Subbasins (Fig. 2.8). It represents a roho system (Hudec & Jackson, 2011), which is defined by seaward-dipping listric normal faults accommodating extension above the roof of salt detachment (Shimeld, 2004; Ings et al., 2006; Albertz et al., 2010; Deptuck & Kendell, 2017).

Accumulation of the overlying Cretaceous deltaic deposits contributed to the salt remobilisation for a distance up to 75 km basinward of its origin. Deptuck & Kendell (2017)

suggested that there are no salt feeders beneath the BSW; therefore, it differs from the other salt-based detachments in the west of the Nova Scotia margin.

2.4. Stratigraphy of the Scotian Shelf and Scotian Basin

The NE-SW-trending Scotian Basin extends an over area of approximately 300 000 km^2 and is bounded by the Yarmouth Arch in the southwest and the Avalon Uplift on the Grand Banks of Newfoundland in the northeast (Fig. 2.8). The sedimentary succession of the Scotian Basin consists of Precambrian-Lower Paleozoic pre-rift, Triassic to Early Jurassic syn-rift and Early Jurassic to present post-rift stratigraphic subdivisions (McIver, 1972; Jansa & Wade, 1975; Wade & MacLean, 1990; MacLean & Wade, 1993; Wade et al., 1995). The total thickness of Mesozoic-Cenozoic sedimentary cover reaches up to 19 km in the central and northeastern segments of the Nova Scotia passive margin and up to 10-12 km in the southwestern segment of the margin (Fig. 2.9).

The stratigraphic units of the Mesozoic-Cenozoic sedimentary cover of the Scotian Basin are described below to summarize the composition, facies, and thickness of main subdivisions and unconformity boundaries between them, as well as corresponding seismic reflection boundaries (Fig. 2.10).

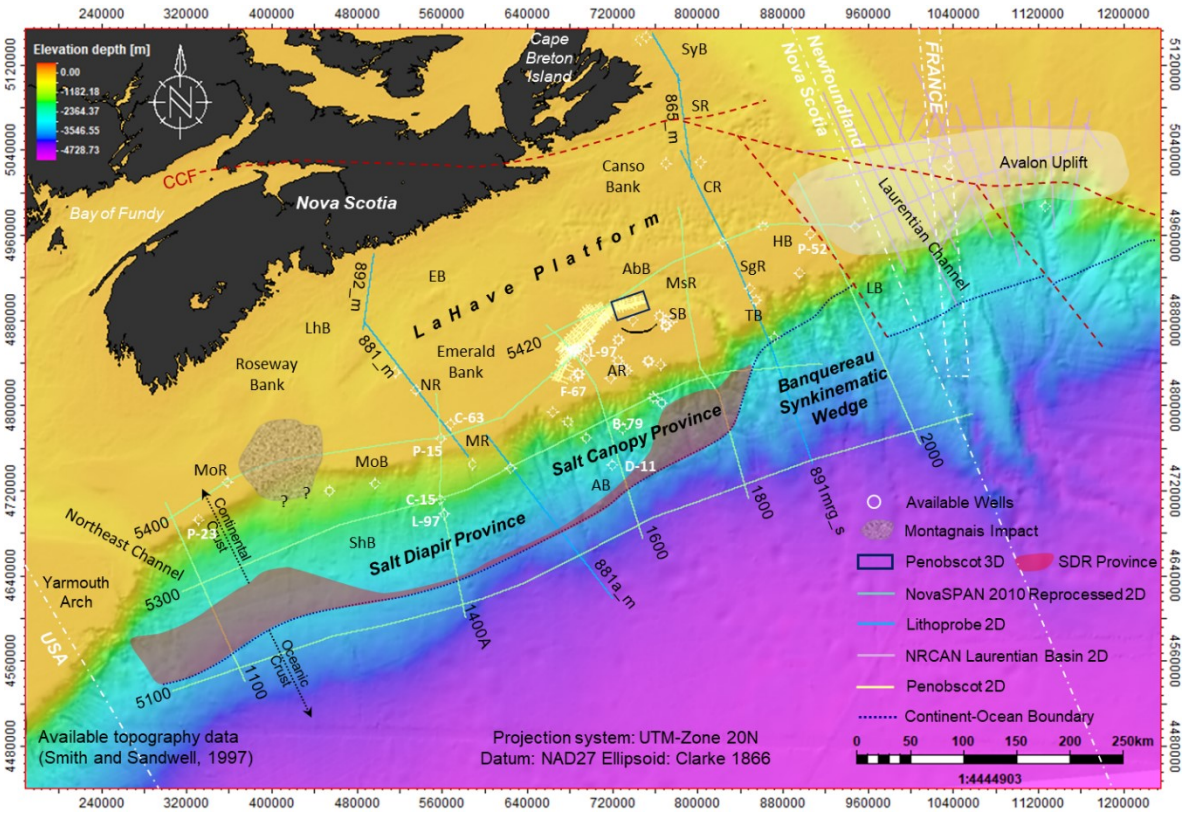

Figure 2.8: The seafloor bathymetry (Smith & Sandwell, 1997, https://topex.ucsd.edu/cgi-bin/get_data.cgi) of the Nova Scotia margin depicts salt tectonic provinces, subbasins, and ridges, available seismic surveys and well data used in this study. AbB: Abenaki Subbasin, AB: Annapolis Subbasin, AR: Alma Ridge, CR: Canso Ridge, EB: Emerald Basin, HB: Huron Subbasin, LB: Laurentian Subbasin, LhB: LaHave Basin, MoB: Mohican Subbasin, MoR: Mohawk Ridge, MR: Moheida Ridge, MsR: Mississauga Ridge, NR: Naskapi Ridge, SB: Sable Subbasin, SgR: South Griffin Ridge, ShB: Shelburne Subbasin, SR: Scaterie Ridge, SyB: Sydney Basin, TB: Tantallon Subbasin, CCF: Cobequid-Chedabucto Fault, SDR: Seaward Dipping Reflectors.

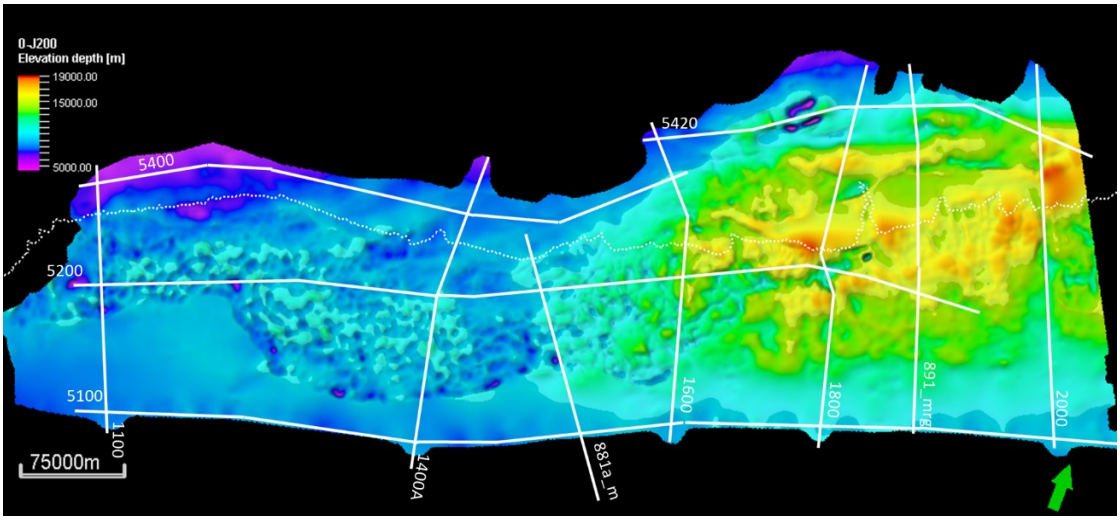

Figure 2.9: The thickness map of Mesozoic-Cenozoic sedimentary cover derived from the previous interpretations (PFA, 2011).

2.4.1. Pre-Rift Units (Carboniferous – Lower-Middle Triassic)

Precambrian and Lower Paleozoic rocks are exposed on Cape Breton Island (Fig. 2.8). These include pre-rift Carboniferous and Permian units that are composed of siliciclastic, carbonates, and sulphate evaporates. These units were penetrated by wells in the Sydney Basin. The drilled thickness is about 1700 m (Pascucci et al., 2000). A series of basement highs (i.e. South Griffin Ridge, Mohawk Ridge, and Alma Ridge) is composed of metamorphic and igneous rocks and exert control on the sediment distribution of the pre-rift units of the basin. Lower Triassic or Carboniferous sedimentary deposits are preserved onshore along the Bay of Fundy (Jansa & Wade, 1975; Wade & MacLean, 1990). The depth of the acoustic basement steadily increases from 3 km at the present-day's continental shelf to more than 12 km in the deep basin in the SW segment of the margin to ~19 km in the NE of the margin (Fig. 2.9).

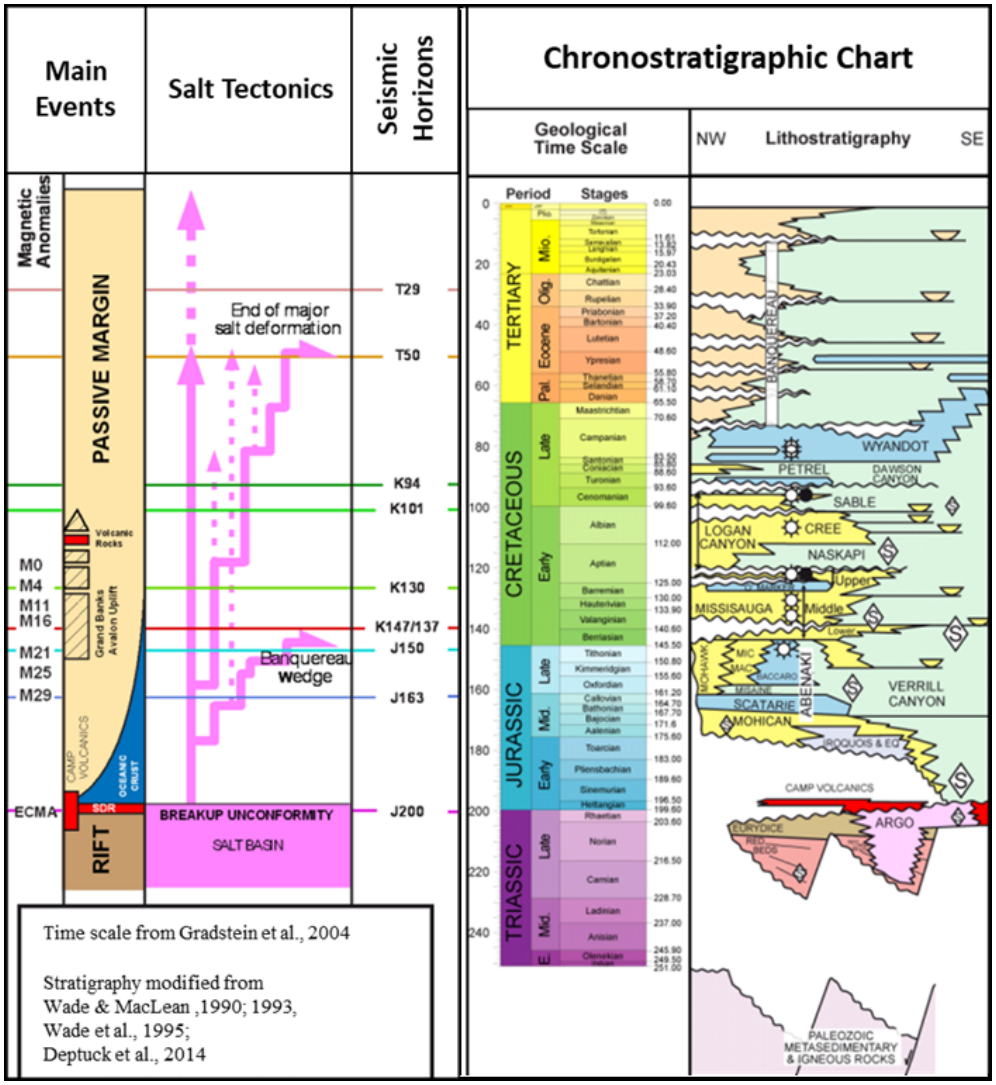

Figure 2.10: Generalized stratigraphic chart of the Scotian Basin and corresponding seismic markers interpreted in this study.

2.4.2. Syn-Rift Units (Upper Triassic- Lower Jurassic)

Upper Triassic-Lower Jurassic syn-rift units (225-200 Ma) are composed of fluvial and lacustrine red sandstones, siltstones, shales, and volcanic rocks ("Glooscap volcanics") of the Eurydice Formation penetrated by the Glooscap C-63 well, and evaporates of the Argo Formation (Fig. 2.10).

The autochthonous salt (Argo Formation) deposits overlie the Eurydice Formation and are formed as a result of the evaporation of a shallow sea in a dry and hot climate (Klein, 1962; Wade & MacLean, 1990). Remobilized allochthonous salt forms salt pillows, canopies, walls,

and diapirs at different structural levels along the margin. The maximum thickness of the Argo Formation reaches 3000 meters in the northern part of the basin (PFA, 2011) (Fig. 2.12).

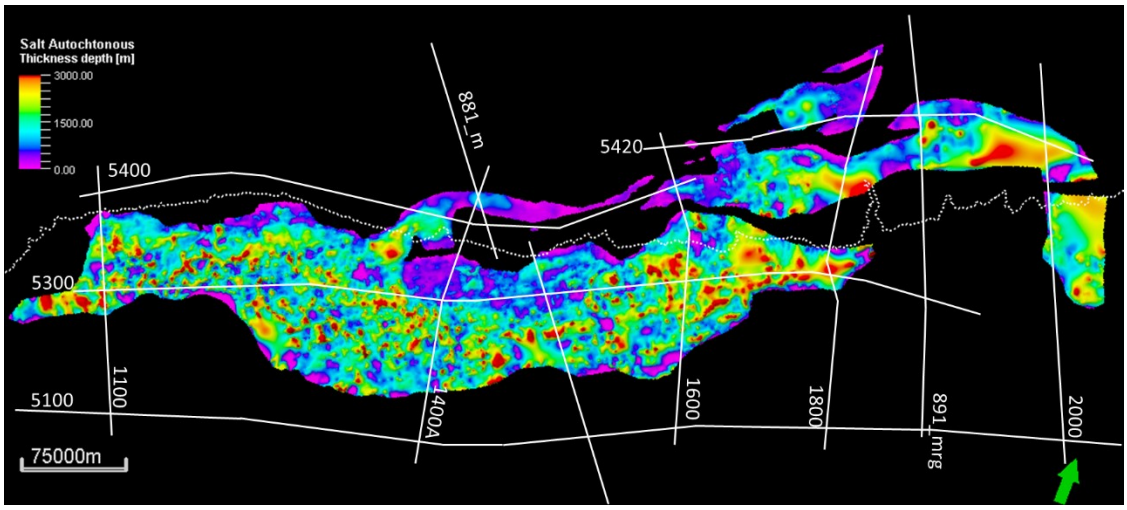

Figure 2.11: The thickness map of the autochthonous salt derived from the previous interpretations (PFA, 2011).

The Eurydice red beds and Argo evaporates are truncated by the Breakup Unconformity (J200) that marks the rift-drift transition, the latest stage of separating the continents of North America and Africa (Fig. 2.3), formation of the oceanic crust, and opening the Atlantic Ocean (Wade & MacLean, 1990).

The Central Atlantic Magmatic Province (CAMP) involves volcanic eruptions that occurred about 201 million years ago, and marks the breakup unconformity J200 (Fig. 2.10). The "Glooscap volcanics" is a 150-m thick basalt sequence located between the Argo and Eurydice Formations and the overlying Mohican Formation. It is correlated with the North Mountain Basalt in the Fundy Basin, which is a part of CAMP and is dated as early Sinemurian (Benson, 2003; Wade & Maclean, 1990). The CAMP lava flows and diabase dykes are also recognized in the Fundy Basin (Fig. 2.8), where they are composed of high-titanium quartz-normative basalts emplaced in less than 1 million years at ~200 Ma (Schlische et al, 2003). The syn-rift CAMP basalt flows and associated Early Jurassic age strata are found only in rift basins in the northern segment of the Central Atlantic margin. The seaward-dipping reflectors (SDRs) (Fig. 2.8) are recognized in seismic lines of the Scotian Basin (Alsop and Talwani, 1984; Benson & Doyle, 1988; Pe-Piper et al., 1992). Although the rocks of SDRs have not been sampled by drilling

because their location is deep within the sedimentary cover, SDRs are assumed to represent a seaward-thickening, wedge-shaped sequence of volcanic and interbedded sedimentary rocks that accumulated within a few million years. These rocks and underlying intrusive and underplated rocks are considered the primary source of the East Coast Magnetic Anomaly (ECMA) (Talwani & Abreu, 2000). Pe-Piper et al., (1992) suggested that the drifting stage, i.e., the stage of intraplate separation and seafloor spreading, for the eastern Canadian margin started near the end of the Bajocian with the formation of the first oceanic crust and the development of SDRs.

2.4.3. Post-Rift Units (Lower Jurassic-Present)

The Lower Jurassic Iroquois Formation (thickness 200 m – 800 m) and its lateral equivalent, the Mohican Formation (Fig. 2.10), were the units deposited after the breakup J200 unconformity. The Iroquois Formation predominantly comprises dolomitic carbonate rocks accumulated under restricted shallow-marine conditions. The Mohican Formation (thickness 300 m – 4000 m) (Given, 1977) consists of fine-grained sandstones and interbedded shales. The Mohican Formation, deposited in the sub-basins along the margin, thins considerably and pinches out at the hinge zone of the present-day shelf (Wade & MacLean, 1990; Deptuck et al., 2014).

The Middle Jurassic – Lower Cretaceous Abenaki Formation (thickness 600 m – 1600 m) (Kidston et al., 2005) is composed of carbonate and clastic rocks, and it is subdivided into four members (from bottom to top): Scatarie, Misaine, Baccaro, and Artimon Members (Fig. 2.10) (Eliuk, 1989; Wade & MacLean, 1990).

The Scatarie Member (thickness 10 m – 600 m), the lowest part of the Abenaki Formation, is primarily an oolithic limestone and packstone (Eliuk, 1978; Kidston et al., 2005). The Top Scatarie (J163) is a key seismic marker due to its traceability and strong positive (peak) reflection in both shelf and distal areas at the acoustic impedance boundary with the overlying clastic deposits of the Misaine Member.

The Misaine Member (thickness 50 m – 300 m), the only clastic interval of the Abenaki Formation, overlies the Scatarie Member. It is mainly composed of dark grey calcareous shale with minor limestone (Fig. 2.10). The member corresponds to the Callovian transgression along

the Jurassic shelf. The shaly unit pinches out landward over the carbonate platform with interfingering proximal sandstone (Kidston et al., 2005).

The thickness of the J200 – J163 interval, which includes the Mohican Formation, Scatarie and Misaine Members of the Abenaki Formation, and Iroquois Formation (Fig. 2.10), varies between 175 m and 6175 m (Fig. 2.12).

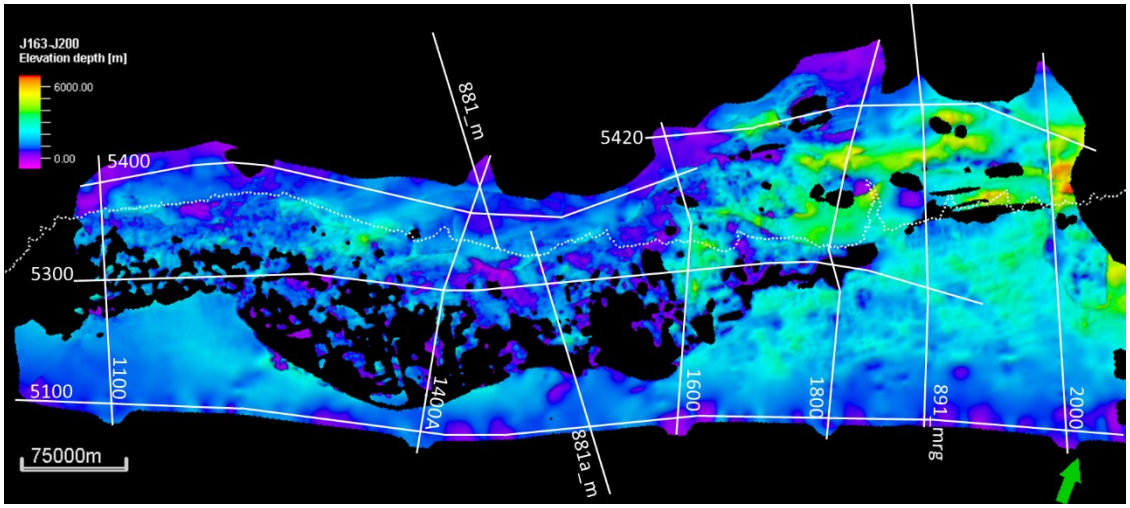

Figure 2.12: The thickness map of the J200 – J163 interval derived from the previous interpretations (PFA, 2011).

The Baccaro Member (thickness 100 m – 1200 m) is composed of limestone with sand and shale interbeds (Kidston et al., 2005). It is the thickest carbonate unit of the Abenaki Formation and was deposited in a shallow marine to the outer neritic setting. On seismic profiles, the Top Baccaro corresponds to the Tithonian Maximum Flooding Surface (MFS) and negative (trough) seismic reflection (J150) at the acoustic impedance boundary with the overlying clastic deposits of the Mic Mac Formation.

The Artimon Member (thickness 30 m – 115 m), the youngest and thinnest member of the Abenaki Formation (Kidston et al., 2005), contains mainly a section of argillaceous limestone interbedded with calcareous shales deposited in a shallow marine setting (Wade & MacLean, 1990).

Upper Jurassic sedimentary units comprise the Mohawk, Mic Mac, and Verrill Canyon Formations (Fig. 2.10). The Mohawk Formation (thickness 600 m to 1000 m) is composed of shallow-water feldspathic sandstone and siltstone recognized on the present-day shelf. The Mic

Mac Formation (thickness 800 m – 5000 m) comprises mixed clastic and carbonate rocks deposited in a shallow marine-outer neritic setting, including interbedded sandstones, shales, and limestones.

The Upper Jurassic-Lower Cretaceous Verrill Canyon Formation (thickness 750 m – 2500 m) mainly comprises dark-coloured calcareous shale interbedded limestone, siltstone, and sandstone (Given, 1977) (Fig. 2.10). It involves distal facies equivalent to the Abenaki, Mohawk, and Mic Mac Formations (McIver, 1972; Given, 1977; Kidston et al., 2005).

The maximum thickness of the Middle and Upper Jurassic interval (J163-J150) reaches 5340 m (Fig. 2.13) beneath the present-day shelf in the Sable and Huron Subbasins to the NE.

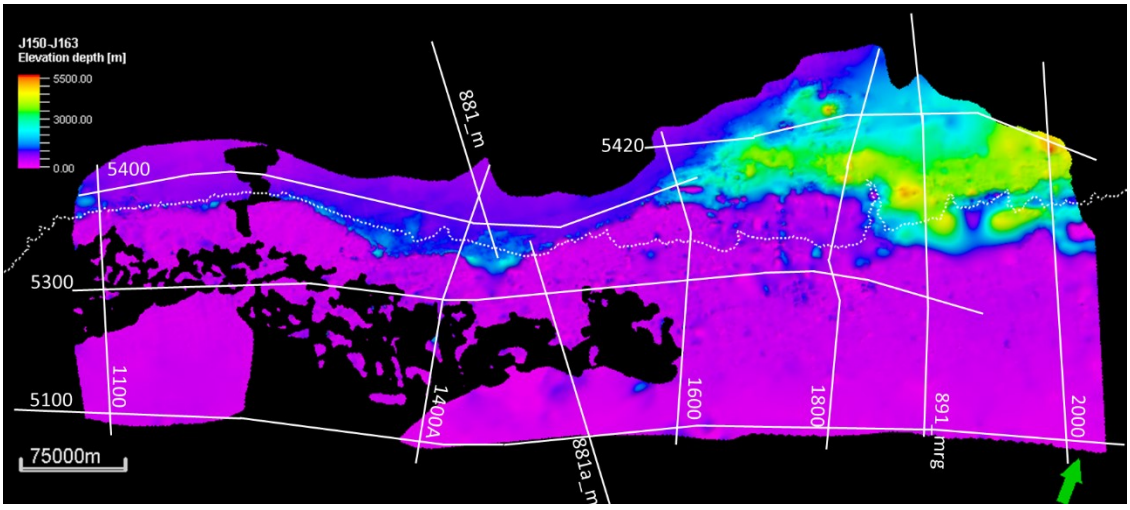

Figure 2.13: The thickness map of the J163 – J150 interval derived from the previous interpretations (PFA, 2011).

The Lower Cretaceous Mississauga Formation (thickness 300m – 3000 m) is composed of deltaic, fluvial, and shallow marine clastic deposits (Fig. 2.10) (Wade & MacLean, 1990; PFA, 2011; Deptuck et al., 2014). It varies in thickness and facies across the margin; the coarse-grained deltaic sediments grades into fine-grained sediments and thins basinward.

The erosional Berriasian-Valanginian Unconformity (Fig. 2.10) corresponds to a negative (trough) seismic reflection (K137) at the acoustic impedance boundary between the overlying

carbonate rocks of the Mississauga Formation and underlying Upper Jurassic-Lower Cretaceous clastic deposits (Wade & MacLean, 1990).

The Kimmeridgian-Berriasian Lower Mississauga Member is characterized by coarsening upward clastic sequence with thin beds of limestone. The maximum thickness of the member reaches 2000 meters at the present-day shelf edge. However, the top of the member Mississauga Formation does not correspond to a strong reflection on seismic profiles as it is underlain by lithologically similar clastic rocks of the Mic Mac Formation. The maximum thickness of the J150 – K137 interval reaches 5600 m in the Laurentian Subbasin within the Banquereau Synkinematic Wedge province (Fig. 2.14).

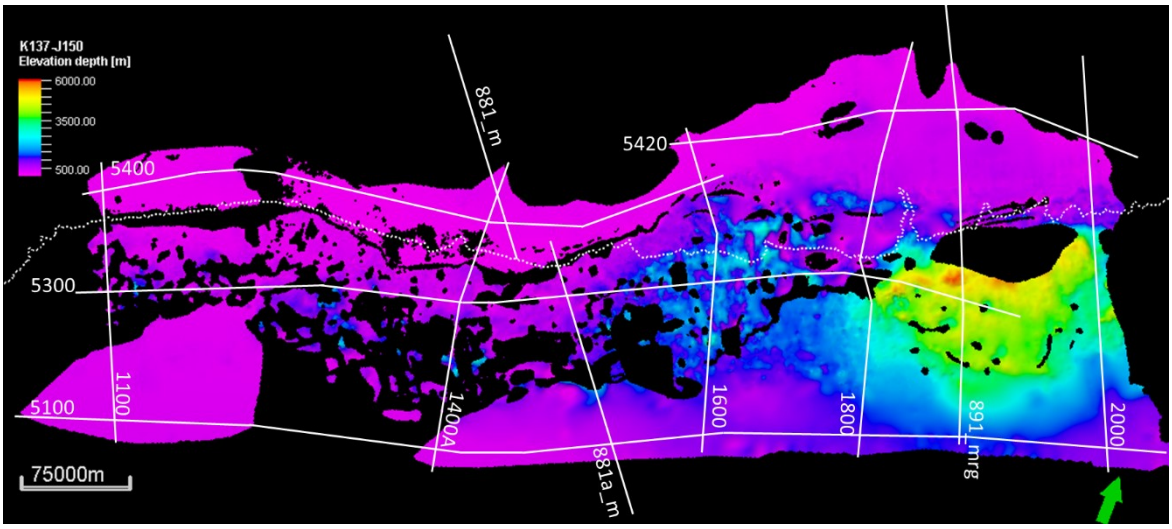

Figure 2.14: The thickness map of the J150 – K137 interval derived from the previous interpretations (PFA, 2011).

The Valanginian-Barremian Middle Mississauga Member (thickness 250 m – 800 m) is predominantly composed of thick sandstone deposited in a fluvio-deltaic environment and regionally extends over the Scotian Basin (Wade & MacLean, 1990). The maximum thickness of the K137 – K130 interval is 5845 m and observed in the Annapolis Subbasin (Fig. 2.15).

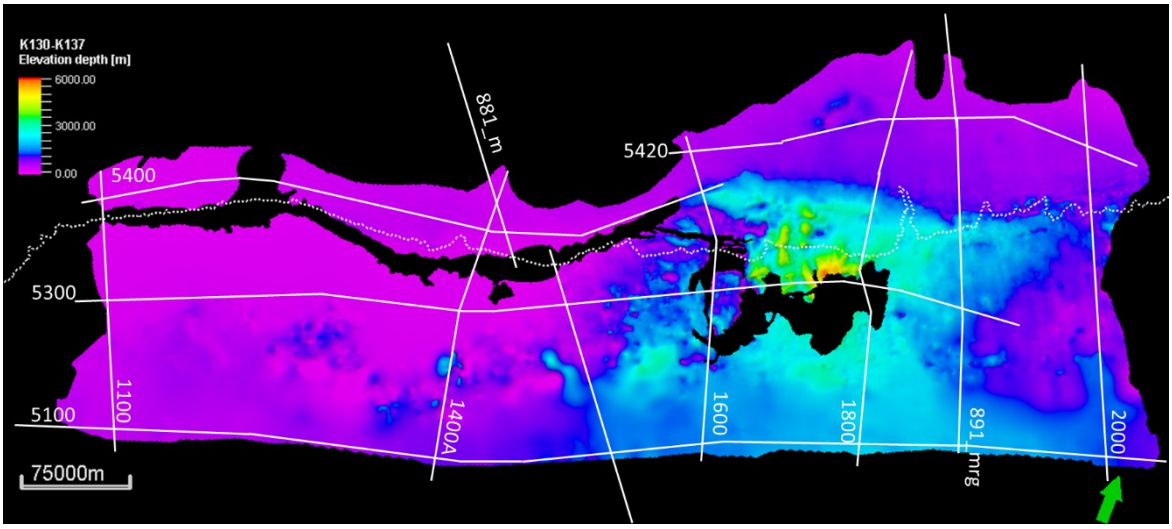

Figure 2.15: The thickness map of the K137 – K130 interval derived from the previous interpretations (PFA, 2011).

The Barremian-Aptian Upper Mississauga Member (thickness 150 m – 250 m) comprises amalgamated channel deposits of interbedded mudstone and limestone (Fig. 2.10). The Hauterivian to Barremian thick oolithic limestone, 'O' Marker, constitutes the base of the member and represents the seismic marker of K130 (Jansa & Wade, 1975; Barss et al., 1980). The seismic marker can easily be picked due to its strong positive amplitude and widespread extent across the margin; however, it attenuates as the oolitic limestone is replaced by shales in a deep-water setting. The K130 marker (Fig. 2.10) is interpreted as the Hauterivian Maximum Flooding Surface (PFA, 2011).

The Aptian-Albian to Cenomanian Logan Canyon Formation (thickness 1000 m – 2500 m) is composed of clastic rocks deposited in shallow marine and estuarine environments (Wade & MacLean, 1990) (Fig. 2.10). It is divided into four members, two of which are sandstone-rich (Marmora and Cree Members); the two others are shale-dominant (Naskapi and Sable Shales) (Wade & MacLean, 1990; MacLean & Wade, 1992; Wade et al., 1995). The Naskapi Member, up to 350 meters thick, consists of shale. The overlying Cree Member is composed of sand-rich facies, and its top corresponds to the Late Albian Unconformity and a positive (peak) seismic reflection (K101) at the acoustic impedance boundary with the overlying shaly units of the Sable Member (PFA, 2011). The maximum thickness of the K101 – K130 interval reaches 4600 m beneath the continental slope in the NE (Fig. 2.16).

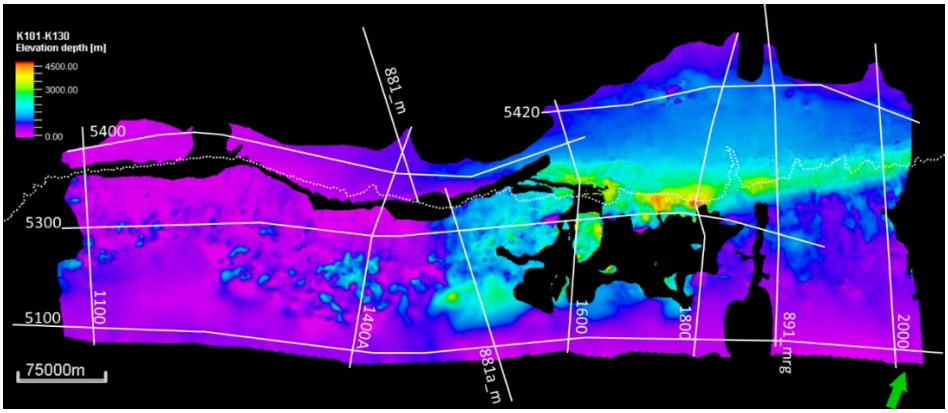

Figure 2.16: The thickness map of the K130 – K101 interval derived from the previous interpretations (PFA, 2011).

Lower Cretaceous volcanic rocks and basalt flow (thickness 800 m – 1500 m) along the Cobequid-Chedabucto Fault Zone are present within the Cree Member (Fig. 2.10) (Pe-Piper & Jansa, 1999). The volcanic rocks formed during the breakup stage (Fig. 2.3) between the Grand Banks and Iberia (Bowman et al., 2012). The Sable Member (250 m) is dominated by shale, thin sandstone, and siltstone beds deposited due to a rapid transgression (McIver, 1972; Jansa & Wade, 1975). The overlying Marmora Member (100 m) is a fining upward sand-rich sequence. Its top corresponds to the Cenomanian-Turonian Unconformity (K94) (Fig. 2.10) and strong negative (trough) seismic reflection at the acoustic impedance boundary at the base of the Ypresian chalk (PFA, 2011). The maximum thickness of the K94 – K101 interval is ~2000 m in the central slope of the margin (Fig. 2.17).

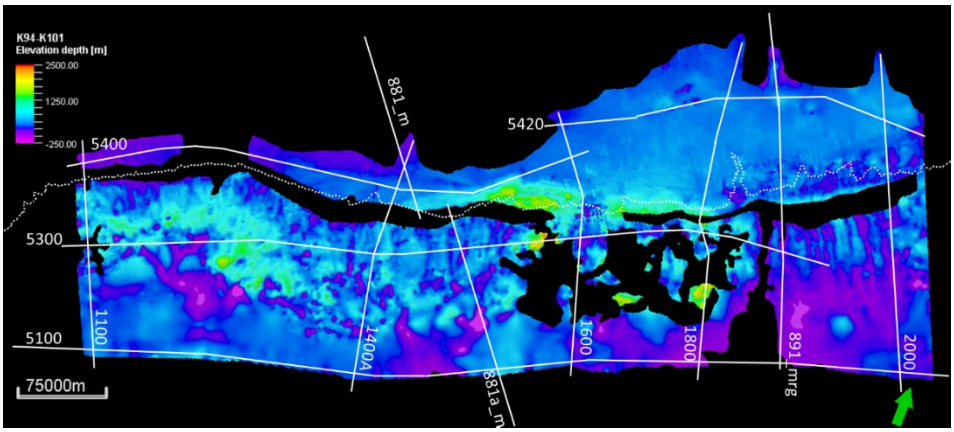

Figure 2.17: The thickness map of the K101 – K94 interval derived from the previous interpretations (PFA, 2011).

Upper Cretaceous-Eocene deposits are recognized as the Dawson Canyon Formation, Wyandot Formation, and Ypresian Chalk (Fig. 2.10) (Jansa & Wade, 1975; PFA, 2011). The Dawson Canyon Formation (>500 m) is composed of marine shales interbedded with thin limestone and chalk layers (Wade & MacLean, 1990). The Wyandot Formation (50 m – 400 m) contains chalk, marl, and minor limestone. The base Ypresian Chalk, corresponding to the key seismic marker T50 (trough), is a strong negative reflection on seismic lines at the acoustic impedance boundary with the overlying chalk unit and underlying clastics of the Banquereau Formation (Fig. 2.18).

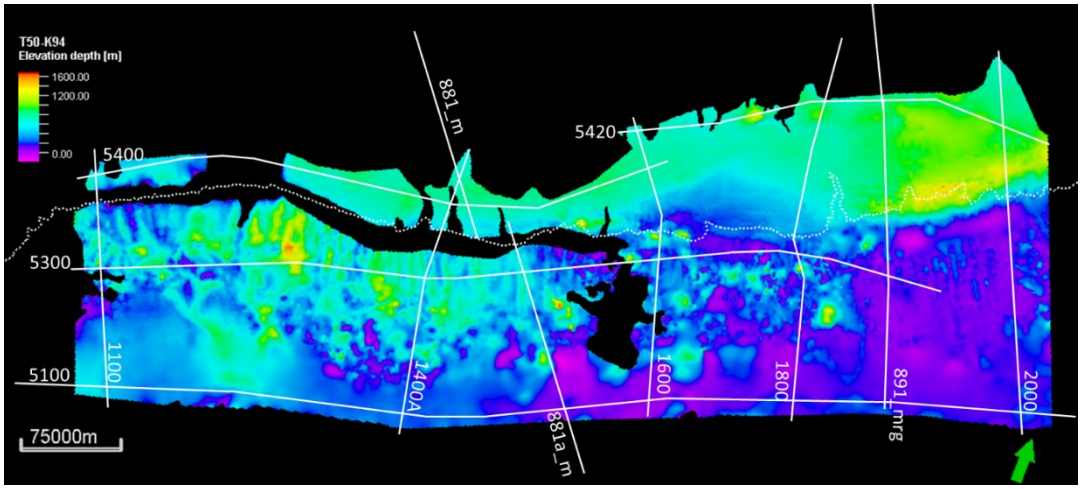

Figure 2.18: The thickness map of the K94 – T50 interval derived from the previous interpretations (PFA, 2011).

There are several unconformities in Cenozoic deposits (Fig. 2.10). The Mid-Oligocene Unconformity T29 (Fig. 2.9) corresponds to the erosional surface resulting from the Oligocene-Quaternary glacial episodes (Wade & MacLean, 1990). The thickness of the T50 – T29 interval varies between 85 m and 2450 m (Fig. 2.19), and it thins landward.

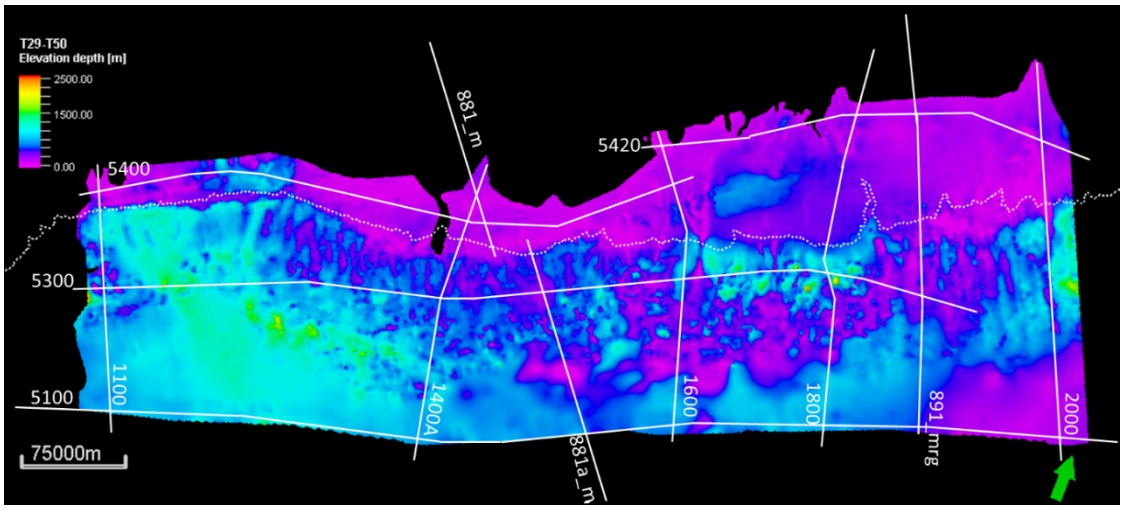

Figure 2.19: The thickness map of the T50 – T29 interval derived from the previous interpretations (PFA, 2011).

The youngest units of the sedimentary cover comprise the glaciomarine clastics of the Banquereau and Laurentian Formations. The thickness of T29 – Seabed interval varies between 105 m and 2465 m. The maximum thickness is observed beneath the southwestern slope of the margin, while it thins landward (Fig. 2.20).

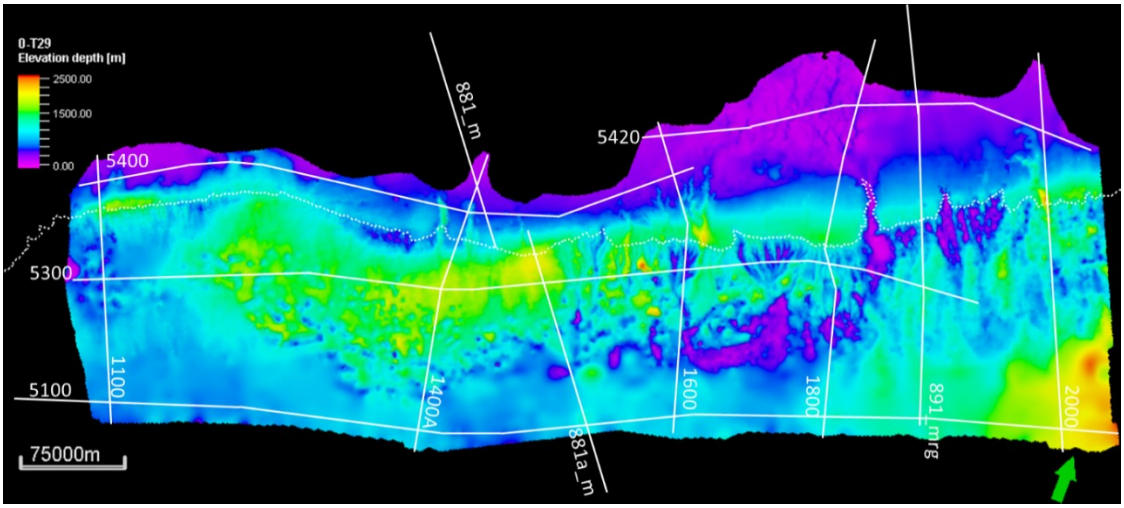

Figure 2.20: The thickness map of the T29 – Seabed interval derived from the previous interpretations (PFA, 2011). Note erosional structures at the break of the present-day shelf.

Chapter 3: Data and Methodology

3.1. Database

The data for seventy-seven wells from the Nova Scotia margin were made available for this project under a non-disclosure agreement (Annex A). Data sets from these wells, which were drilled in shelf to deep-water settings, included formation tops, well reports, well trajectories, log suites (GR, DT, RHOB, Resistivity, and Caliper), and checkshot surveys from the CNSOPB (Canada-Nova Scotia Offshore Petroleum Board). In addition, 10 000 km of post-stack 2D seismic surveys (Fig. 2.8) that were acquired and reprocessed during fifty-year-old exploration history have been provided by the NSDRR (Nova Scotia Department of Natural Resources and Renewables) and downloaded from open-source websites given in Annex B. The surveys of Penobscot 2D, 3D and NRCAN Laurentian Basin 2D are in the time domain, surveys of Novaspan 2010 2D and Lithoprobe 2D are both time and depth domains (Table 3.1). In addition, the seismic velocities of the Novaspan 2010 survey that have been used to build a velocity model were also shared by the NSDRR.

Table 3.1: The summary of available seismic surveys.

Seismic Survey	Total Length/Area	Number of Line	Record Length
Novaspan 2010 Reprocessed 2D-Time	3370 km	9	16 s
Novaspan 2010 Reprocessed 2D-Depth	3370 km	9	40 km
Lithoprobe 2D-Time	2015 km	6	21.5 s
Lithoprobe 2D-Depth	650 km	3	35 km
Penobscot 2D	1895 km	54	7 s
NRCAN Laurentian Basin 2D	2675 km	34	7 s
Penobscot 3D	82 km^2	600 IL/480 XL	6 s

The Novaspan 2010 reprocessed seismic lines are oriented parallel and orthogonal to the Nova Scotia shore line and characterized by highest coverage density; they were used in structural interpretation and 2D kinematic restoration. The NW-SE-striking Lithoprobe 2D seismic lines (881, 892, 891, and 865) extend from shelf to deep-water setting and were also used in structural interpretation. The densely spaced Penobscot 2D lines and Penobscot 3D

seismic survey cover very limited area and are located to the northwest of Sable Island. The NRCAN Laurentian Basin 2D survey, the easternmost data set, is situated in the Laurentian Subbasin (Fig. 2.8); it was not used in this study. The surfaces of key seismic markers (Fig. 2.10) in time and depth provided by the CNSOPB and NSDRR were used as a guide in refined structural seismic interpretation of this study.

The magnetic anomaly data (Miles & Oneschuk, 2016) gridded to 1 km intervals, and the bathymetry (Smith, 1997) and high-density free-air gravity anomaly data gridded to 1 minute were downloaded from https://topex.ucsd.edu/cgi-bin/get_data.cgi (Sandwell et al., 2014) and were also integrated with seismic reflection data to recognize different crustal structural boundaries.

3.2. Methods

3.2.1. Seismic Interpretation

The seismic interpretation was conducted in Petrel Slb to characterize the tectonic structure of the margin. It included steps of seismic mis-tie, QC of well logs, seismic-well tie, and picking faults and horizons in time and depth domains. In addition, seismic reflections at main acoustic impedance boundaries (sea floor, tops of carbonates, volcanics, salt and acoustic basement) were compared to reflection coefficients estimated from acoustic impedance in wells to determine the polarity and phase of seismic surveys.

The different sets of 2D seismic surveys were previously acquired, processed and reprocessed with different parameters during fifty years of exploration history of the Nova Scotia margin. Therefore, a mis-tie analysis was required to match seismic lines at the intersection of different seismic surveys. As the long-offset Novaspan 2010 reprocessed survey provides extended coverage from shelf to deep-marine settings, they served as reference lines for the mis-tie analysis. Hence, every event's times on the Lithoprobe lines were shifted up 35 milliseconds to adjust two seismic surveys (Fig. 3.1). Similarly, the time shift of 20 milliseconds and phase shift of 180º applied for the mis-tie eliminations between the Novaspan 2010 reprocessed and Penobscot 2D seismic surveys (Fig. 3.2). The Laurentian 2D survey is similarly shifted 25 milliseconds up as a result of mis-tie analysis.

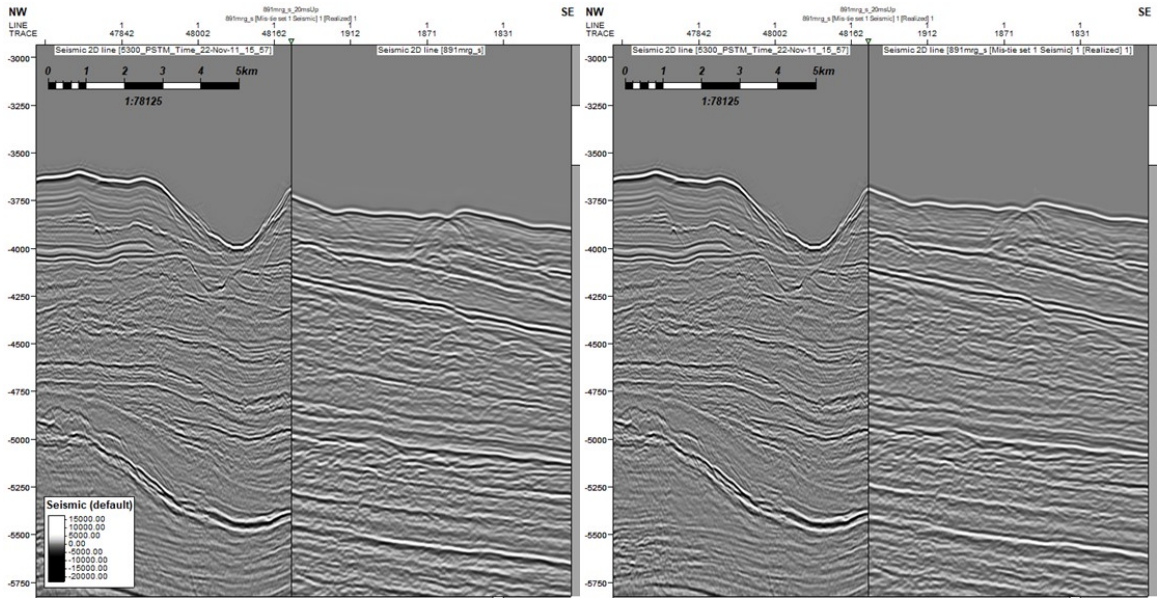

Figure 3.1: The composite lines between the Novaspan 5300 and Lithoprobe 891mrg_s lines before (left side) and after (right side) the mis-tie analysis, the vertical scale is TWT, ms.

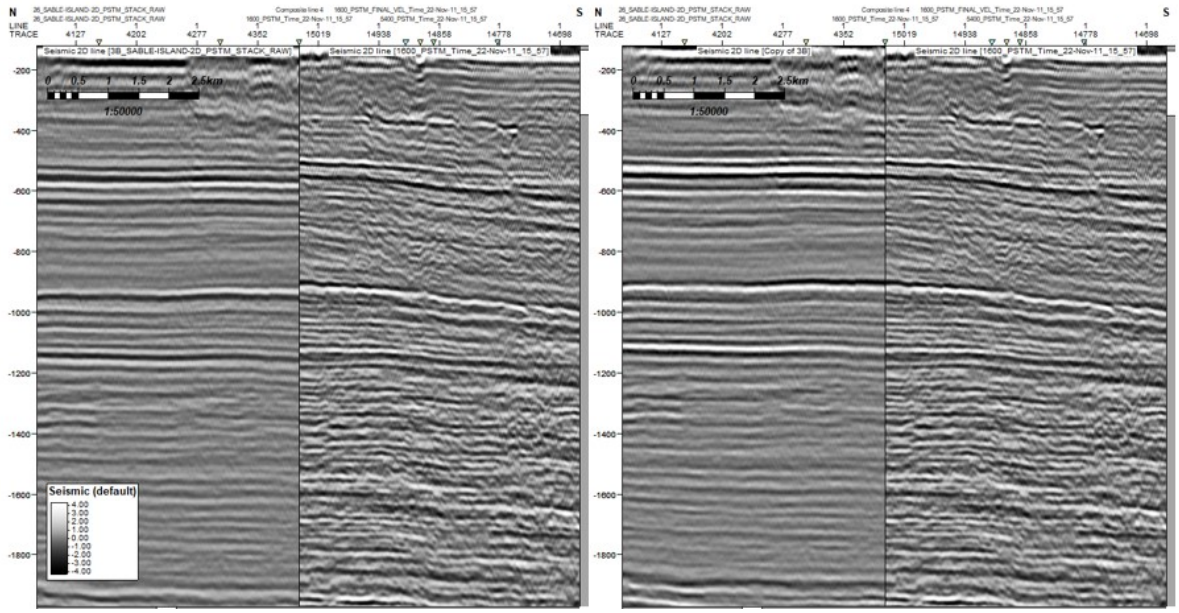

Figure 3.2: The composite lines between the Novaspan 1600 and Penobscot 3B lines before (left side) and after (right side) the mis-tie analysis, the vertical scale is TWT, ms.

To prepare the seismic-well tie analysis, the compressional wave sonic (DT) and density (RHOB) well logs were QC and despiked by using control from GR and caliper logs. The seismic-well tie process (Fig. 3.3) consists of the computation of acoustic impedance using the

sonic and density well log (Simm & Bacon, 2014). First, the reflection coefficient is computed at each interface between velocity and density contrasts along a well trajectory. The wavelets were extracted for each seismic line in a time window and a shot points range around the analyzed well to obtain a better correspondence between the generated synthetic seismogram and seismic data (Fig. 3.4). The wavelets were extracted based on bandwidth and frequency response from the seismic data near the well. The wavelets are convolved with the reflection coefficients to generate a synthetic seismogram (Fig. 3.4). In this study, synthetic seismograms of fifteen wells were created to correlate formation tops and key seismic markers, which were defined in the reports of the Play Fairway Analysis (PFA), 2011. Available checkshot and VSP surveys of the wells were used as input time-depth relationship (TDR) data. These data show two different trends in average velocity for wells drilled on the continental shelf and on the slope and deeper part of the Scotian Basin (Fig. 3.5).

Ten seismic markers (PFA, 2011), tops of autochthonous and allochthonous salt bodies (Table 3.2), and faults in both time and depth domains were interpreted in Petrel along the profiles of the 2D Novaspan 2010, 2D Lithoprobe and Penobscot 2D and 3D surveys.

Table 3.2: Interpreted seismic markers and their polarities identified in seismic well tie studies.

Seismic Marker	Stratigraphic Surface	Polarity
Seabed/0	Unconformity	Positive
T29	Unconformity	Positive
T50	Maximum Flooding Surface/Unconformity	Negative
K94	Unconformity	Negative
K101	Unconformity	Positive
K130	Maximum Flooding Surface	Positive
K137	Unconformity	Negative
J150	Maximum Flooding Surface	Positive
J163	Maximum Flooding Surface	Positive
Post-rift basement	Break-up Unconformity	Positive
Top Salt	Unconformity	Negative

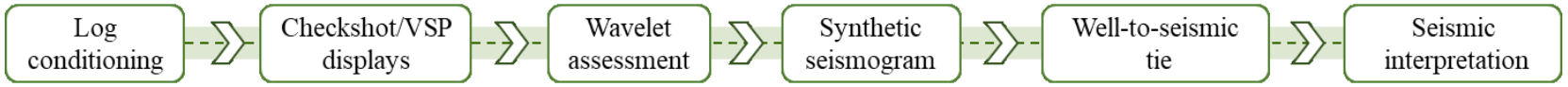

Figure 3.3: Well-to-seismic tie workflow.

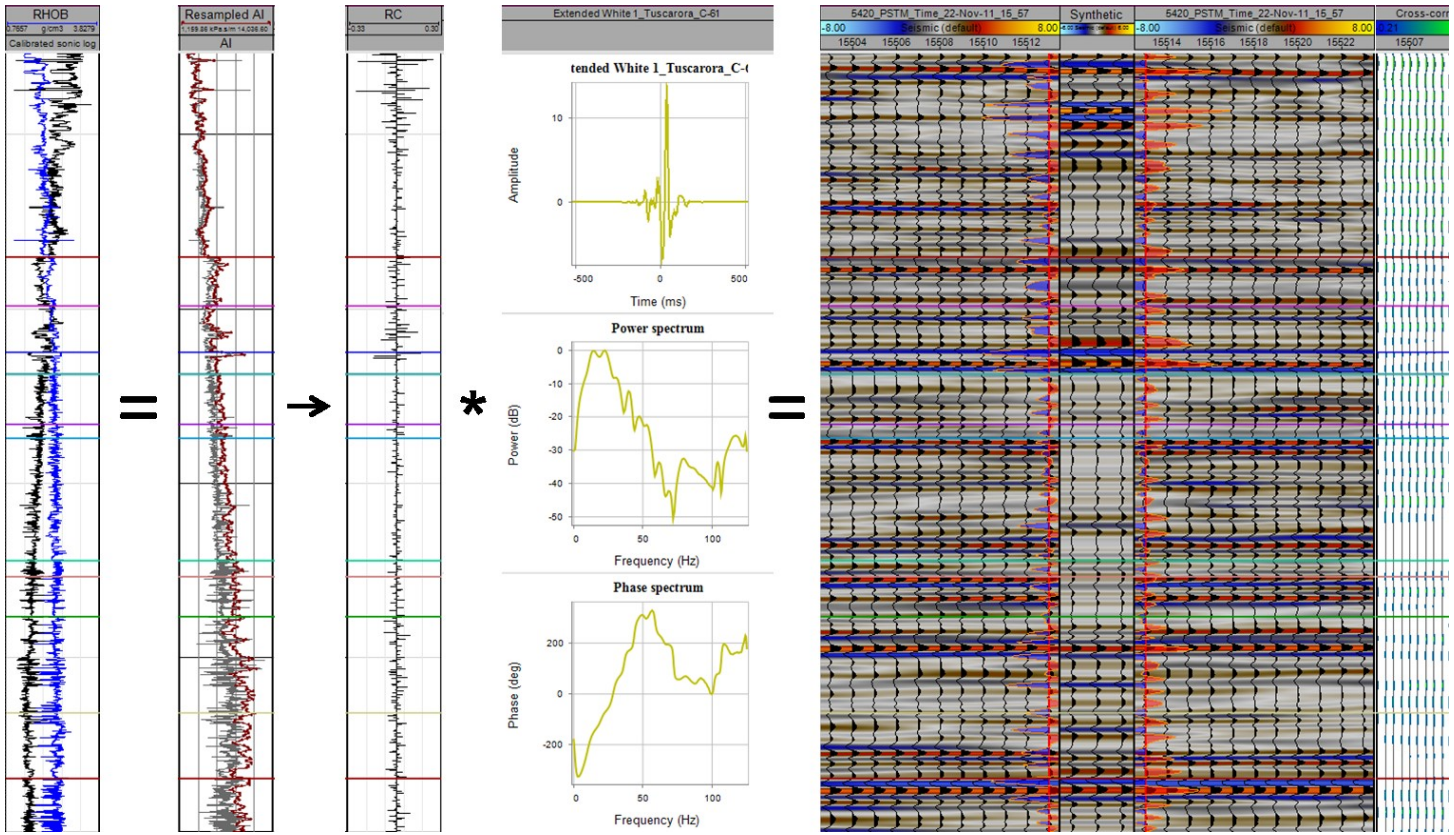

Figure 3.4: The synthetic seismogram of the Tuscarora C-61 well tied to Novaspan PSTM Line of 5420.

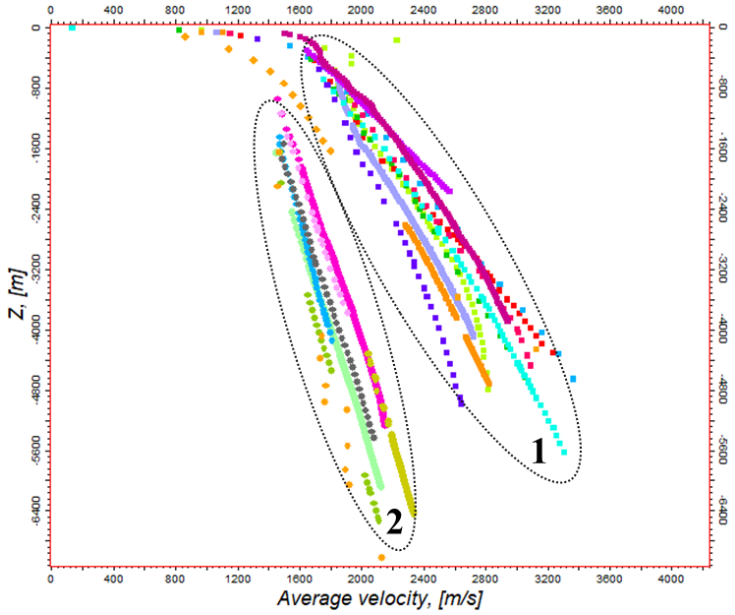

Figure 3.5: Two main trends of average velocities derived from the checkshot surveys in 27 wells in the Nova Scotia margin located: on shelf and close to the shelf break (1), and on the continental slope and in the deeper part of the basin (2).

3.2.2. 2D Sequential Restoration

The 2D sequential restoration is a numerical modelling approach used in sedimentary basin analysis and structural restoration (Gibbs, 1983; Groshong, 2006; Macaulay, 2017). In this study, the 2D kinematic modelling is conducted through MOVE Petroleum Experts Ltd. Several steps are completed during the 2D kinematic restoration that are subsequently applied for each time step/horizon. At the beginning, the beds are unfolded and fault offsets are restored. Next, the effects of sediment compaction and isostasy are reconstructed. Finally, thermal subsidence is estimated and compensated. The reconstruction allows us to analyze paleobathymetry and reconstruct tectonic deformation during the basin evolution. In particular, the simulation results help to quantify the amount of tectonic extension, thermal subsidence, decompaction, and isostatic response for each stratigraphic unit. 2D kinematic restoration is completed along the four NW-SE-striking seismic profiles in the depth domain (Novaspan PSDM lines of 2000, 1600, 1400A, and 1100) located in the SW, central and NE segment of the Nova Scotia passive margin (Fig. 2.8).

The workflow of the 2D kinematic restoration involves the processes of fault offset restoration, unfolding, thermal subsidence, isostasy, and decompaction for each time-step (Fig. 3.6). The selected seismic lines are sub-parallel to the NW-SE orientation of extension during the Atlantic Ocean opening. The orientation of extension can be interpreted from the NE-SW orientation of axes of syn-rift sub-basins and NE-SW-striking seafloor magnetic anomalies (Fig. 2.6) (Karner & Watts, 1982; Wade et al., 1995; Funck et al., 2004; Deptuck & Kendall, 2017). Thus, no angle correction was applied when restoring extension along the 2D lines.

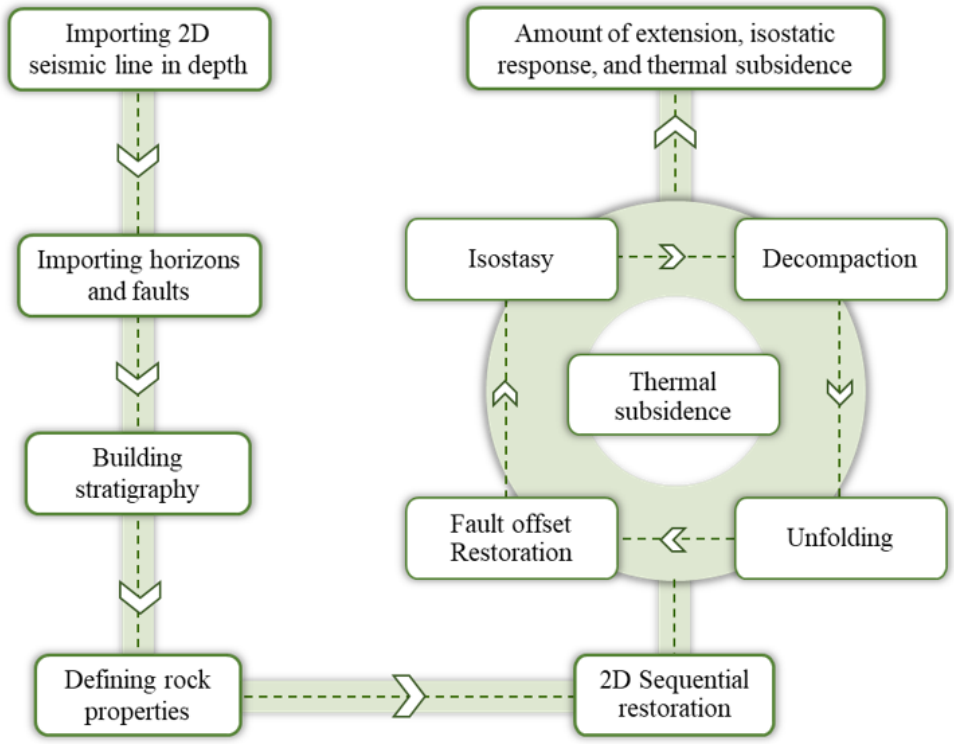

Figure 3.6: The workflow chart of the 2D kinematic restoration in MOVE.

The information on the sedimentary succession includes dominant lithology, grain size, thickness, and age of each unit, which were determined using available well logs, cuttings reports, biostratigraphy reports and composite logs. Information on rock properties included shale volume, porosity, Young's modulus and Poisson's ratio were determined from well logs and calibrated by test results in core cutting reports. The shale volume (V_{sh}) was estimated from gamma-ray logs for each reference wells (Eq. 1).

$$V_{sh} = \frac{GR_{log} - GR_{clean\,rock}}{GR_{shale} - GR_{fluiclean\,rock}} \quad (1)$$

Total porosity (Φ) was calculated from the density logs (Eq. 2).

$$\Phi_d = \frac{\rho_{matrix} - \rho_{log}}{\rho_{matrix} - \rho_{fluid}} \quad (2)$$

Where:

Φ_d : Density porosity

ρ_{matrix} : Density of matrix (2.65 gr/cm^3 for sandstone, 2.71 gr/cm^3 for limestone, 2.85 gr/cm^3 for dolomite)

ρ_{fluid} : Density of fluid (1 gr/cm^3 for fresh water)

ρ_{log} : Bulk density of log reading

The V_p profiles were estimated from compressional wave sonic logs and calibrated by the average compressional wave velocity ($V_{average}$) estimated from checkshot surveys (Fig. 3.5). The V_s profiles were estimated from V_p using Greenberg & Castagna (1992) correlation (Eqs. 3a, b, c).

$$V_s \text{ (sandstone)} = 0.8042V_p - 855.9 \quad (3a)$$

$$V_s \text{ (limestone)} = 1.0167V_p - 1030.5 \quad (3b)$$

$$V_s \text{ (shale)} = 0.7697V_p - 867.4 \quad (3c)$$

Where:

V_p : Compressional wave velocity

V_s : Shear wave velocity

$$Edyn = \frac{\rho Vs^2(3Vp^2 - 4Vs^2)}{(Vp^2 - Vs^2)} \quad (4)$$

$$\upsilon dyn = \frac{(Vp^2 - 2Vs^2)}{2(Vp^2 - Vs^2)} \quad (5)$$

Input parameters characterizing the properties of crustal and lithosphere of the Nova Scotia margin (Table 3.3) included thickness and density of water, crust, and lithosphere mantle (Dehler & Keen, 1993; PFA, 2011; Watts, 2001). These parameters were previously obtained from crustal-scale modelling and calibrated by gravity and magnetic data (Dehler, 2012; Dehler

& Welford, 2013). Elastic thickness of lithosphere (Table 3.3) was estimated based on the age of the lithosphere (Watts, 1981) and magnetic anomalies (Funck et al., 2004). The non-uniform stretching factor (Table 3.3) was applied with the consideration of previous results (Dehler & Welford, 2013), as explained below. Thermal properties of the Nova Scotia margin (Table 3.4) were also obtained from literature data (Dehler & Keen, 1993).

Table 3.3: Crustal properties of the Nova Scotia margin (Dehler & Keen, 1993; Watts, 1981; PFA, 2011; Dehler & Welford, 2013).

Crustal Properties of the Nova Scotia Margin	
Rifting period	225-200 Ma
Crustal thickness	35 km
Lithospheric thickness	125 km
Elastic thickness of lithosphere	20 km-30 km
Mantle density	3340 kg/m^3
Crust density	2870 kg/m^3
Water density	1030 kg/m^3
Stretching factor	1.1-2.2

Table 3.4: Thermal properties of the Nova Scotia margin (Dehler & Keen, 1993).

Thermal Properties of the Nova Scotia Margin	
Temperature of asthenosphere	1400 ºC
Thermal conductivity (grain)	2.092 (w/(mºC))
Thermal conductivity (basement)	2.929 (w/(mºC))
Thermal expansion coefficient	3.5x10^{-5}
Radiogenic heat production (grain)	0.837 (μW/m^3)
Radiogenic heat production (basement)	2.092 (μW/m^3)

3.2.2.1. Fault Offset Restoration

The normal fault offset restoration technique may involve different deformation mechanisms (simple shear, fault parallel flow, fault bend fold algorithm, trishear, and elliptical fault flow). The fault parallel flow algorithm (Kane et al., 1997; Egan et al., 1997) was applied in

this study for each stratigraphic unit. It is based on these principles: (1) the footwall is not deformed or translated, (2) the horizon length is preserved (Fig. 3.7). To estimate total amount of extension (%) along a given 2D line, the final (restored) and initial length of the profile were used.

$$Extension\ amount = \frac{(Lf - Li)}{Li} * 100 \quad (6)$$

Where:

L_f : Final length

L_i : Initial length

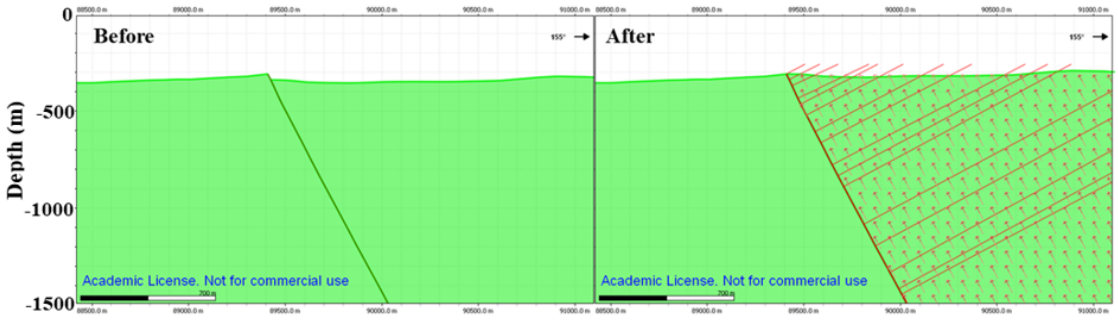

Figure 3.7: The 2D offset restoration (36 m) for the horizon K101 displaced by the normal fault shown for the deformed and restored state. Solid red lines represent the poles to the fault's plane and red arrows depict the restored displacement along the fault. The cross-section is in depth domain (PSDM), no vertical exaggeration.

3.2.2.2. Unfolding

The unfolding technique allows stratigraphic units to be restored to the pre-deformed state along a regional line, using algorithms such as simple shear, flexural slip, and line length unfolding. The simple shear algorithm was used in this study (Fig. 3.8) as it is best suited for flattening horizons in extensional settings where complex fold and thrust structures are not observed. It is based on these principles: (1) if the bed length is not preserved, the surface area of the bed is not preserved; (2) the surface area of horizons does not remain the same before and after the unfolding; (3) when the top bed is being unfolded to a regional line, the area of the bed, which topographically exceeds the regional line is removed, and the exceeding area is added to the volume of the unfolded bed.

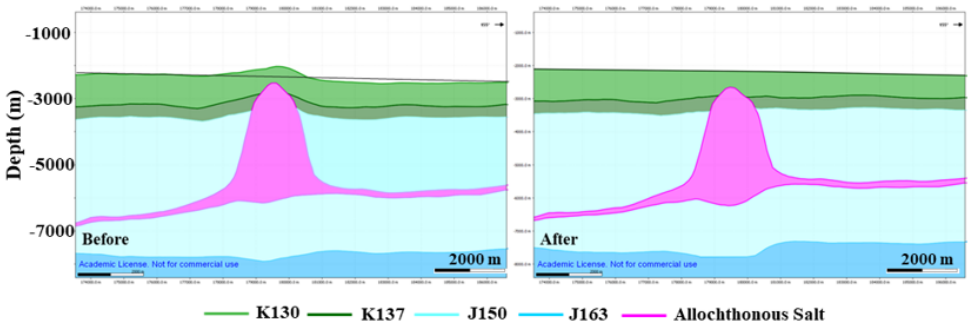

Figure 3.8: The cross-section before and after the unfolding of horizon K130 using the regional line (shown in black color). The cross-section is in depth domain (PSDM), no vertical exaggeration.

3.2.2.3. Thermal Subsidence

The thermal subsidence step of the kinematic restoration restores tectonic subsidence caused by cooling of the lithospheric mantle after the end of main rifting phase. The response of the lithosphere to extension during and after the rifting can be quantified to calculate the subsidence. The subsidence (S_i) (Eq. 7) caused by syn-rift faulting and the subsidence (S_t) generated by exponential thermal cooling (Eq. 8a-b) both define the total subsidence (ST) (Eq. 9), which persists until isostatic equilibrium is achieved (McKenzie, 1978).

$$s_i = \frac{a\left[(\rho_0-\rho_c)\frac{t_c}{a}\left(1-\alpha T_1\frac{t_c}{a}\right)-\frac{\alpha T_1\rho_0}{2}\right]\left(1-\frac{1}{\beta}\right)}{\rho_0(1-\alpha T_1)-\rho_w} \quad (7)$$

Where:

S_i : Initial subsidence

a : Thickness of lithosphere

ρ_0 : Mantle density

ρ_c : Continental crust density

ρ_w : Sea water density

α : Thermal expansion coefficient

T_1 : Temperature of asthenosphere

β : Stretching factor

t_c : Initial thickness of the continental crust

$$e_{(t)} = \frac{\alpha\rho_0\alpha T_1}{\rho_0-\rho_w}\left\{\frac{4}{\pi^2}\sum_{m=0}^{\infty}\frac{1}{(2m+1)^2}X\left[\frac{\beta}{(2m+1)\pi}sin\frac{(2m+1)\pi}{\beta}\right]\exp\left(-(2m+1)^2\frac{t}{\tau}\right)\right\} \quad (8a)$$

Where:

$e_{(t)}$: Elevation change at time t

α : Thickness of lithosphere

ρ_0 : Mantle density

ρ_w : Sea water density

α : Thermal expansion co-efficient

T_1 : Initial thickness of continental crust

β : Beta factor

t : Time (in millions of years) since rifting

τ : Lithosphere thermal time constant (tau)

$$S_t = e_0 - e_t \quad (8b)$$

Where:

S_t : Subsidence since extension

e_0 : Thermal subsidence at time 0

e_t : Thermal subsidence at time t

Total subsidence is, then, calculated by:

$$S_T = S_t + S_i \quad (9)$$

Where:

S_T : Total subsidence

S_t : Thermal subsidence since extension

S_i : Initial subsidence

In MOVE, the McKenzie model (1978) is used to restore thermal subsidence. The stretching factor (β) is defined as the ratio of the final (stretched) length to the initial (unstretched) length of the lithosphere. This assumes deformation occurs through pure shear and that area is preserved in 2D, with volume preserved in 3D. The stretching factor can also be calculated from changes in thickness of the lithosphere using the same assumptions, but in this case the stretching factor would be the ratio of the initial (unstretched) thickness to the final (stretched) thickness of the lithosphere. A uniform single-layered lithospheric stretching model is used in MOVE, and there is no option to account for different stretching factors for the crust and rigid-mantle parts of the lithosphere. At the same time, the β factor, with options of uniform and non-uniform values along the cross-section, can be applied to calculating thermal subsidence. Both uniform and non-uniform β values along the cross-section were tested through the burial curve in sensitivity tests to evaluate the stretching factor. As there is a change from the continental to oceanic crust along the NW-SE cross-sections, non-uniform values of β factor are expected to better respond to the tectonic settings of the Nova Scotia margin.

In this study, non-uniform stretching factor (β) was applied along the cross-section with increasing values from 1.1 at the continental shelf to 2.2 in the oceanic crust (Fig. 3.9). The estimated total subsidence increases with increasing value of beta factor (Fig. 3.10). The non-uniform beta helps to improve the reliability of the reconstruction of paleobathymetry for each time step compared to the uniform β values. Additionally, the parameter of the elastic thickness of the lithosphere (T_e) contributes to the variation of the thermal subsidence. Therefore, the sensitivity tests performed for β and T_e.

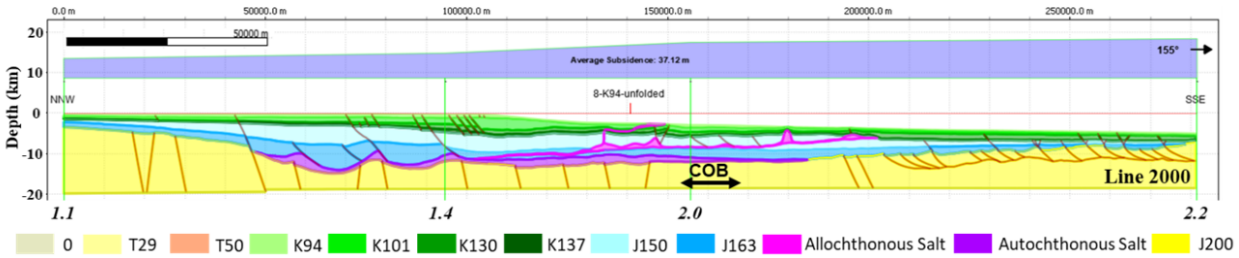

Figure 3.9: The thermal subsidence stage of the K94 along Line 2000 with an increased stretching factor (β). COB, continent-ocean boundary. The cross-section is in depth domain (PSDM), no vertical exaggeration.

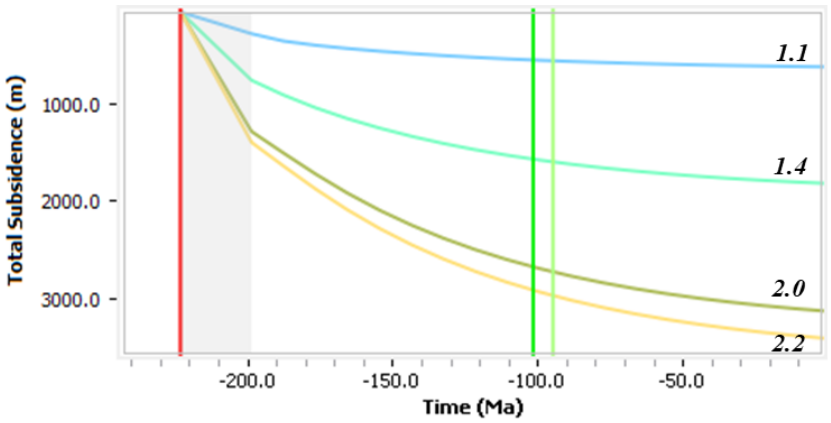

Figure 3.10: The total (thermal) subsidence curves estimated forof the K94 horizon at different beta factor that increases from 1.1 in the NW to 2.2 in the SE along Line 2000 (see Fig. 3.9). The red line represents the time of the beginning of rifting, and the grey shaded area corresponds to the syn-rift stage. Subsidence curves shown in different colours correspond to the increased β values.

3.2.2.4. Isostasy

The isostasy, the state of gravitational equilibrium between outermost layers of the Earth, is based on the Archimedes' principle stating the upward buoyant force P that is exerted on a body immersed in a fluid, whether fully or partially, is equal to the weight (h×ρ×g) of the fluid that the body displaces (Fig. 3.11).

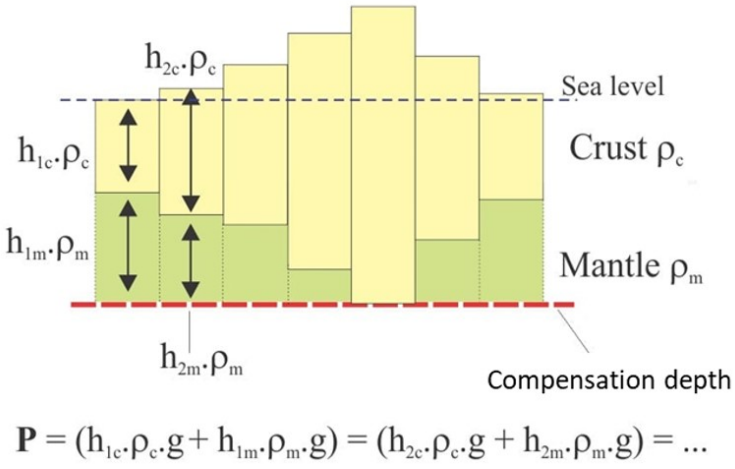

Figure 3.11: The diagram explaining Archimedes' principle of the isostasy, after (Allen & Allen, 2005).

The MOVE provides two options for calculating isostatic response: the Airy isostasy and flexural isostasy, combined with the decompaction process. The flexural isostasy algorithm was

performed in this study as the length of the reconstructed cross-sections is greater than 10 km, and the thickness of stratigraphic units was laterally variable.

Turcotte & Schubert (1982) proposes the equations below (Eqs. 10a-b-c) to calculate lithospheric deflection from the load at a given distance and model flexural response.

$$\sum_{n=0}^{n=w} \frac{L_n.\alpha^3}{8.D} e^{\frac{-x}{\alpha}} \times \left(\cos\left(\frac{x}{\alpha}\right) + \sin\left(\frac{x}{\alpha}\right)\right) \quad (10a)$$

Where:

D_x : The deflection of the lithosphere at distance from the load (L)

L : The load

D : Flexural rigidity

α : Flexural parameter

The equation 10b defines the flexural rigidity D as below.

$$D = \frac{E \times Te^3}{12 \times (1-\upsilon^2)} \quad (10b)$$

E : Young's modulus

υ : Poisson ratio

T_e : Effective elastic thickness of lithosphere (km)

The equation 10c defines the flexural parameter as below.

$$\alpha = \left[\frac{4 \times D}{(\rho_m).g}\right]^{\frac{1}{4}} \quad (10c)$$

ρ_m : Density of material below the lithopshere (normally the density of the mantle)

g : Gravity

The effective elastic thickness, T_e, is constrained by the rheological thickness of the lithosphere and geothermal gradient (Eq. 10b). T_e controls the wavelength of the lithospheric flexure and magnitude of the sedimentation (Roberts et al., 1998; Watts, 2001). Watts (1981)

proposes an estimation of T_e, corresponding to the oceanic isotherms of 300 to 600 ºC, based on the cooling plate model (Fig. 3.12).

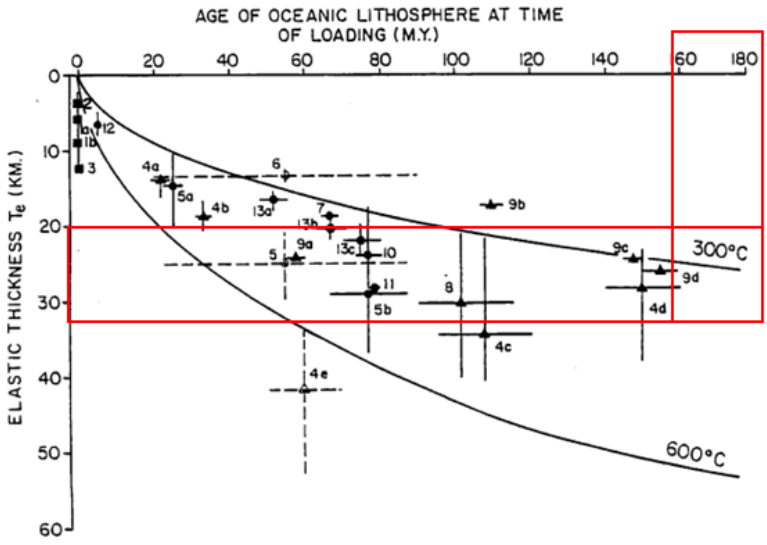

Figure 3.12: The elastic thickness of the lithosphere T_e against the age of the oceanic lithosphere at the time of loading (Watts, 1981). The solid lines are the 300°C and 600°C oceanic isotherms based on a cooling plate model. The red boxes represent age of the lithosphere (160-180 Ma) and T_e values (20 km-30 km) used in this study.

According to the model, Te increases with the thermal age of the lithospheric plate (Eq. 11) (Bodine et al., 1981).

$$\mathrm{Te} = aAge^{1/2} \tag{11}$$

Where a = 4.3± 0.5 (dry) and a = 3.3± 0.5 (wet)

In this study, the T_e of the reconstructed cross-sections is evaluated as ranging between 20-30 kilometres as the age of the oceanic lithosphere in the oceanic domain (SE of the cross-sections) varies between 160 Ma and 180 Ma (Fig. 3.12). The sensitivity testing was performed for the T_e.

3.2.2.5. Decompaction

The porosity is a ratio of a pore volume to total rock volume and refers to the storage capacity of a rock. The compaction defines the decrease in pore volume resulting from the porosity loss with increased burial depth; it is represented by the compaction curves (Fig. 3.13).

The decompaction module in MOVE estimates tectonic loads generated by overlying sedimentary succession and seawater and contributes to the restoration of burial history. Decompaction helps to restore rock volume when the overburden is removed. The decompaction for each time step was integrated with the restoration of the effects of thermal subsidence to estimate total isostatic rebound and analyze resulting paleobathymetry (Fig. 3.14) that was subsequently compared to the biostratigraphy data from wells.

In MOVE, the decompaction tool allows either using model (default) compaction based on Sclater & Christie (1980), Baldwin & Butler (1985), and Dickinson (1953) or importing user-defined porosity-depth relationships (Fig. 3.13). The curve of Sclater & Christie (1980) is derived from normally pressured stratigraphic units of the North Sea. The curve of Baldwin & Butler (1985) was proposed for calculating shale compaction.

In this study, density porosity curves were derived from the bulk density (RHOB) logs (Eq. 1) of wells located on or nearby (at less than ~20 km from) the analyzed cross-sections. There is a high uncertainty of the porosity of sedimentary units in the shallow intervals as neither RHOB nor DT logs are usually available in the upper interval of 0 -1500 m in wells. In these intervals, two compaction curve were used for calibration (Fig. 3.13). One default curve from Sclater & Christie (1980) and another estimated for Sable Island C-67 well by Watts and Steckler (1979).

Thus, the shape of the compaction curve at shallow depth intervals strongly affects decompaction results for the underlying units.

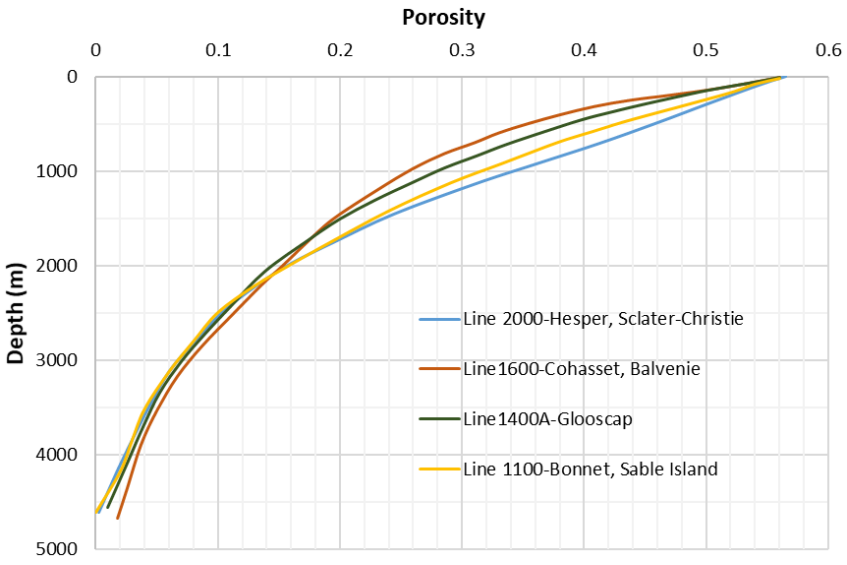

Figure 3.13: The compaction curves built in this study for indicated reference wells by using density porosity logs estimated from bulk density logs. Variations in the compaction curves are more important for shallower sections (<1500 m).

Applying variable compaction curves for the cross-section results in a significant variation of restored paleodepth for the stratigraphic units and, subsequently, the location of depocenters and sediment distribution modelling. In shallower depths (<1500 m), the compaction curve mostly affects the restored paleodepth of horizons. Therefore, sensitivity tests were carried out to calibrate the effect of the compaction curve on paleobathymetry, especially for the shallow intervals.

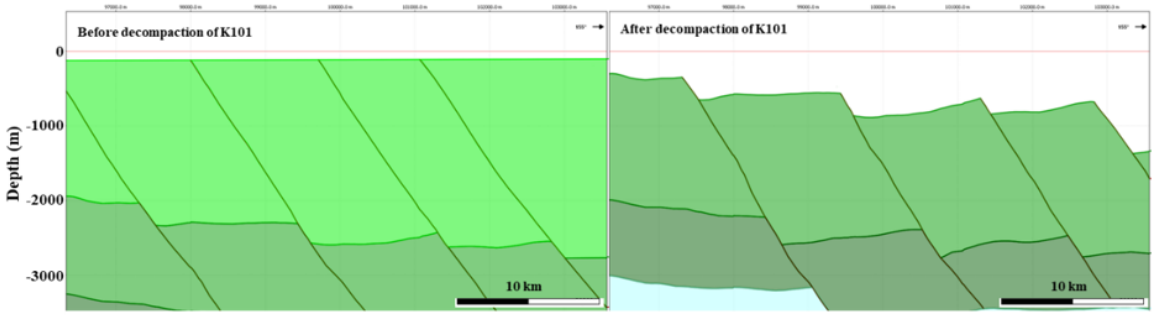

Figure 3.14: The example of decompaction + thermal subsidence restoration for K101 horizon along line 2000. The cross-section is in depth domain (PSDM), no vertical exaggeration. The location of the sections are shown in Figure 2.8.

The combined effects of unfolding, decompaction, and removal of thermal subsidence results were modeled to estimate a paleodepth of each stratigraphic unit. The reconstructed paleodepth was compared to the paleodepth range analyzed from biostratigraphy data of stratigraphic units in available well reports (Weston et al., 2012; Parthasarathy et al., 2017) for wells located nearby the cross-section.

Chapter 4: Results

This chapter describes the results of this study in two groups. The first part includes the horizon and fault interpretation based on 2D regional seismic data. The second part comprises the results of the 2D backstripping modelling built for four cross-sections.

4.1. Seismic Interpretation

4.1.1. Horizon Interpretation

Ten seismic markers identified in previous study (PFA, 2011) based on the biostratigraphy studies, tops of autochthonous and allochthonous salt, and faults were interpreted along the Lithoprobe and Novaspan surveys in time and depth domains. The horizons were traced based on well tops and well-to-seismic tie results through Petrel. The seismic surveys display positive polarity convention and zero phase. Seismic characteristic patterns of units (Fig. 4.1) were considered in the interpretation in the areas with limited or no well control.

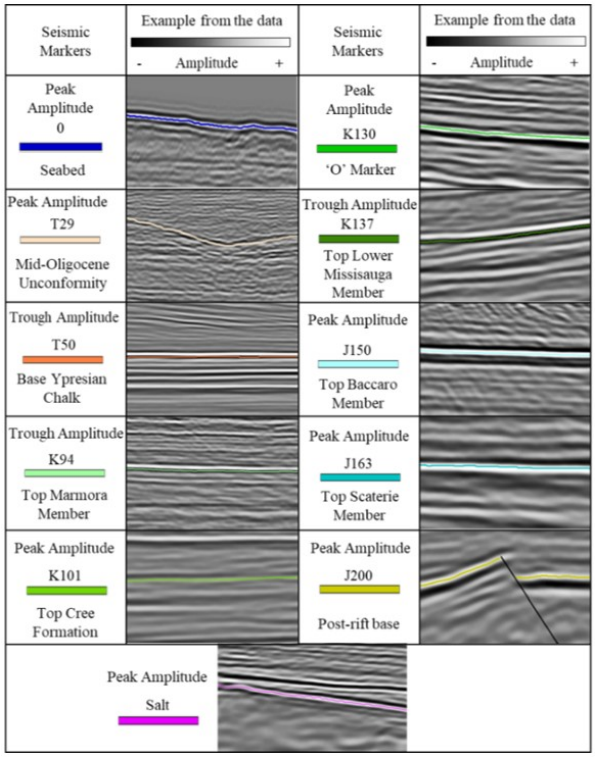

Figure 4.1: Seismic characteristic patterns and prominent amplitude response at the top of the interpreted seismic markers. See Figure 2.10 for correlation of the seismic markers with stratigraphic units.

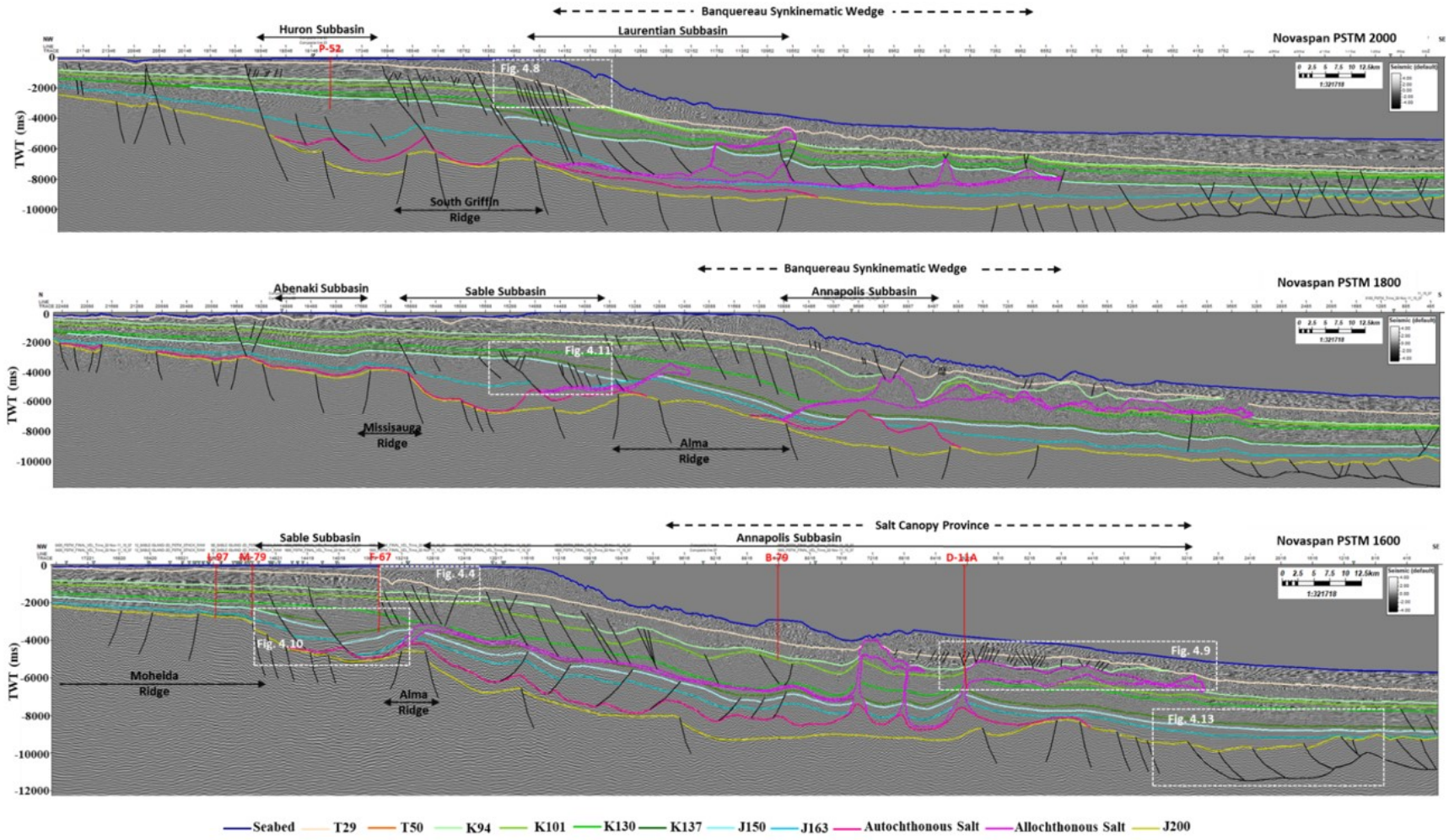
Banquereau Synkinematic Wedge
Huron Subbasin
Laurentian Subbasin
Novaspan PSTM 2000
P-52
Fig. 4.8
TWT (ms)
South Griffin Ridge
Banquereau Synkinematic Wedge
Abenaki Subbasin
Sable Subbasin
Annapolis Subbasin
Novaspan PSTM 1800
Fig. 4.11
Missisauga Ridge
Alma Ridge
Salt Canopy Province
Sable Subbasin
Annapolis Subbasin
Novaspan PSTM 1600
L-97
M-79
F-67
B-79
D-11A
Fig. 4.4
Fig. 4.10
Fig. 4.9
Fig. 4.13
Moheida Ridge
Alma Ridge
Seabed
T29
T50
K94
K101
K130
K137
J150
J163
Autochthonous Salt
Allochthonous Salt
J200

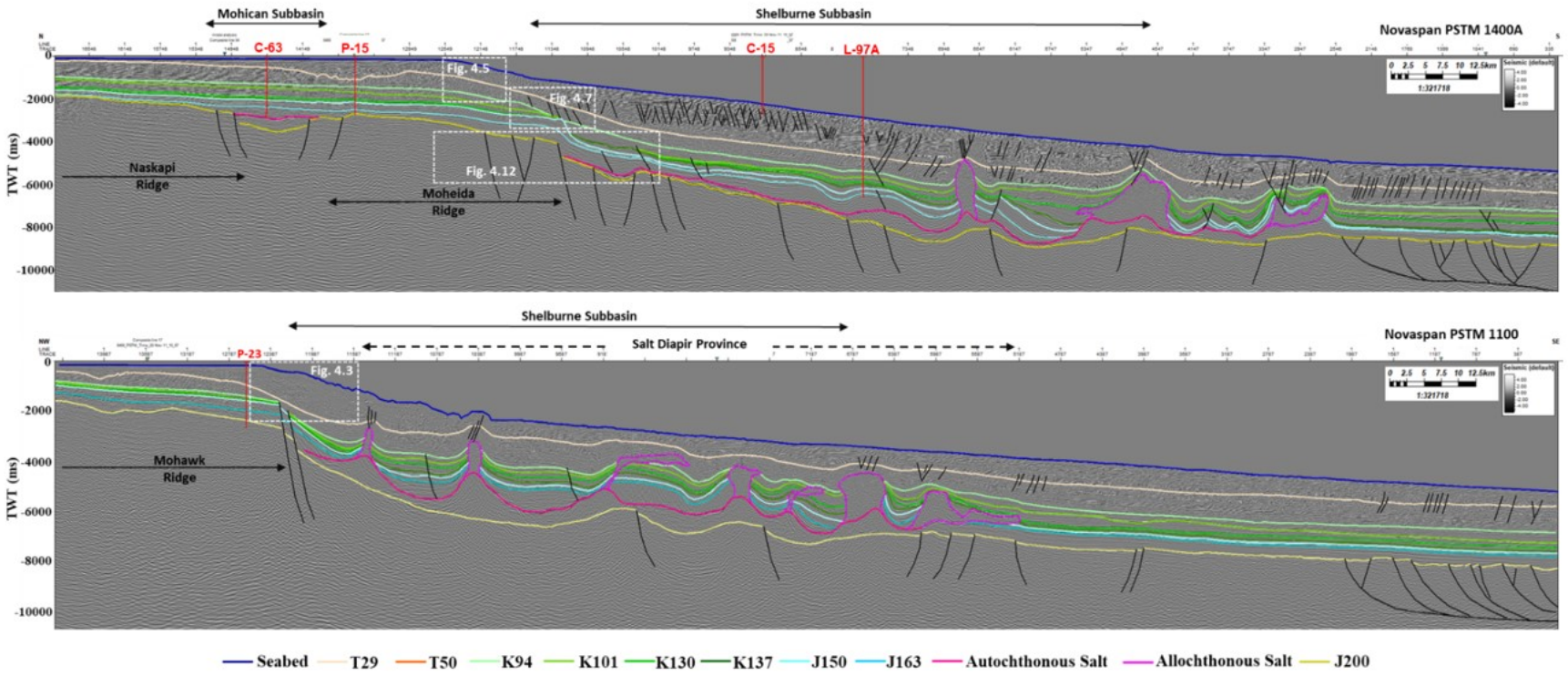

Figure 4.2: Structural interpretation of the NW-SE Novaspan 2010 PSTM lines across the Nova Scotia margin basin. Vertical scale is in time. See Figure 2.8 for the location of lines.

4.1.1.1. The 0 – T29 Interval

The seabed corresponds to the acoustic impedance boundary between water and the clastic deposits, and it is represented by positive (peak) reflection (Fig. 4.3). The youngest units of the basin consist of prograding, coarsening-upward sequences of the Banquereau Formation and glaciomarine clastics of the Laurentian Formation. The reflection configuration of the unit is subparallel to slightly divergent on the shelf, highly divergent on the slope, and parallel to subparallel in the distal part of the basin.

The interval thickness changes from 105 m to 2465 m (Fig. 2.20), reaching its maximum beneath the southwestern slope. Incised canyons along the shelf and downlapping sequences are widespread within the unit (Fig. 4.3), especially in the central and NE segments of the margin.

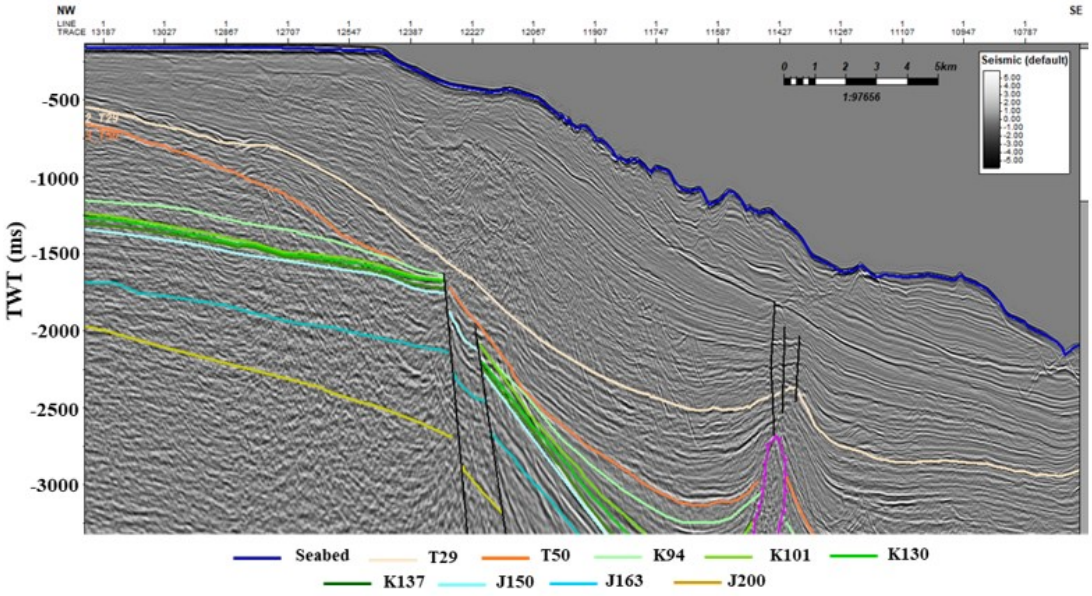

Figure 4.3: Increase in thickness and downlapping sequence observed within the interval T29-seabed beneath the outer shelf and upper slope along Line 1100. Vertical scale is in time. See Figs. 2.8 and 4.2 for the line location.

4.1.1.2. The T29 – T50 Interval

The T29 Mid-Oligocene Unconformity (Fig. 2.10) corresponds to the erosional surface (Fig. 4.1) resulting from the Oligocene-Quaternary glacial episodes; therefore, T29 is characterized by a variable AI boundary changing from peak to trough depending on the rock lithology above and below it. The most characteristic feature of T29 horizon is a shape that

reflects incised valleys and channel geometries (Figs. 2.19, 4.4). These valleys are 2-7 km wide, 100-800 m deep and ~25-50 km up to 75 km long based on the interpretation of the PSDM lines. T29 is overlain by a prograding Upper Tertiary clastic sequence (Fig. 4.5) beneath the continental slope. Thickness of the interval T29-T50 vary from zero in the incised valleys to ~2450 m below the continental slope of the SW segment of the margin (Fig. 2.19).

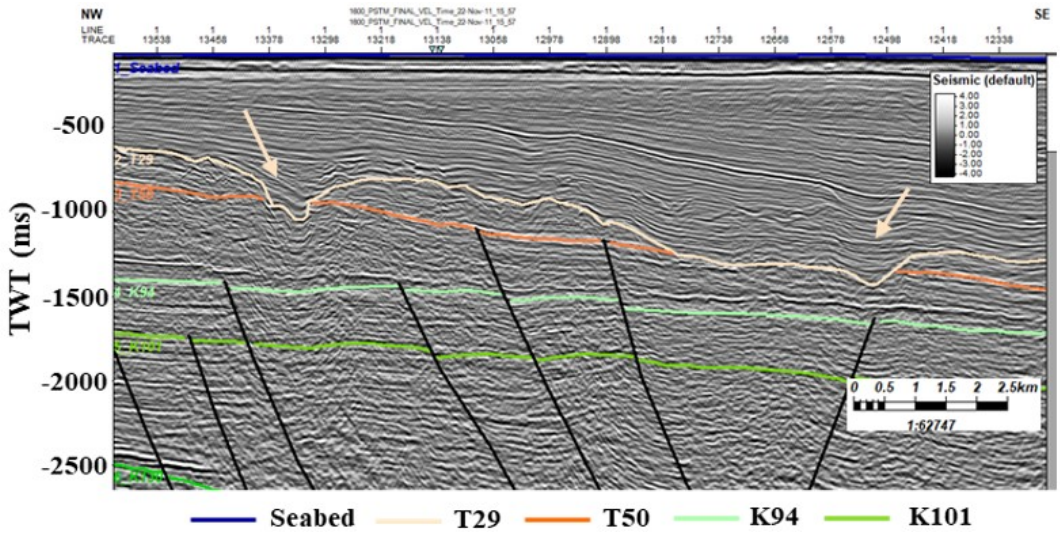

Figure 4.4: The incised canyons shown by arrows in the shelf area along the Novaspan PSTM 1600 line. T29 erodes T50 for ~200-350 m. Vertical scale is in time. See Figs. 2.8 and 4.2 for the line location.

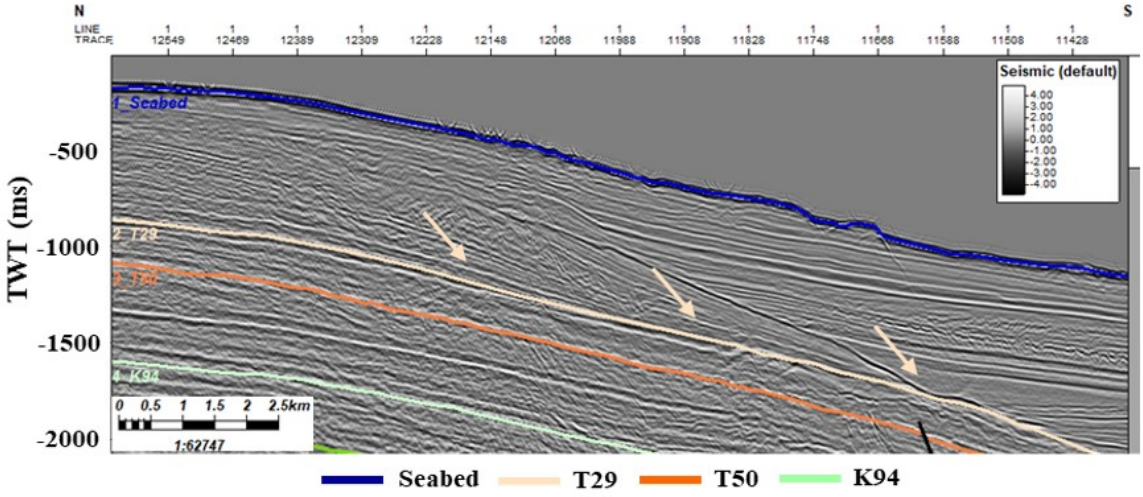

Figure 4.5: The prograding sequences in the interval T29-seabed shown by arrows beneath continental slope along Novaspan PSTM 1400A line. Vertical scale is in time. See Figs. 2.8 and 4.2 for the line location.

4.1.1.3. The T50 – K94 Interval

T50, defined as the base of the Ypresian Chalk, corresponds to the beginning of the latest chalk deposition during the Tertiary (Fig. 2.10). T50 is represented by a negative (trough) reflection (Fig. 4.1), as it corresponds to the AI boundary between the hard chalk above to the less hard clastic units of the Banquereau Formation below it. The chalky unit reaches a maximum thickness of ~30 m in the shelf area; therefore, the seismic marker is more traceable landward. The interpretation of T50 is mainly guided by its strong negative reflection on the continental slope.

The Montagnais structure with a diameters of ~45 km (Jansa et al., 1989) was caused by a meteorite impact in the southwestern part of the present-day shelf (Fig. 4.6). The impact overprinted the reflections of all units older than T50. The T50 is eroded by Oligocene-Miocene unconformity (T29) within the shelf and continental slope.

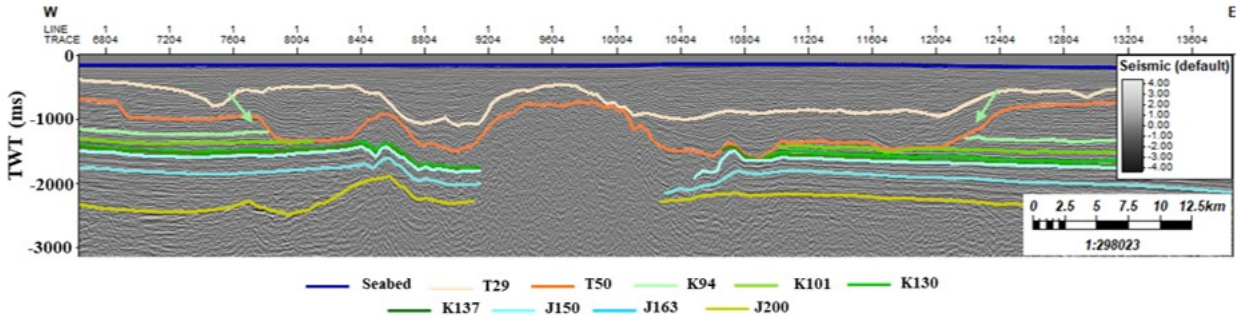

Figure 4.6: The Montagnais impact structure interpreted on the Novaspan PSTM Line 5400. Vertical scale is in time. See Figs. 2.8 and 4.2 for the line location.

The T50-K94 interval thickness ranges from 75 to 11575 m (Fig. 2.18), and T50 reaches the maximum depth of 6700 m (TVDSS) in the northeastern part of the deep basin (Fig. 4.14).

4.1.1.4. The K94 – K101 Interval

K94, the Turonian-Cenomanian Unconformity, defines a submarine erosional surface (PFA, 2011) and also marks the onset of chalk production in the basin. It is equivalent to base of the chalky unit of the Dawson Canyon Formation on the shelf (Fig. 2.10).

The reflections of K94-K101 interval are parallel to slightly divergent on the shelf; progradational in dip direction beneath the northeastern slope; distorted and wavy related to salt tectonism beneath the southwestern slope; and parallel in the basin plain.

The K94 corresponds to the boundary between chalk above and sand below it, and it is represented by strong negative (trough) amplitude on seismic profiles (Fig. 4.1). It can be easily recognized on the shelf; however, chalky facies is replaced by shale distally, and the amplitude contrast between overlying and underlying units relatively disperses.

The thickness of K94-K101 interval significantly changes from 450 m to 100 m to 0 m, where this interval is eroded by slope failure (Figs. 2.17, 4.7) above the edge of the Jurassic carbonate platform below the present-day continental slope. Locally, K94-K101 interval is destroyed by the Montagnais impact structure.

K94 reaches the maximum depth of 7100 m (TVDSS) (Fig. 4.14) in the northeastern part of the basin. Total thickness of the K94-K101 interval changes between 80 m to 2000 m (Fig. 2.17).

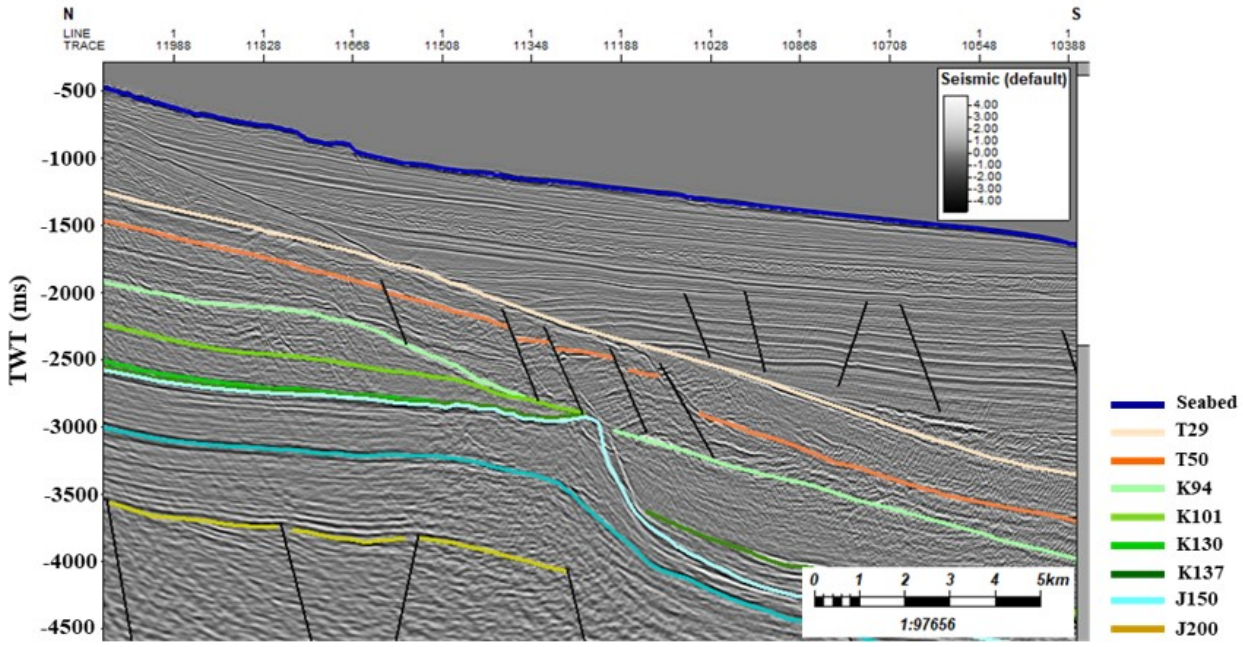

Figure 4.7: K94 and K130 are eroded by slope failure above the edge of the Jurassic carbonate platform interpreted on the Novaspan Line 1400A. Vertical scale is in time. See Figs. 2.8 and 4.2 for the line location.

4.1.1.5. The K101 – K130 Interval

K101 is the Late Albian Unconformity (PFA, 2011) that separates the sand-rich Cree Member from the overlying shaly unit at the base of the Sable Member of the Logan Canyon Formation (Fig. 2.10). K101 is represented by a downward increase in AI and corresponds to a moderate positive (peak) amplitude (Fig. 4.1). The picking was based on well tops derived from biostratigraphy reports and the reflection characteristics in the areas without well control.

The reflections of the sand-rich clastic deposits K101-K130 are subparallel to slightly divergent on the shelf; oblique reflections indicate the presence of clinoform and progradational deposits advancing in dip direction beneath the northeastern slope (Fig. 4.8); divergent and distorted reflections are related to salt tectonism beneath the southwestern slope; parallel reflections are typical in the deeper part of the basin.

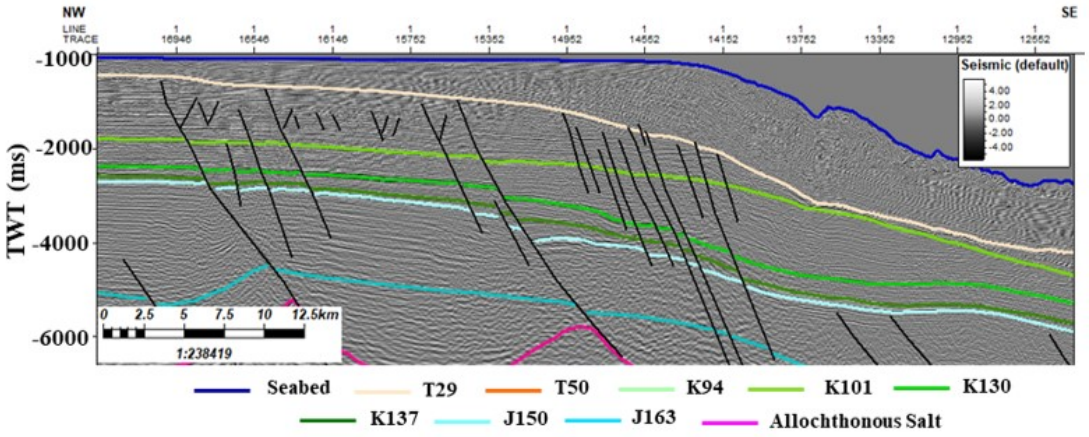

Figure 4.8: Seismic characteristics of the K101-K130 interval: subparallel to oblique reflections in the clinoform interpreted along the Novaspan PSTM 2000. Vertical scale is in time. See Figs. 2.8 and 4.2 for the line location.

The NE-SW-striking growth faults affect K101-K130 interval beneath the present-day continental slope along the margin with the vertical offset of 50 m – 100 m in the northeastern and central parts of the basin (Fig. 4.8).

The unit is not affected by salt tectonics on the shelf. Basinward, K101 overlies the top of salt canopies in the Annapolis Subbasin, and salt diapirs pierce the unit in the Shelburne Subbasin (Fig. 4.2). The thickness of K101 – K130 ranges from 40 m in the SW to 4600 m (Fig. 2.16) to the northeastern part of the basin.

4.1.1.6. The K130 – K137 Interval

K130 is defined as the Hauterivian Maximum Flooding Surface (PFA, 2011) and coincides with the top of 'O' Marker on the shelf (Fig. 2.10). K130 is a boundary separating shale above it from limestone below it on the shelf, and it corresponds to an increase in AI downward across the boundary and a strong positive (peak) amplitude (Fig. 4.1). Basinward, the amplitude of the seismic reflection slightly weakens in response to an increased shale component in the underlying beds of the K130-137 interval.

The reflections of the unit K130-K137 are parallel to slightly divergent within the northeastern shelf and slightly to highly divergent in the southwestern shelf near the growth faults; wavy beneath the northeastern slope and distorted beneath the southwestern slope where salt diapirs are dominant; parallel distally.

K130 is discontinuous over the edge of the Jurassic carbonate platform (Fig. 4.7) in the SW and is continuous below the present-day continental slope in the NE (Fig. 4.8). The K130-137 interval is strongly deformed in the northeastern and central parts of the Scotian Basin, where expelled salt canopies pierce or uplift the deposits of the interval (Fig. 4.9). Toward the SW, K130-K137 interval deposits are pierced by dome-shaped salt diapirs with a diameter of 750 m- 5500 m and fill isolated mini-basins.

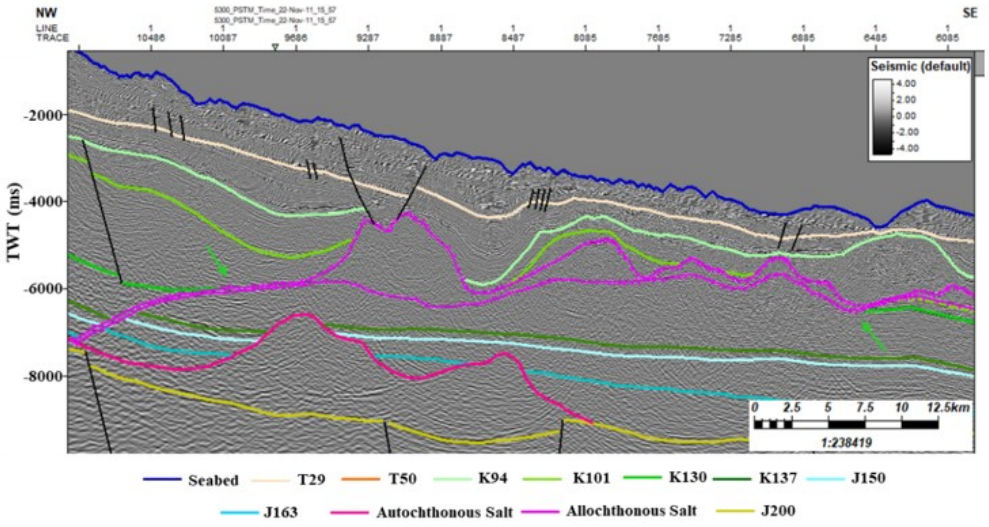

Figure 4.9: Disruption of K130 horizon caused by the emplacement of salt canopy in the central part of the Scotian Basin, segment of the Novaspan PSTM 1600. Vertical scale is in time. See Figs. 2.8 and 4.2 for the line location.

In the shelf area, K130 dips uniformly to the SE and is faulted by only a few SE-dipping normal faults with vertical offset of 50 m – 100 m. However, K130 is structurally distinctive on the slope settings. K130 is offset by a series of NE-SW-striking growth faults on the northeastern slope (Fig. 4.8), which is a clastic-dominated margin; to the SW, K130 is affected by a slope gliding (Fig. 4.7) above the edge of the Jurassic-rimmed carbonate platform caused by sediment starvation during Cretaceous-Tertiary times (PFA, 2011).

The thickness of K130 – K137 interval ranges from 30 m in the SW segment of the margin to 5845 m in the NE segment of the margin (Fig. 2.15) within the Banquereau Synkinematic Wedge province.

4.1.1.7. The K137 – J150 Interval

K137 corresponds to the Berriasian-Valanginian Unconformity (PFA, 2011) and it is related to the Avalon Uplift. The uplift triggered notable uplift, deformation, and significant erosion of Jurassic and older units that resulted in a drastic decrease in accommodation (Jansa & Wade, 1975; MacLean et al., 1989; Wade & MacLean, 1990). K137 is presented by a strong negative (trough) amplitude (Fig. 4.1) as it represents an interface between the clastic deposits above it and carbonate deposits below it.

The reflections of the K137-J150 interval are parallel to slightly divergent on the shelf except for the Sable Subbasin; slightly divergent on the northeastern slope and wavy and distorted on the central and southwestern slope; parallel basinward.

K137 is generally unaffected by salt tectonics on the shelf; however, salt depletion (removal) caused by sediment loading in the Sable Subbasin resulted in the emplacement of growth normal faults that offset the K137-J150 interval deposits within the shelf of the central part of the Scotian Basin (Fig. 4.10). Basinward, remobilized salt diapirs and amalgamated salt canopies deform the K137-J150 interval.

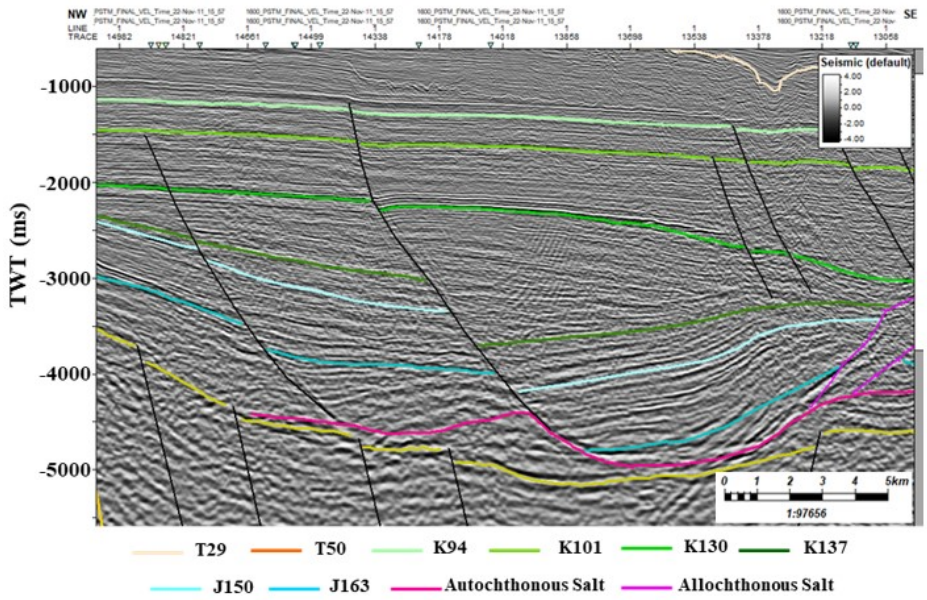

Figure 4.10: The K137-J150 interval deposits offset by the SE-sipping growth faults in response to depletion (removal) of salt in the Sable Subbasin, central part of the Scotian Basin, interpreted along the Novaspan PSTM 1600 line. Vertical scale is in time. See Figs. 2.8 and 4.2 for the line location.

The deposits of the K137-J150 interval gently dip to the southeast in the shelf along the entire basin but they are offset by the SE-dipping normal growth faults in the central part of the Scotian Basin caused by salt removal and migration basinward. The K137 boundary is defined as an angular unconformity in the northeastern shelf associated with the Avalon Uplift; while it gradually changes into relatively conformable boundary in the southwest of the basin boundary (MacLean et al., 1989).

The thickness of K137 – J150 interval ranges from 50 m in the SW to 5600 m in the NE of the basin (Fig. 2.14).

4.1.1.8. The J150 – J163 Interval

J150 is defined near the Tithonian Maximum Flooding Surface based on biostratigraphy studies (Eliuk, 1978; Kidston et al., 2005). It corresponds to the top of the Baccaro carbonates of the Abenaki Formation in the SW and to the top of sandstones of the Mic Mac Formation in the NE, where the deltaic system was developed (PFA, 2011). J150 corresponds to a strong positive (peak) amplitude (Fig. 4.1) due to higher AI in the underlying carbonate units compared to the overlying clastic units of the interval K137-J150.

The seismic reflectors of J150 are predominantly parallel on the southwestern shelf except for the Jurassic rimmed-carbonate platform, where they are mounded; slightly to highly divergent near growth faults in the Sable, Tantallon, and Laurentian Subbasins in the northwestern shelf; deformed and tilted in the continental slope; parallel with high continuity in the distal part of the basin.

J150 was not affected by salt tectonics along the present-day continental shelf except for the Sable Subbasin. However, J150 was strongly affected along the slope by salt mobilization in the Salt Diapir, Salt Canopy Provinces, and the Banquereau Synkinematic Wedge.

The SE-dipping growth faults deformed J150 in the Huron and Sable Subbasins, where a significant deltaic depocenter developed in Jurassic time in the northeastern shelf (Fig. 4.11). To the southwestern shelf, the Jurassic rimmed carbonate platform, lying along Moheida and Mohawk Ridges, was preserved (Fig. 4.7). Along the modern slope of the entire basin, seaward-dipping growth faults strongly deformed J150 and formed extensional turtle structures and roll-over anticlines within the Banquereau Synkinematic Wedge. Basinward, J150 also was slightly affected by the SE-dipping normal faults.

The thickness of J150 – J163 ranges from 60 m in the SW to 5340 m in the NE, where it reaches the maximum thickness beneath the northern shelf (Fig. 2.13).

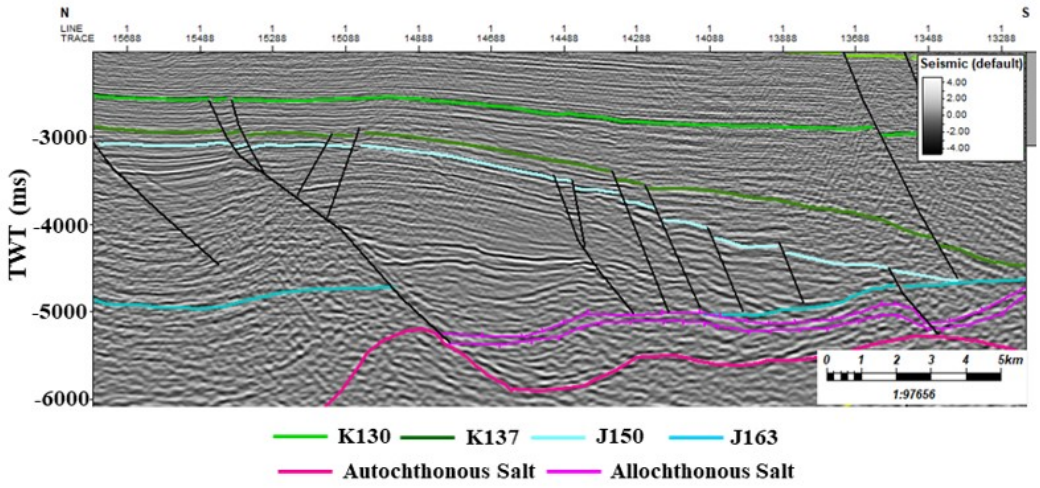

Figure 4.11: The Jurassic deltaic progradational clastic package in the interval J150-J163 interpreted above the salt canopy in the Sable Subbasin in the northeastern shelf, Novaspan PSTM 1800 line. Vertical scale is in time. See Figs. 2.8 and 4.2 for the line location.

4.1.1.9. The J163 – J200 Interval

J163 is defined near the Callovian Maximum Flooding Surface based on biostratigraphy studies (Eliuk, 1978; Kidston et al., 2005) and corresponds to top of the Scaterie carbonates of the Abenaki Formation (Fig. 2.10). The unit also represents the onset of the shallow marine carbonate production. J163 is presented by a strong positive (peak) amplitude (Fig. 4.1) due to increase in AI across the boundary from the overlying shaly Misaine Member downward to the carbonate deposits below it.

The seismic reflectors of the J163-J200 interval are parallel to divergent near growth faults in the Sable, Tantallon, and Laurentian Subbasins to the northwestern shelf; wavy and distorted within the Diapir and Canopy Provinces, deformed and tilted within the Banquereau Synkinematic Wedge along the slope; parallel with high continuity in the deeper part of the basin. Carbonate facies are interpreted in the SW of the Nova Scotia margin and fine-grained sandstones intercalated with limestone in NE part of it based on well data, both grade into prodelta and deep marine shales in deeper parts of the Scotian Basin.

J163 was not affected by salt tectonics along the modern continental shelf except for the Sable Subbasin. However, J163 was strongly deformed by salt remobilization in the Salt Diapir, Salt Canopy Provinces, and the Banquereau Synkinematic Wedge along the slope (Fig. 4.2).

The thickness of J163 – J200 ranges from 175 m in the SW to 6175 m in the NE of the margin, where its maximum thickness is observed (Fig. 2.12).

4.1.1.10. The Autochthonous Salt

The top salt is picked as a reflection with negative (trough) amplitude (Fig. 4.1) that corresponds to a decrease of acoustic impedance from the overlying sedimentary units to the underlying salt.

The salt bodies are characterized by an absence of strong internal seismic reflections and chaotic seismic pattern. In the deeper part of the basin, the complexity of the allochthonous salt bodies decreases the quality of seismic imaging below the salt and results in high uncertainty while picking the bottom of canopies or diapirs with subvertical or negative dip angles.

The thickness of the autochthonous salt changes from 100 m to 3000 m (Fig. 2.11). The maximum thickness is observed on the slope setting within the Salt Canopy Province and Banquereau Synkinematic Wedge.

The autochthonous salt was deposited in the rift basins of the margin and bounded by normal faults beneath the modern shelf and slope settings. The southeastern limit of the autochthonous salt marks the volcanic ridge separating the continental and oceanic crusts. The structure of the salt bodies is discussed in the chapter of the Salt Tectonics.

4.1.1.11. The J200 Reflector

J200 corresponds to the base of the post-rift sediments (PFA, 2011) and is the deepest interpreted seismic marker. It corresponds to the top of the acoustic basement. It is overlain by sedimentary rocks of J163-J200 interval on the shelf (Fig. 4.12, to the left), by autochthonous salt on the slope (Fig. 4.12, to the right), and by sedimentary rocks in the deeper part of the basin (Fig. 4.13). The J200 horizon is picked as a positive (peak) amplitude (Fig. 4.1) due to higher AI in the basement rocks than in the overlying sedimentary deposits, including syn-rift deposits.

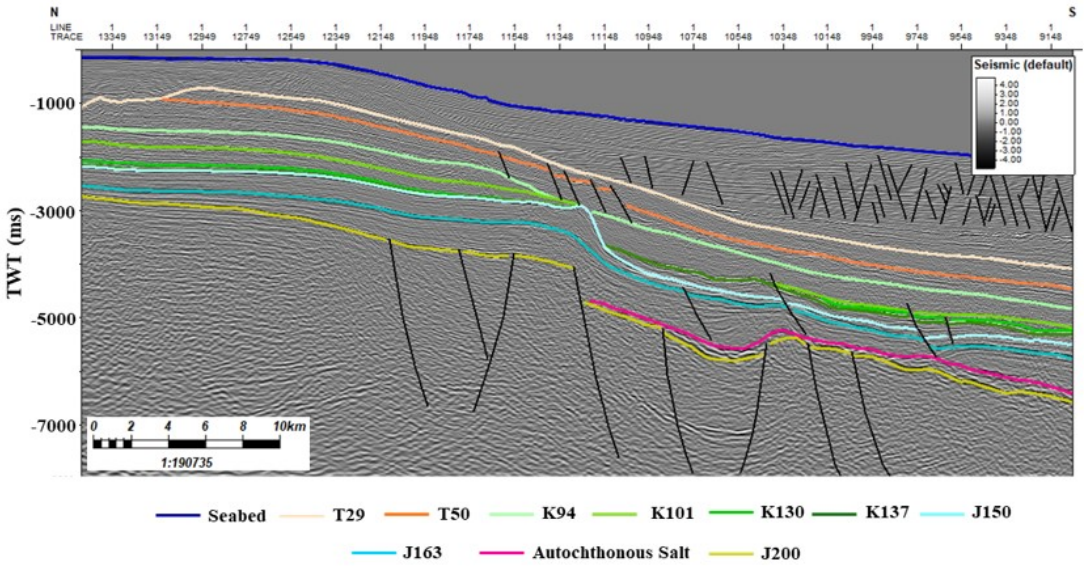

Figure 4.12: The J200 horizon overlain by sedimentary rock on the Moheida Ridge (to the left) and by the autochthonous salt in the Shelburne Subbasin (to the right) interpreted along the Novaspan PSTM 1400A line. Vertical scale is in time. See Figs. 2.8 and 4.2 for the line location.

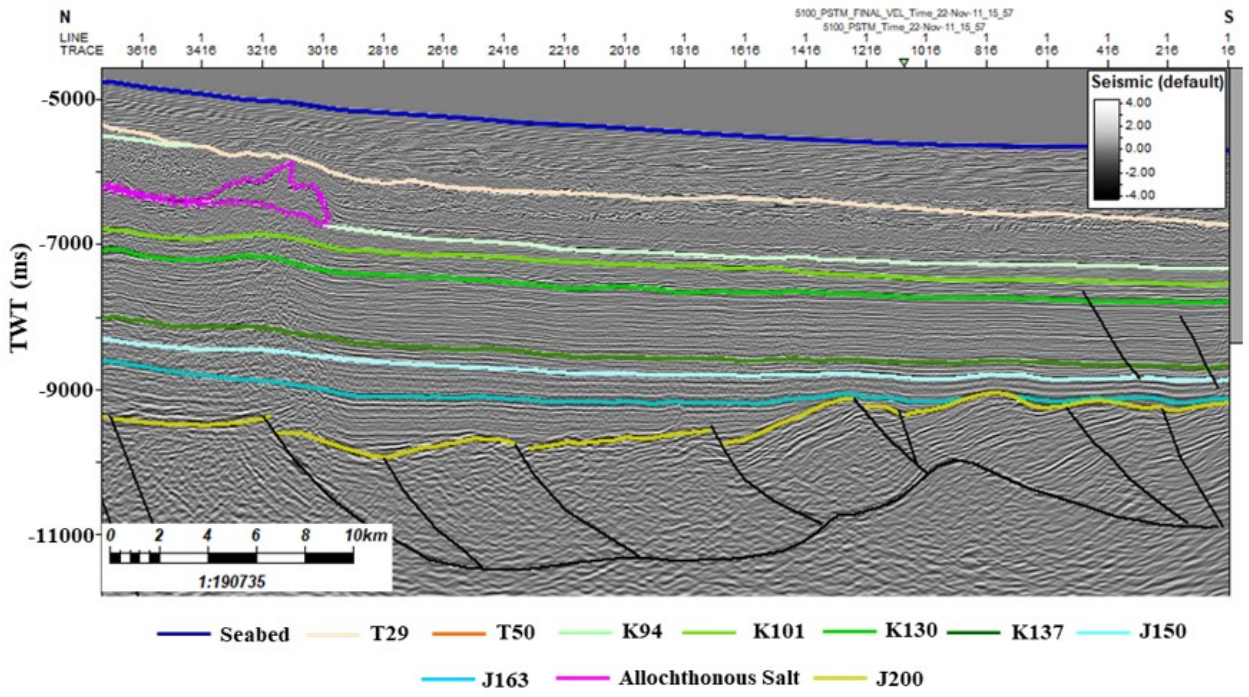

Figure 4.13: The J200 horizon is overlain by sedimentary rocks in the deeper part of the basin (oceanic domain), interpreted along the Novaspan PSTM 1600 line. Vertical scale is in time. See Figs. 2.8 and 4.2 for the line location.

The maximum depth of the J200 reaches ~19 km TVDSS within the Banquereau Synkinematic Wedge (Figs. 2.9, 4.14).

Regarding confidence of the seismic picking, it is confident on the shelf. The Tertiary and Cretaceous units are mostly traced by well control. The picking of the Jurassic units (J150 and J163) comprising carbonate facies on the southwestern shelf is quite confident due to the high acoustic impedance contrast with overlying clastic deposits. Picking the Jurassic clastic units is less confident on the northeastern shelf and supported by well control and identified reflections patterns. The seaward-dipping growth faults and salt remobilization downward the continental slope decrease seismic imaging quality, particularly within the Salt Canopy Province and the Banquereau Synkinematic Wedge. Picking sub-salt units is based on horizon thickness and previous interpretations by PFA (2011). The interpretation is also confident in the basin's distal domain, out of the salt tectonics, guided by strong seismic reflections and seismic patterns typical for each interval.

4.1.2. Fault Interpretation

In this study, five different sets of normal faults were identified on seismic profiles in the Nova Scotia margin (Fig. 4.14).

(I) NE-SW-striking syn-rift planar normal faults offset the acoustic basement (Figs. 4.1, 4.14). The geometry of the syn-rift faults varies across the Nova Scotia passive margin. The faults are planar in the upper crust below the continental shelf and slope of the continental domain dipping both to the NW and SE. The vertical offset of J200 horizon by faults in the continental domain ranges from 30 m to 500 m. The main structures in the basement include NE-SW-oriented ridges and subbasins on the shelf and continental slope (Fig. 4.14).

(II) SE-dipping syn-rift listric normal faults developed in the acoustic basement in the oceanic domain (Figs. 4.14a, b, c, d). These faults merge into a flat basal detachment at ~15 km of depth. The emplacement of faults of sets I and II corresponds to the onset of rift-to-drift transition during the Triassic and Early Jurassic. The vertical offset of J200 by faults in the oceanic domain ranges from 145 m to 550 m. Some of the listric faults within the northeastern segment of the margin (line 2000) were reactivated, resulting in small-scale displacement (80 m – 120 m) of the overlying Jurassic and Cretaceous units (Fig. 4.16a).

(III) SE- and NW-dipping post-rift listric faults developed in the Jurassic and Cretaceous strata. These faults merge into a basal detachment either along the top of the autochthonous salt (lines 2000, 1600, 1400A) or along the extended thin salt canopies progressed to the SE (line 2000). The faults of set IIIa merging into the top of the autochthonous salt are interpreted below the present-day shelf and slope in the NE segment of the margin (Huron, Sable and Annapolis Subbasins), dipping towards the root of the thin and highly extended salt canopy (Figs. 4.14a and b, lines 2000 and 1600). The faults of set IIIb merge into the top of the allochthonous thin extended canopy and dip to the SE, accommodating the SE-ward salt propagation (Fig. 4.14a, line 2000). In the central segment of the margin, the faults of set IIIa faults are recognized in the deeper part of the Shelburne Subbasin, dipping toward the root of an isolated salt diapir (Fig. 4.16c,

line 1400A). J163, J150, and K137 are faulted by the NE-SW-striking growth faults caused by salt remobilization initiated by sediment loading in the Huron, Sable, Annapolis, and Shelburne Subbasins (Figs. 4.14a, b, c).

(IV) NE-SW-striking post-rift planar normal faults are interpreted in the central and NE segments of the margin (Figs. 4.14a, b, c, lines 2000, 1600, and 1400A). They offset the Cretaceous and Tertiary clastic units below the present-day shelf and/or continental slope. These faults control thickness of the Cretaceous and Tertiary progradational clastic wedges accumulated below the present-day continental slope in the central and northeastern segments of the margin (Figs. 2.14, 2.15, 2.16, and 2.17).

(V) The set of youngest post-rift faults is represented by small-scale conjugated planar normal faults associated with crestal deformation of Tertiary deposits above salt diapirs in the southwestern (line 1100) segment of the margin (Fig. 4.14d). The NE-SW-striking faults dip to NW and SE with a vertical offset of 20 m to 55 m.

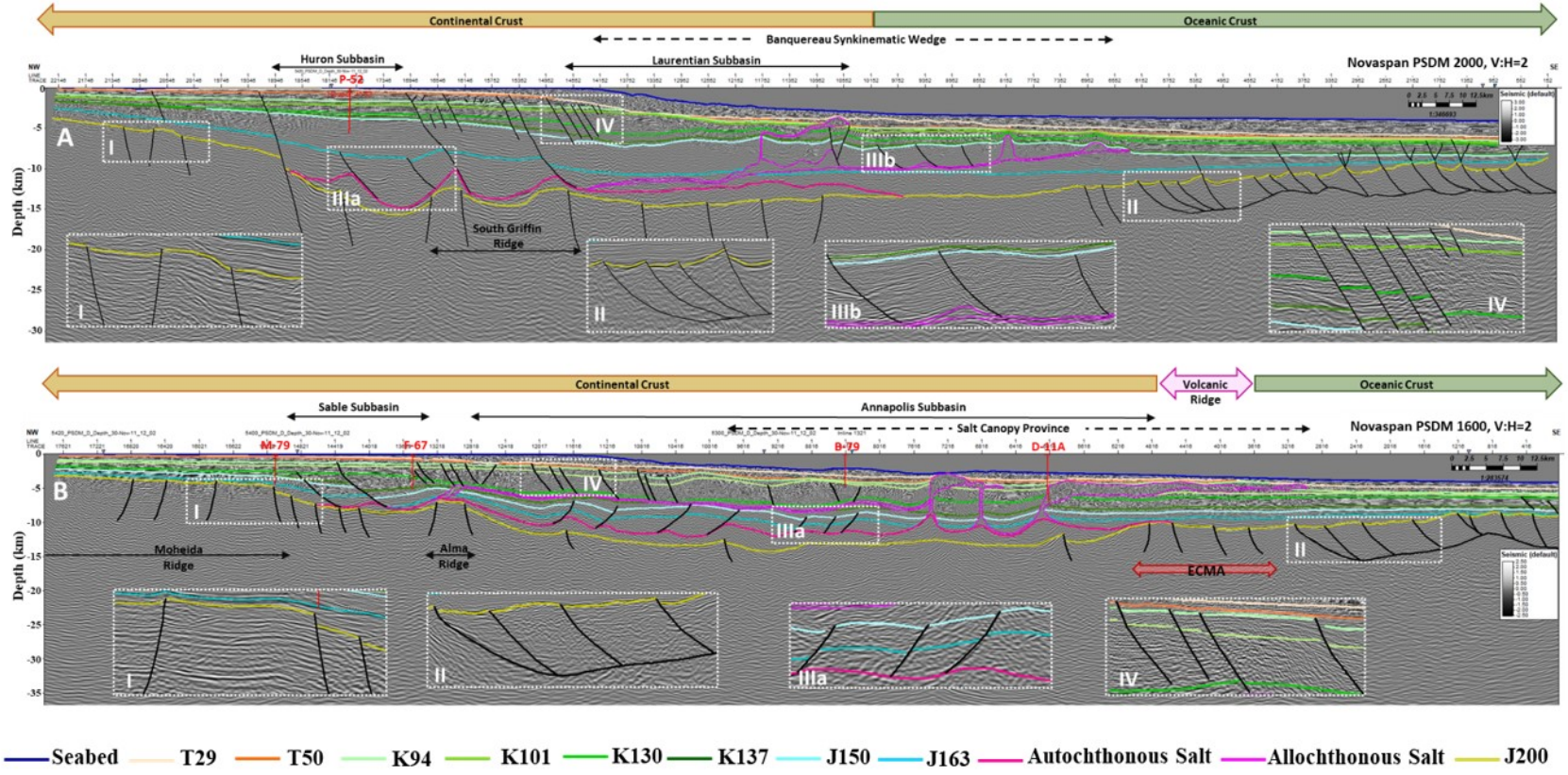
Continental Crust
Oceanic Crust
Banquereau Synkinematic Wedge
Huron Subbasin
Laurentian Subbasin
Novaspan PSDM 2000, V:H=2
P-52
A
I
IV
IIIb
IIIa
II
South Griffin Ridge
Depth (km)
Continental Crust
Volcanic Ridge
Oceanic Crust
Sable Subbasin
Annapolis Subbasin
Salt Canopy Province
Novaspan PSDM 1600, V:H=2
M-79
F-67
B-79
D-11A
B
Moheida Ridge
Alma Ridge
ECMA
Seabed
T29
T50
K94
K101
K130
K137
J150
J163
Autochthonous Salt
Allochthonous Salt
J200

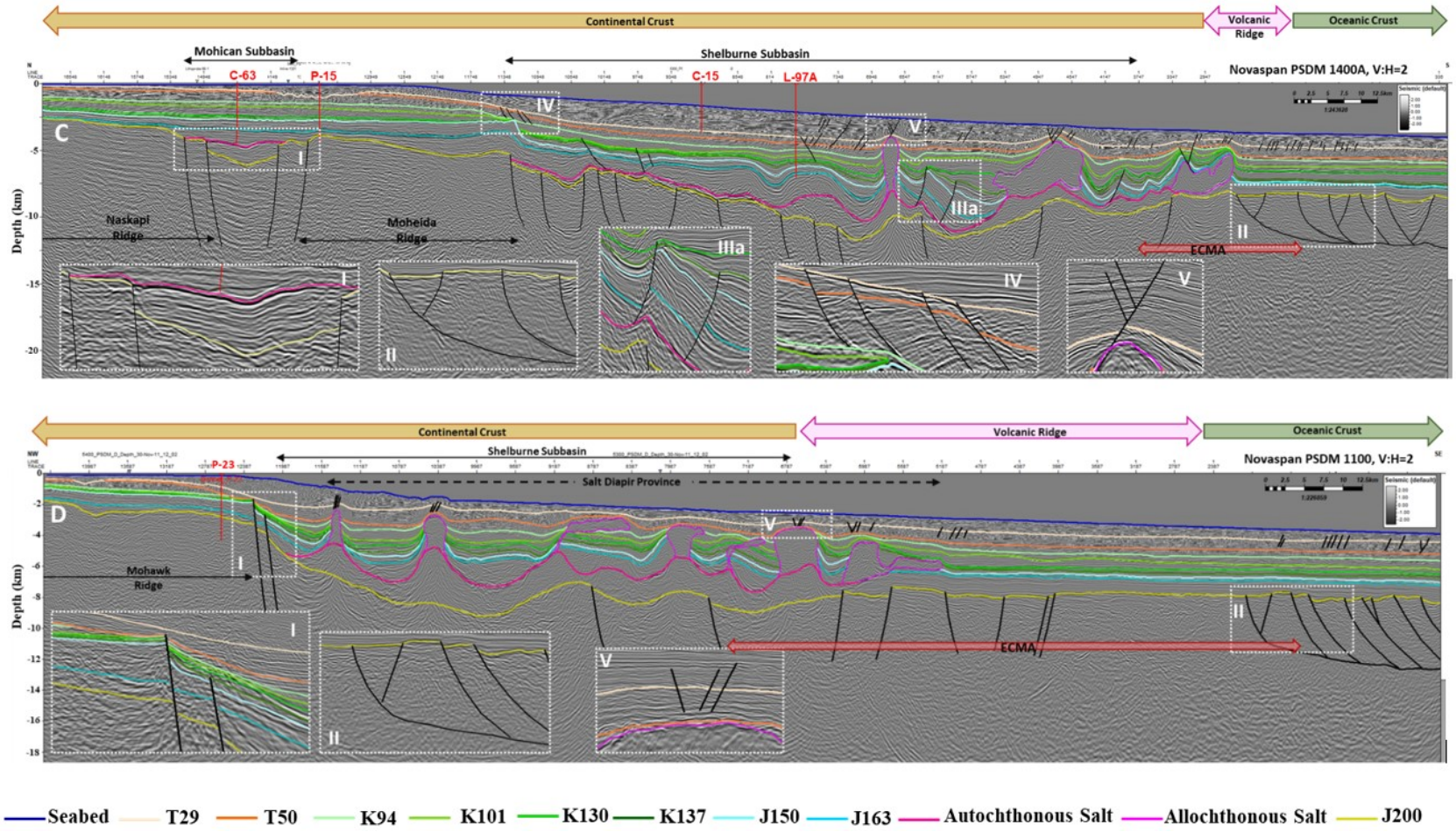

Figure 4.14: Structural interpretation of the NW-SE Novaspan 2010 PSDM lines across the Nova Scotia margin. Several sets of normal fault are identified along the lines from the northeastern (A) to southwestern (D) segment of the margin. Vertical scale in depth, V:E=2. See Figure 2.8 for the location of lines. I, II, III, IV, and V correspond to the fault sets described in the text.

4.1.3. Salt Tectonics

Salt accumulations are divided into two groups: the autochthonous salt that was deposited from the Late Triassic to Early Jurassic on top of the rifted basement and allochthonous salt (canopies and diapirs) that was remobilized during post-rift extension moving vertically and laterally and was fed from the autochthonous salt. The timing of emplacement and geometry of the allochthonous salt bodies vary between recognized tectonic zones in the Scotian Basin (Chapter 2.2).

The autochthonous salt bodies with a thickness of ~400 m are bounded by the NE-SW-striking normal faults beneath the present-day shelf in the northeastern and southwestern parts of the basin (Fig. 4.14). Salt basins approximately 15-km-wide are present beneath the northeastern shelf. The autochthonous salt pillows were expelled ~80 km progressively basinward (Fig. 4.14a) as a response to an increase in the thickness of the Jurassic prograding sedimentary wedge in the central part of the basin (Laurentian and Annapolis Subbasin)

Allochthonous salt geometries vary in a NE-SW direction. At the northeastern slope of the basin, the amalgamated salt canopies and salt nappes within Banquereau Synkinematic Wedge are widespread (Figs. 4.14a and b). SE-dipping faults in Upper Jurassic strata evacuate the salt and form salt nappes climbing Lower Cretaceous and Upper Jurassic stratas (Fig. 4.15). The thickness of salt canopies and salt nappes vary between 900 m and 2400 m, and their width ranges from 2.5 km to 10 km.

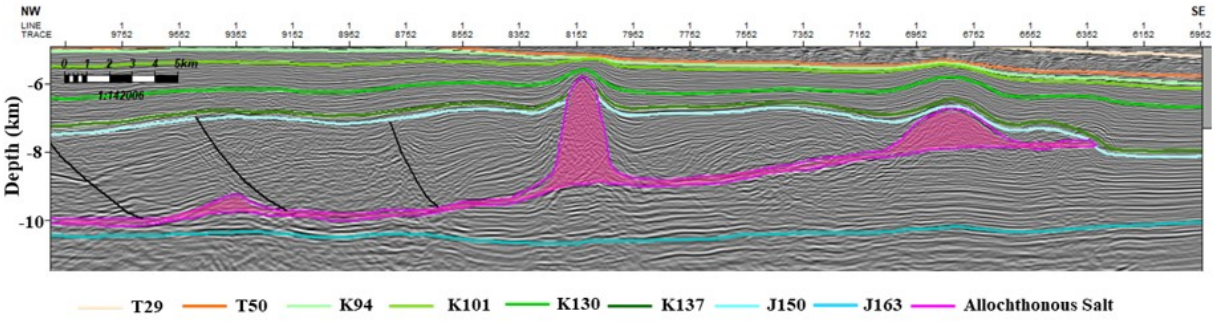

Figure 4.15: The allochthonous salt nappe climbing up through the Jurassic deposits for ~ 40 km to the SE across the Scotian basin, interpreted along the Novaspan PSDM Line 2000. Vertical scale in depth, see Figure 2.8 for the line location.

Amalgamated salt tongues (Fig. 4.16) and salt-cored detachment folds are dominant at the central segment of the margin, which includes the Abenaki, Annapolis, and Sable Subbasins. The salt bodies were remobilized during the Cretaceous-Tertiary and formed seaward-leaning canopies expelled ~80 km. The thickness of a 10 – 35 km-wide salt canopies is ~2.5 km.

The symmetrical salt diapirs dominate the southwestern slope of the margin and form the isolated mini-basins in the Shelburne Basin (Fig. 4.17). Further seaward, diapirs are bulb-shaped and reach 5-15 km in width and 1-6 km in length. Most of the diapirs were expelled for a distance of 10-80 km far from the present day's continental slope; they continued to rise in Tertiary time, arching the overlying T50 and T29 deposits around the domes. The highly squeezed diapirs in the southwestern part of the basin cause up to 200 m of seafloor bathymetric relief.

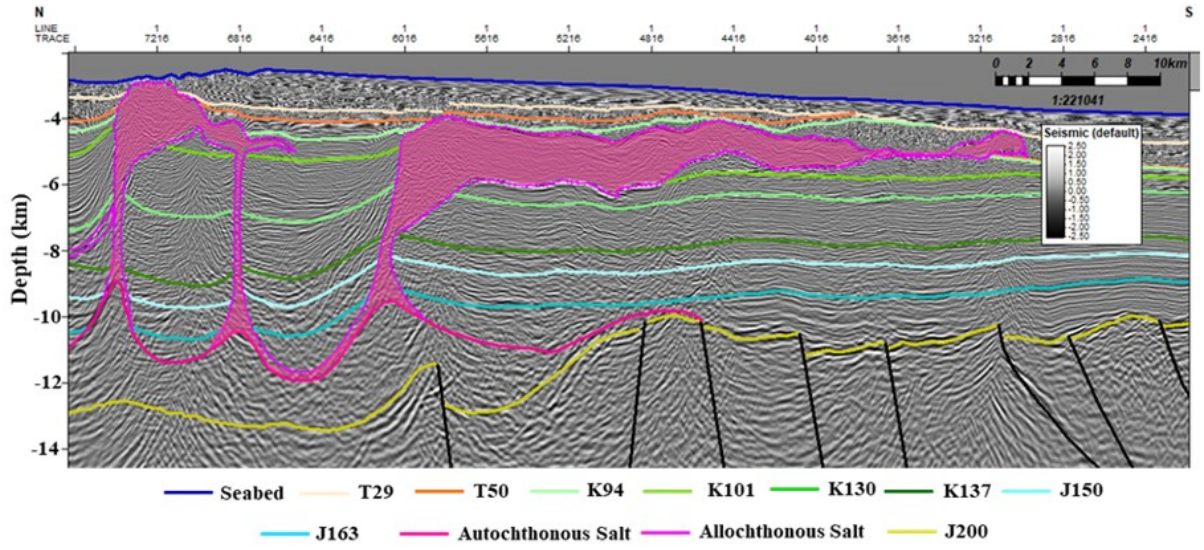

Figure 4.16: The prograding basinward-leaning salt tongues in the Annapolis Subbasin, interpreted along the line 1600. Vertical scale in depth, see Figure 2.8 for the line location.

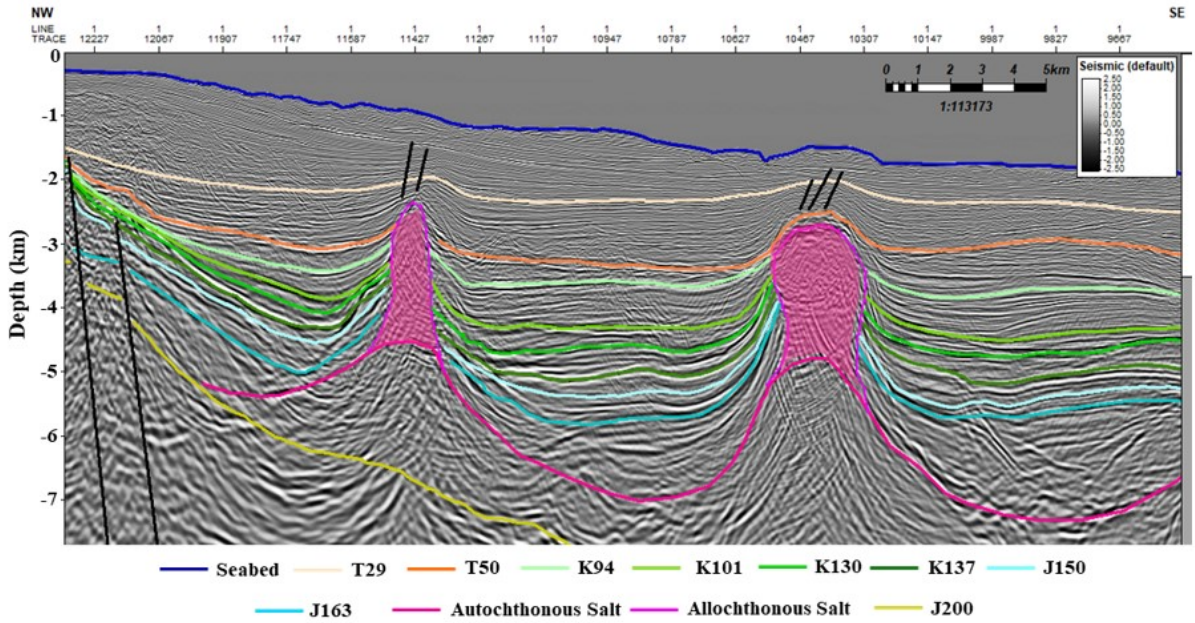

Figure 4.17: The symmetrical salt diapirs and mini basins between them interpreted in the Shelburne Subbasin along the Novaspan PSDM line 1100. Vertical scale in depth, see Figure 2.8 for the line location.

4.2. 2D Backstripping Modelling

The intent of the 2D sequential restoration of deformation of the Mesozoic-Cenozoic sedimentary succession of the Scotian Basin is to quantify the variation in the amount of tectonic extension, subsidence, decompaction, and the isostatic response at each time step across the Nova Scotia passive margin and evaluate the impact of these parameters on tectonic evolution scenarios.

The 2D kinematic restorations were conducted along the NW-SE-striking cross-sections based on four Novaspan PSDM seismic profiles 1100, 1400A, 1600, and 2000 located in the southwestern, central and northeastern segments of the Nova Scotia passive continental margin (Fig. 2.8). The depth interval of the PSDM seismic profiles that was used in 2D restorations is limited to the upper 13 km-20 km.

The total present-day length of the cross-sections used in the restoration varies from 185 km to 281 km (Fig. 4.14). The distance between the profiles ranges from 110 km to 250 km (Fig. 2.8). The continent-ocean boundary (COB) transition on cross-sections is interpreted as the location of serpentinized mantle along Line 2000 (Fig. 2.15, Funck et al., 2004) or zone of

magmatic underplating ("volcanic ridge") along lines 1600, 1400A, and 1100 (Fig. 4.14) that are recognized between the continental and oceanic domains (Funck et al., 2004; Dehler, 2012; Dehler & Welford, 2013). The COB is about 55 km wide in the SW segment of the Nova Scotia margin, where the ECMA is prominent (Fig. 2.6), while it is about 10-13 km in the central and NE segment of the margin (Fig. 4.14). The mid-crustal detachment within the continental domain is located at ~22 km below the present-day shelf getting shallower to ~18 km below the continental slope (Figs. 4.18, 4.22, 4.26 and 4.30) (Funck et al., 2004; OETR, 2009; PFA, 2011; Dehler, 2012; Dehler & Welford, 2013).

4.2.1. Novaspan PSDM Line 2000

The line is 280 kilometres long and passes through the Huron Subbasin, South Griffin Ridge, and Laurentian Subbasin from the shelf to the distal part of the Scotian Basin in the NE segment of the Nova Scotia margin (Fig. 4.18). The continent-ocean transition zone is located at ~ 150-160 km from the NW end of the line based on the location of serpentinized mantle between the continental and oceanic domains interpreted along the closely located Lithoprobe 891 line (Fig. 2.3). The maximum thickness of the continental crust along the line 2000 is close to 40 km (Dehler & Welford, 2013) beneath the present-day continental shelf, and toward the southeast, it decreases to around 8 km in the oceanic domain. The depth interval of the PSDM seismic profile that was used in 2D restorations is 20 km.

The well reports and logs of the 12-km-offset Hesper P-52 were used to compile primary input parameters for lithology, grain size, and thickness and compaction curve of each stratigraphic unit. The 2D sequential restoration (Fig. 4.19) for line 2000 were conducted for 11 time steps starting from present-day back to the onset of the rifting phase (T225), using the iterative workflow (See Chapter 3). The top surface of each cross-section displays the pre-deformed paleobathymetry at a given time step annotated on the cross-sections.

The changes in the length of horizons before and after 2D restoration are used to estimate the extension amount for each time interval (Table 4.1). The NE-SW-striking syn-rift normal faults (sets I and II) that are located in the basement (J200) below the autochthonous salt accommodate the maximum extension amount along the cross-section. The planar normal faults in the basement within the continental domain (set I) contributed 14% of extension, while the

listric normal faults in the oceanic domain (set II) accommodated 86% of extension of the 2.70% extension estimated for T225 horizon.

The SE-dipping growth faults (set III) that are interpreted in the Cretaceous and Jurassic deposits and merge into the detachments at the top of the autochthonous or allochthonous salt of the Banquereau canopy or along shales units accommodate 1.02% extension. The total extension amount along line 2000 is estimated as 3.72% as a sum of extension obtained along each horizon. The main contribution to the total extension along line 2000 is associated with the syn-rift normal faulting in the acoustic basement.

Table 4.1: The length of the restored cross-sections along line 2000 and extension amounts for each time step.

Time (Ma)	Restored Length (m)	Extension Amount (%)
0	281,888.3	0.00
T29	281,888.0	0.00
T50	281,833.0	0.02
K94	281,492.0	0.12
K101	281,158.0	0.12
K130	281,040.0	0.04
K137	280,740.0	0.11
J150	280,404.0	0.12
J163	279,148.0	0.45
J200	279,031.0	0.04
T225	271,708.0	2.70
Total extension amount		3.72

The amount and distribution of thermal subsidence vary across the margin along the line 2000. It increases basinward for each horizon. Initial rapid thermal subsidence by the end of the rifting stage was accommodated by syn-rift faults interpreted in the basement (set I and II). It was followed by slow post-rift thermal subsidence with a stair-like distribution for each seismic marker along the line (Fig. 4.20). The maximum thermal subsidence of 1035 m is reconstructed in the deep-water setting and 175 m in the shelf area by the end of rifting (J200). The subsidence for the post-rift units is ~25 m in the shelf, increasing in the deep basin. The subsidence of T50 (230 m), K101 (300 m), and J150 (207 m) is more significant than the subsidence of T29 (26 m) and K94 (58 m) in the deeper basin.

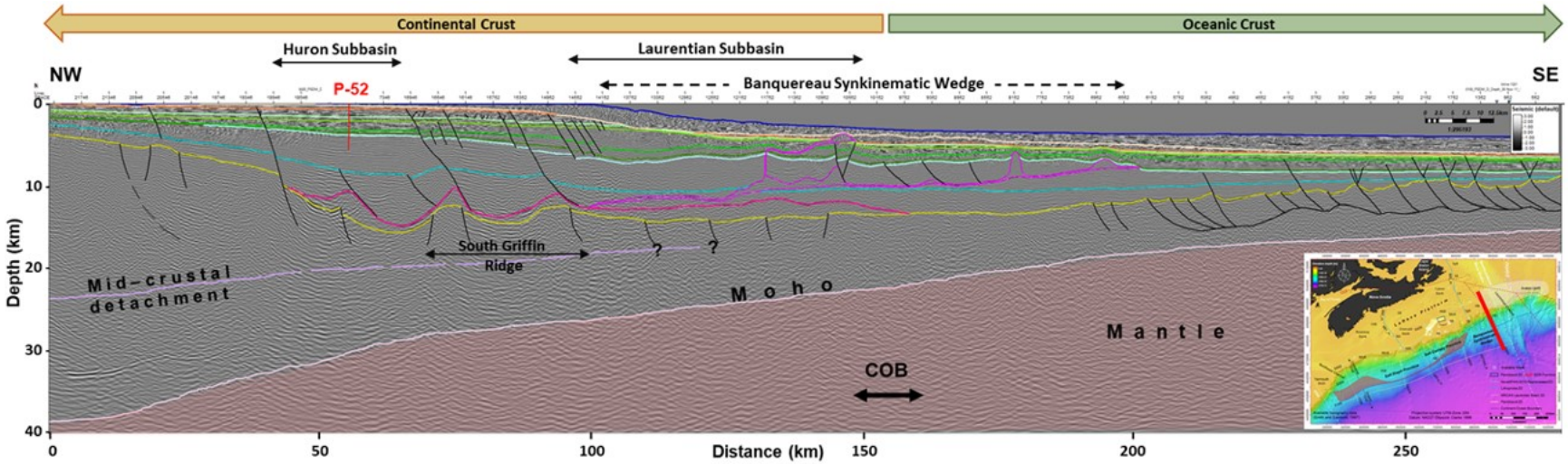

Figure 4.18: The structural interpretation of Novaspan PSDM Line 2000. Lateral limits of the continental crust and COB, oceanic crust (PFA, 2011), the mid-crustal detachment (Funck et al., 2004; Dehler &Welford, 2013) are shown. No vertical exaggeration.

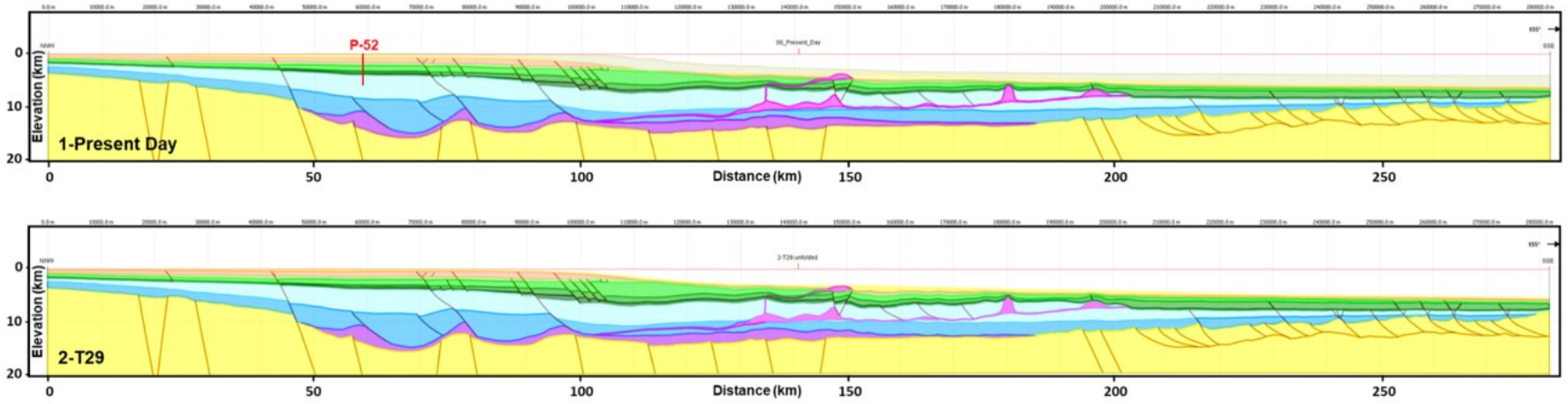

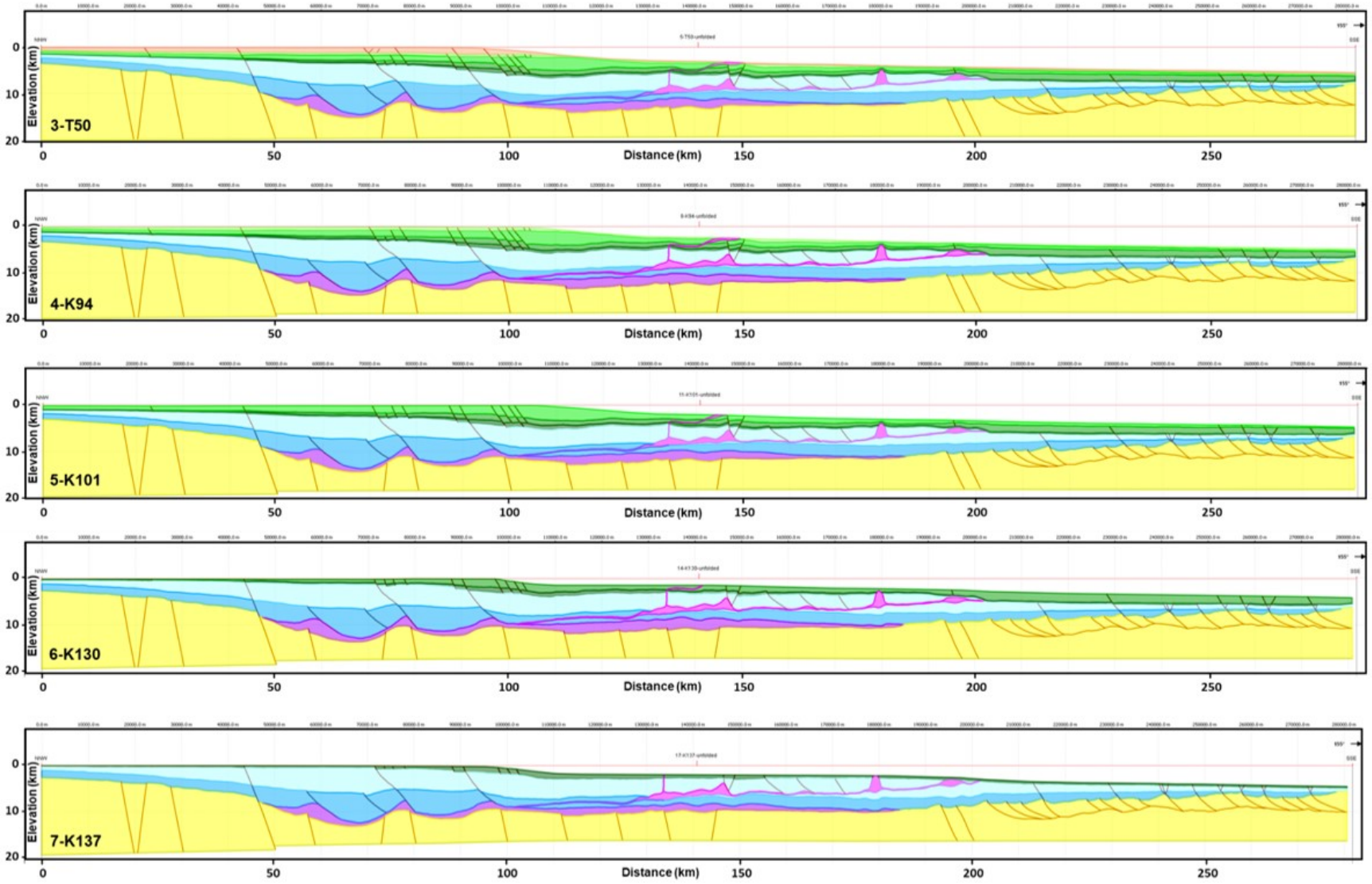
3-T50
4-K94
5-K101
6-K130
7-K137
Elevation (km)
Distance (km)
0
10
20
50
100
150
200
250

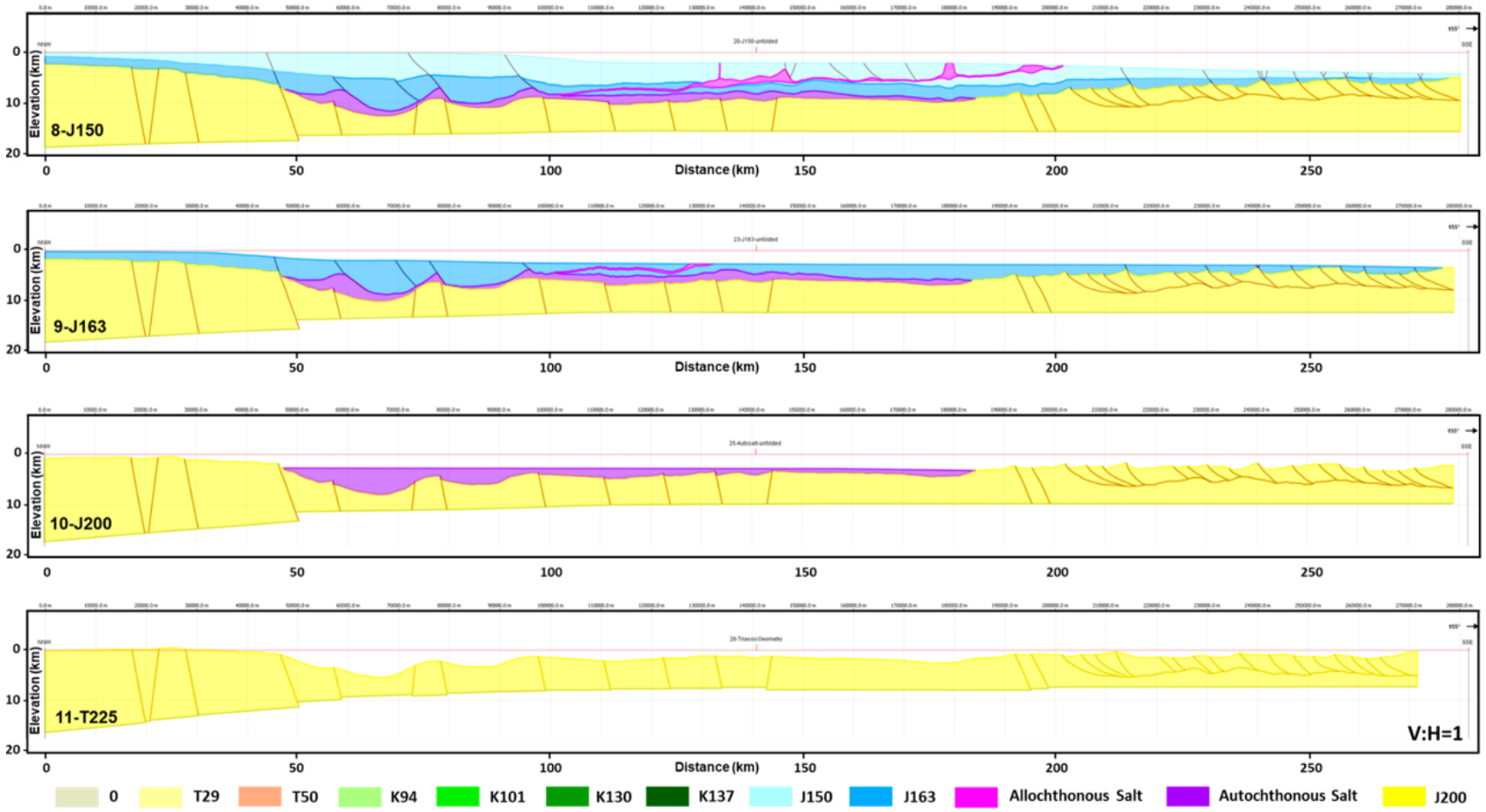

Figure 4.19: The 2D sequential restoration along the Novaspan PSDM 2000 line. Each cross-section is restored to the time step when the deposition of the top unit ended. The cross-sections are in depth domains, no vertical exaggeration.

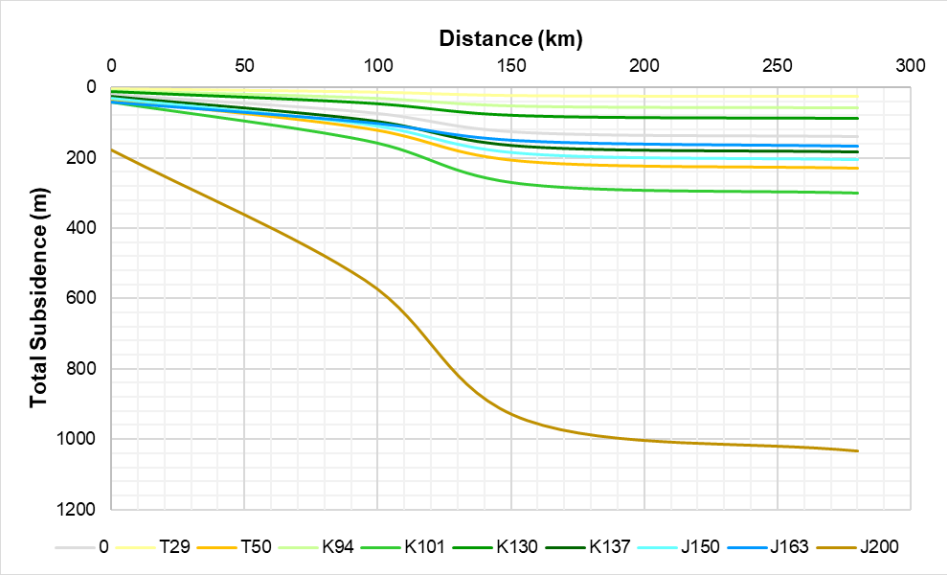

Figure 4.20: The amount of thermal subsidence of each horizon along line 2000.

The estimated decompaction and isostatic rebound are more significant in the depocenters with higher thickness of sedimentary cover. The highest isostatic rebound of 2610 m is estimated for the Jurassic strata (J150-J163) in the Huron Subbasin and ~500 m for the Lower Cretaceous reconstructed in the Laurentian Subbasin (Fig. 4.21). The SE-dipping normal faults (set I) below the present-day shelf edge (Fig. 4.19) at the NW side of the Laurentian Subbasin accommodate the main depocenter within the basin, where maximum thickness of Cretaceous-Tertiary deposits (K137-T29) occur (See Chapter 2, Figs. 2.13-2.19).

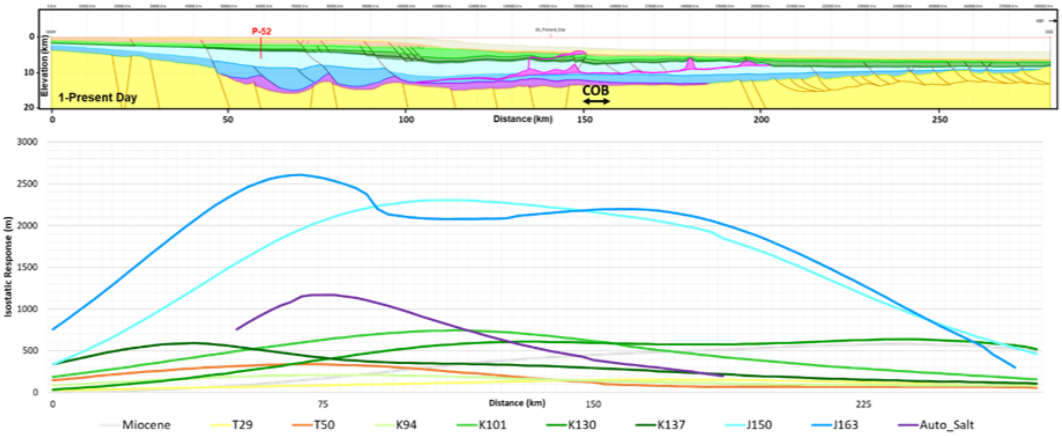

Figure 4.21: The present-day interpretation of the PSDM line 2000 (top figure) and the total isostatic response simulated for each horizon (bottom figure).

4.2.2. Novaspan PSDM Line 1600

The PSDM 1600 line is 225 kilometres long and is located in the central part of the Scotian Basin (Fig. 4.22). The COB transition zone corresponds to the location of the volcanic ridge, approximately within 165-177 km interval from the NW end of the line (PFA, 2011). The line crosses the Moheida Ridge, Sable Subbasin, Alma Ridge, and Annapolis Subbasin from the shelf to the deep water setting (Fig. 2.8). The crustal thickness along the line ranges from 40 km in the northwest to ~7 km in the southeast (Dehler & Welford, 2013). The restoration is carried out for the depth interval of 18 km (Fig. 4.22).

Cohasset L-97, Alma F-67, Balvenie B-79, and Aspy D-11A from NW to SE were reference wells for rock properties of Cretaceous and Jurassic stratigraphic units, while there was no well logs recorded in the Tertiary units. As Balvenie B-79 well is situated on the slope and penetrates mostly Tertiary deposits, the RHOB log from this well was used to compile the compaction curve in the Tertiary deposits.

Each time steps of 2D sequential restoration for line 1600 are shown in Figure 4.23. The top surface of each cross-section displays the restored paleobathymetry of each time step annotated on the profiles.

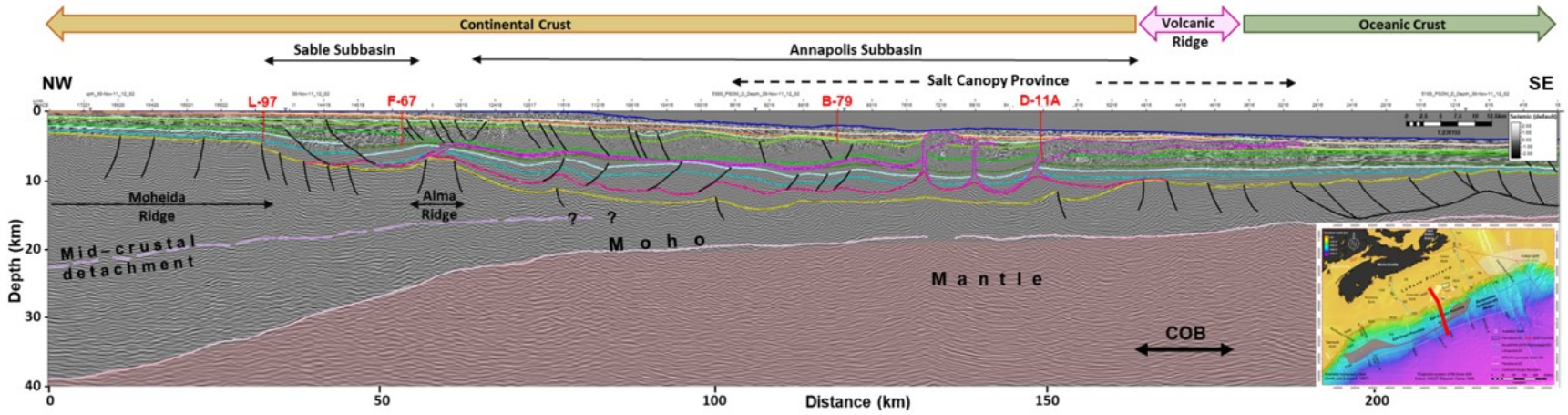

Figure 4.22: The structural interpretation of Novaspan PSDM line 1600. Lateral limits of the continental crust and COB, oceanic crust (PFA, 2011), the mid-crustal detachment (Funck et al., 2004; Dehler & Welford, 2013) are shown. No vertical exaggeration.

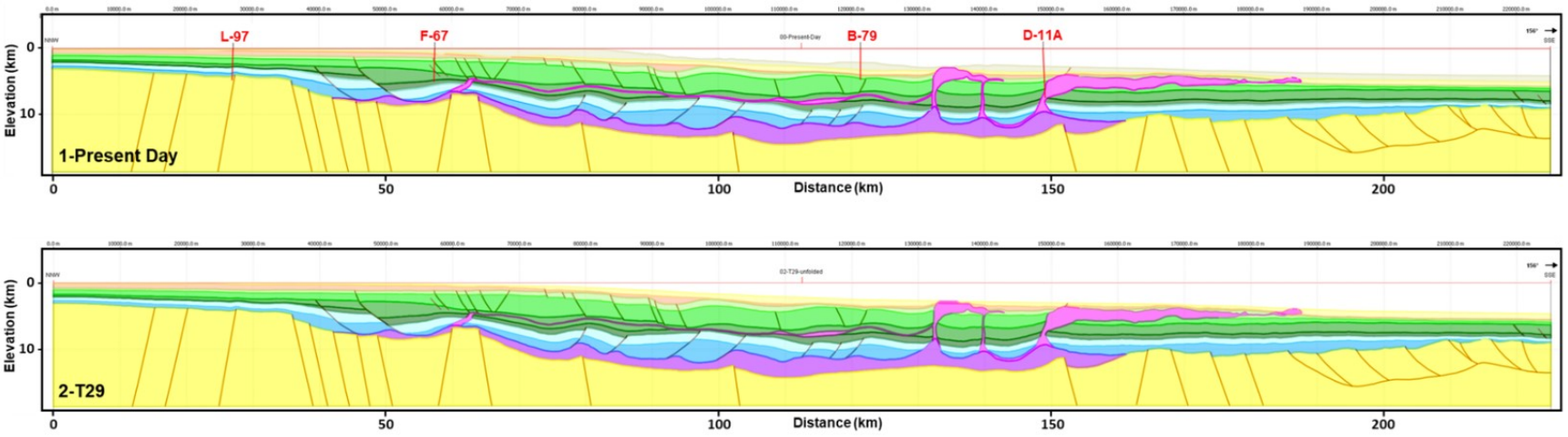

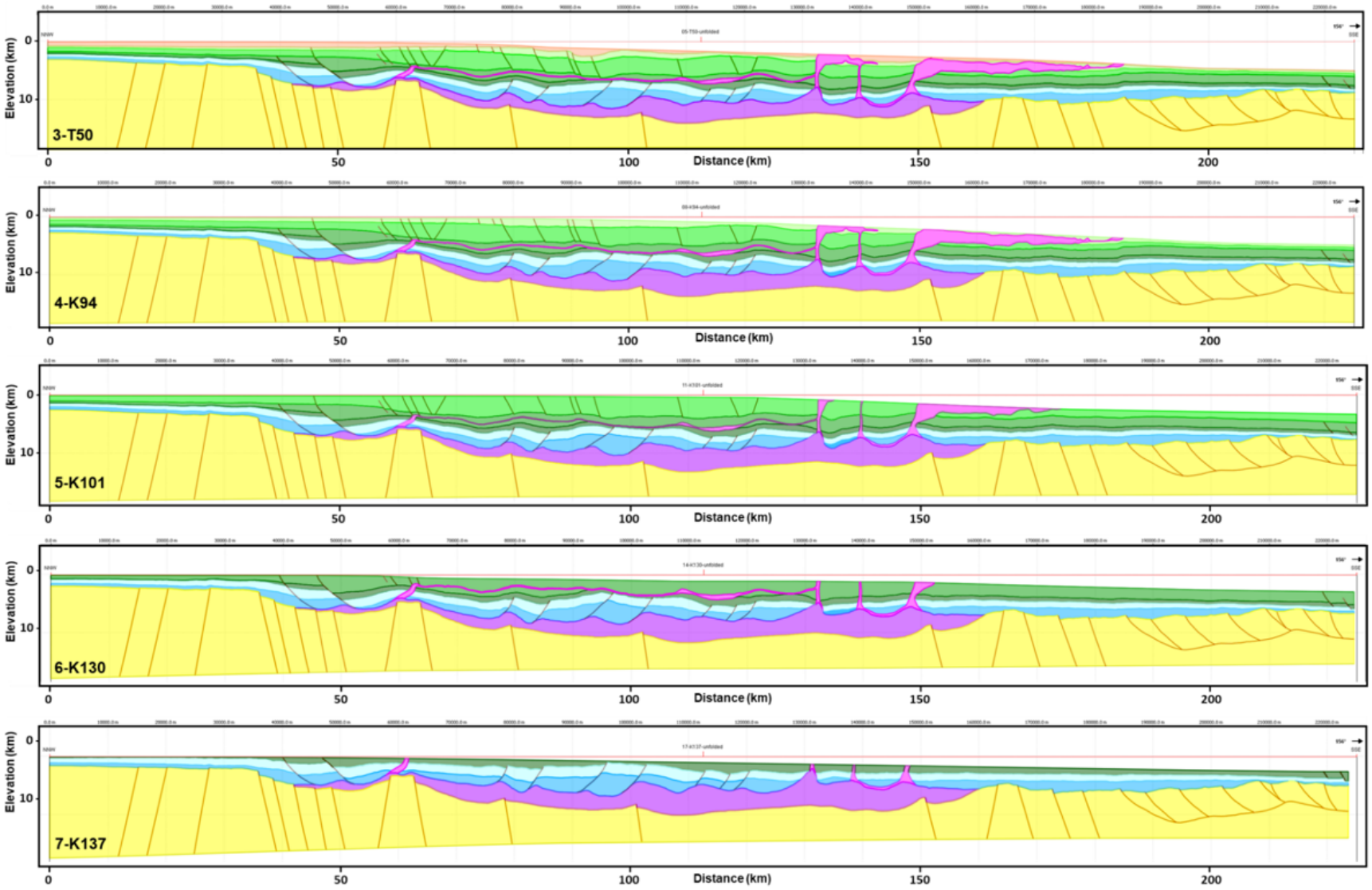
Elevation (km)
0
10
3-T50
0
50
100
Distance (km)
150
200
4-K94
5-K101
6-K130
7-K137

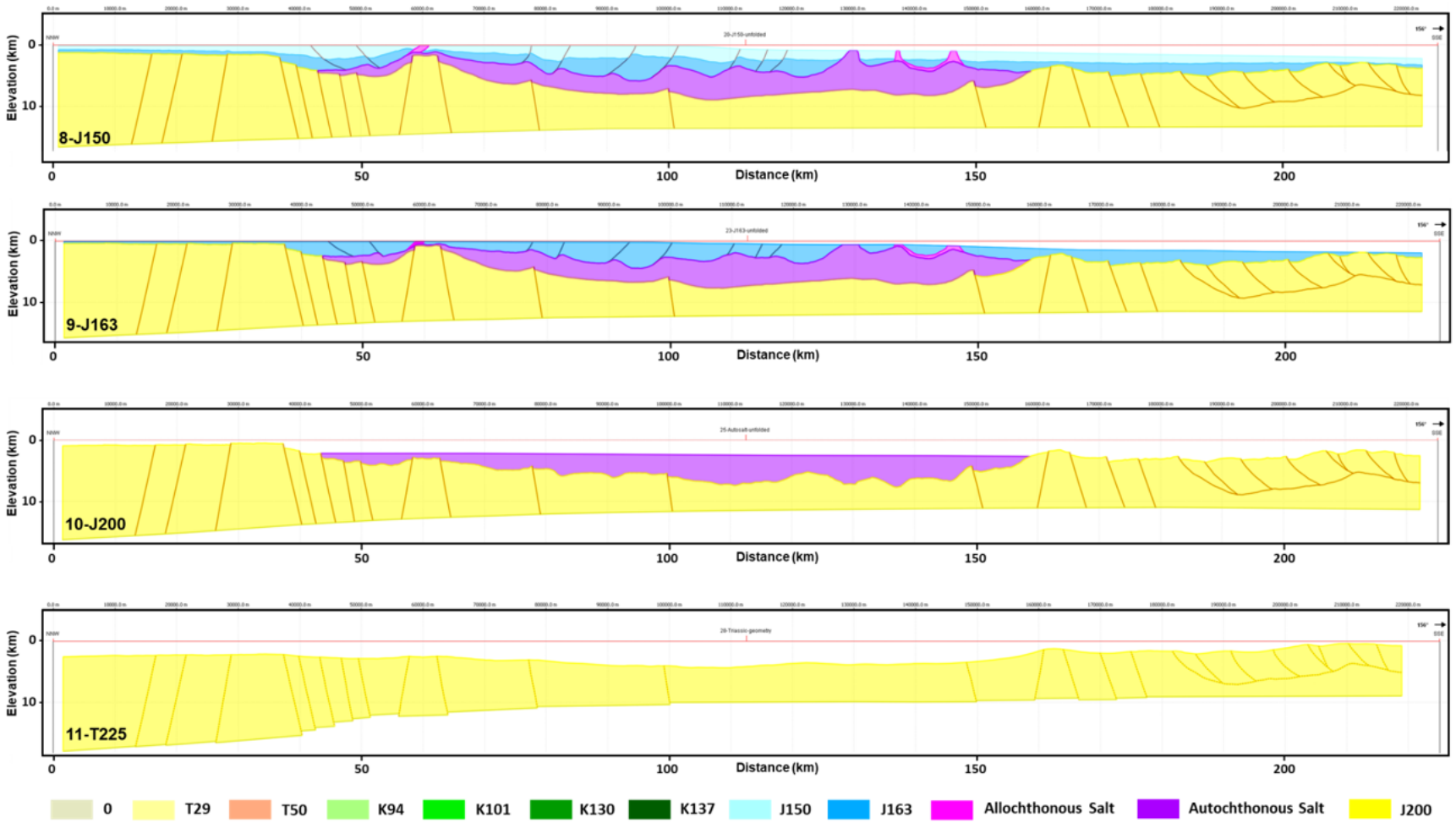

Figure 4.23: The 2D sequential restoration of the Novaspan PSDM 1600 line. Each cross-section is restored to the time step when the deposition of the top unit ended. The cross-sections are in depth domains, no vertical exaggeration.

The restored length of cross-sections and calculated extension amounts for each time step are given in Table 4.2. The NE-SW-striking syn-rift normal faults (sets I and II) in the acoustic basement accommodate an extension amount (1.23%) along the profile. The SE-dipping and NW-dipping growth faults in the units of Jurassic (set III) contribute to the extension with a total amount of 1.62%. The seaward-dipping growth faults in Cretaceous units (set IV) beneath the shelf edge and slope accommodate only 0.57% of extension. The total extension amount of line 1600 is estimated 3.53%. The planar normal faults in the basement within the continental domain (set I) contributed 42% of extension compared to the listric normal faults in the oceanic domain (set II) 58% of extension.

Table 4.2: The length of the restored cross-sections along line 1600 and extension amounts for each time step.

Time (Ma)	Restored Length (m)	Extension Amount (%)
0	225,187.8	0.00
T29	225,187.8	0.00
T50	224,986.5	0.09
K94	224,785.3	0.09
K101	224,436.0	0.16
K130	224,021.3	0.19
K137	223,719.0	0.14
J150	221,748.0	0.89
J163	220,132.3	0.73
J200	220,000.4	0.06
T225	217,410.7	1.19
Total extension amount		3.53

The total subsidence increases along and across the line 1600 from the NW to the SE for each seismic marker. The maximum subsidence was completed by the end of the rifting stage, followed by slow post-rift thermal subsidence for each seismic marker along the line (Fig. 4.8). The maximum thermal subsidence of 1200 m is estimated in the distal part of the Annapolis Subbasin and 220 m in the shelf area by the end of rifting (J200). Subsidence for the post-rift units is ~20 m in the shelf, increasing in the deep basin. The subsidence of K101 (230 m), J150 (255 m), and J163 (363 m) is more significant than the subsidence of T29 (36 m) and K94 (35 m) in the deeper basin (See Chapter 2, Figs. 2.13-2.19).

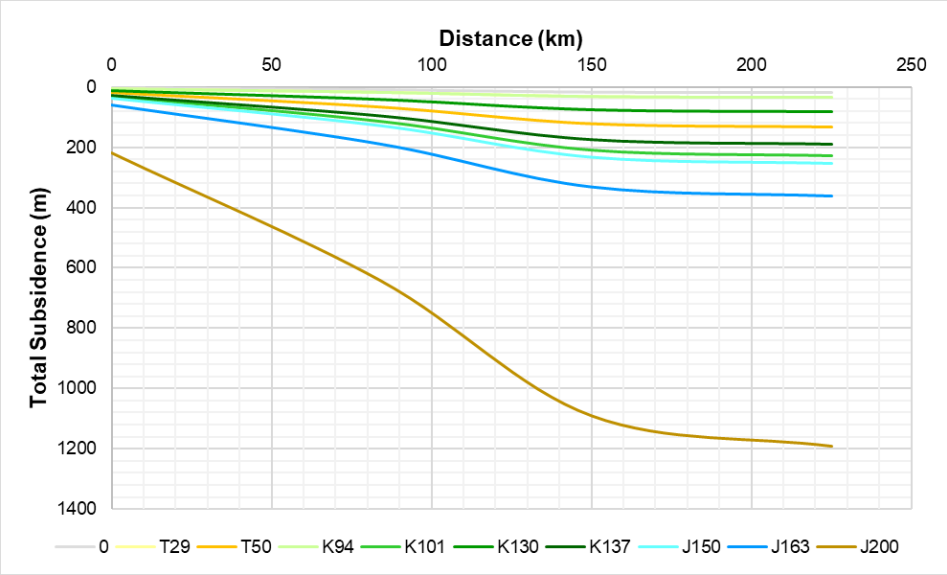

Figure 4.24: Reconstructed total subsidence of each horizon along line 1600.

The maximum isostatic rebound of ~1050 m is reconstructed for the Jurassic units below the continental slope as a result of subsidence and accommodation along the NW-dipping listric faults (set III) merging into the detachment along the top of the autochthonous salt (Fig. 4.25, J150-J163). The highest maximum isostatic rebound of 1180 m is estimated for K101 horizon and 1100 m for K130 horizon below the present-day continental slope (Fig. 4.25). It is correlated with the thickness of prograding clastic sequences of K101 and K130 units in a depocenter, where subsidence was accommodated by SE-dipping faults (set IV) merging into the salt canopy detachment emplaced within K130 horizon (Fig. 4.23, K101-K130). The maximum isostatic rebound of ~200 m is reconstructed for T50 below the present-day shelf. The estimated decompaction and isostatic rebounds correlate well with the thickness of restored sedimentary units in main depocenters (See Chapter 2, Figs. 2.13-2.19).

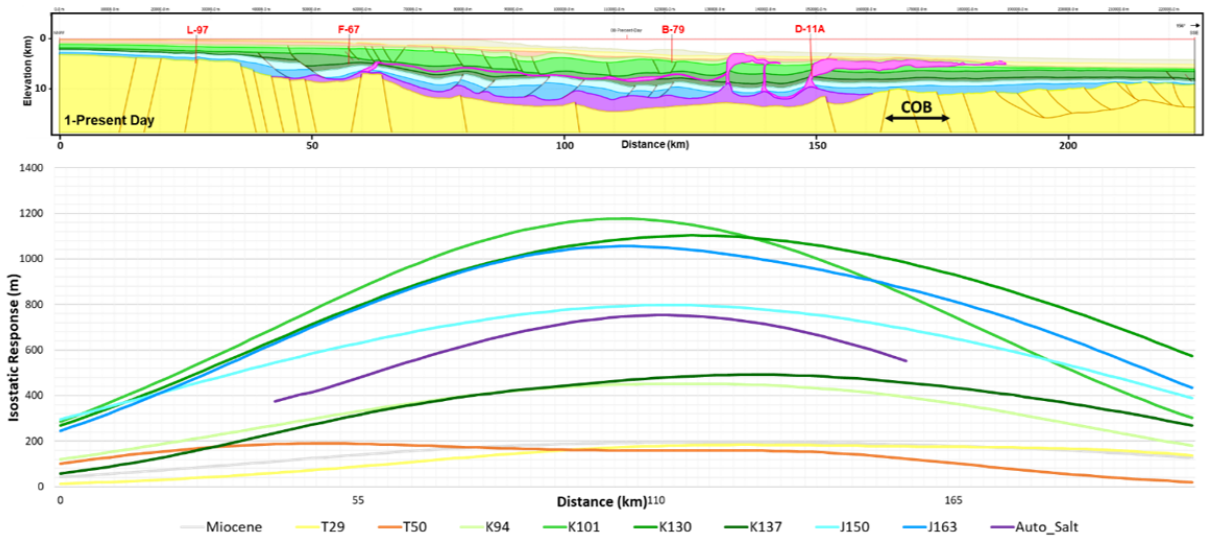

Figure 4.25: The present-day interpretation of the PSDM line 1600 (top figure) and the total isostatic response simulated for each horizon (bottom figure).

4.2.3. Novaspan PSDM Line 1400A

The line is 214 kilometres long (Fig. 4.26) and it passes through the Naskapi Ridge, Mohican Subbasin, Moheida Ridge, and Shelburne Subbasins from the shelf to the deep-water settings in the central part of the NS margin (Salt Diapir Province). The COB transition in this line is represented by the area of magmatic underplating ("volcanic ridge") located between 175 km and 185 km from the NW end of the line based on magnetic map (Fig. 2.6) (PFA, 2011; Miles & Oneschuk, 2016). It separates the continental crust domain in the NW from the oceanic domain in the SE. The maximum crust thickness of ~32 km is at the north end of the profile, and toward the south, it is around 6 km (See Chapter 2, Fig. 2.4) (Dehler & Welford, 2013). The depth interval of the PSDM seismic profile that was used in 2D restorations is 15 km (Fig. 4.26).

The Moheida P-15 located on the line 1400A on the shelf was used as a reference well for the rock properties of stratigraphic units and compaction curve. The well reports of Glooscap C-63, Torbrook C-15, and Cheshire L-97A were used for compiling rock properties of stratigraphic units. The complete sequential restoration results for line 1400A are shown in Figure 4.27. The top surface of each cross-section displays the restored paleobathymetry of each time step annotated on the cross-sections.

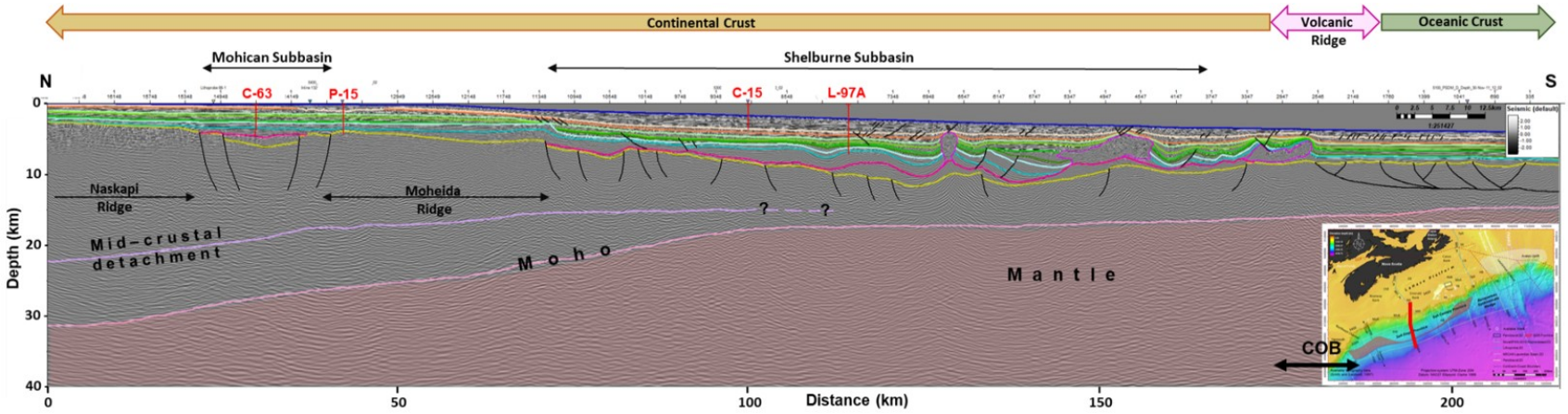

Figure 4.26: The structural interpretation of Novaspan PSDM line 1400A. Lateral limits of the continental crust and COB, oceanic crust (PFA, 2011), the mid-crustal detachment (Funck et al., 2004; Dehler & Welford, 2013). No vertical exaggeration.

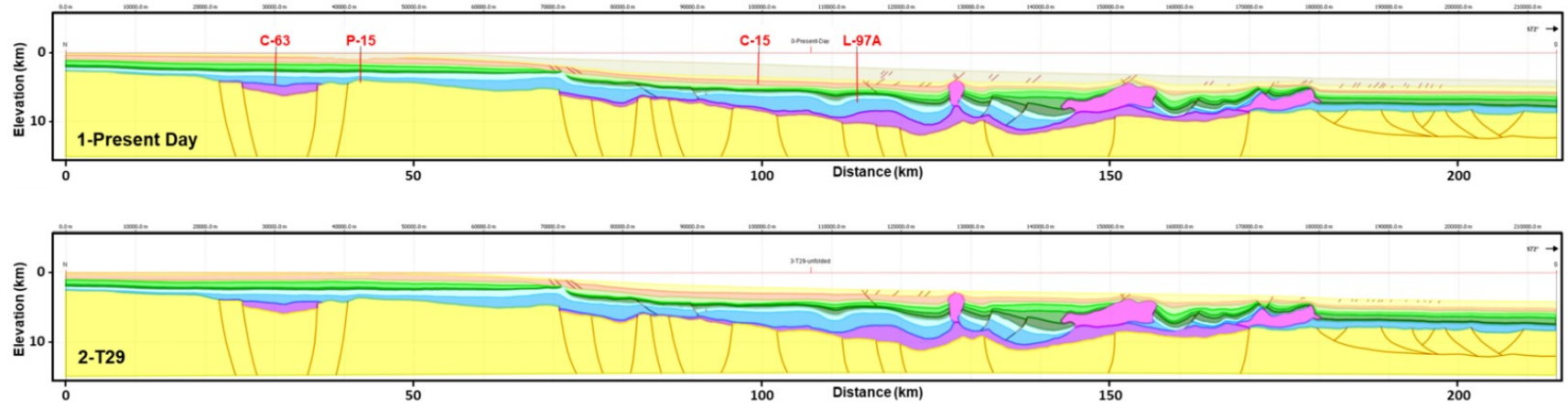

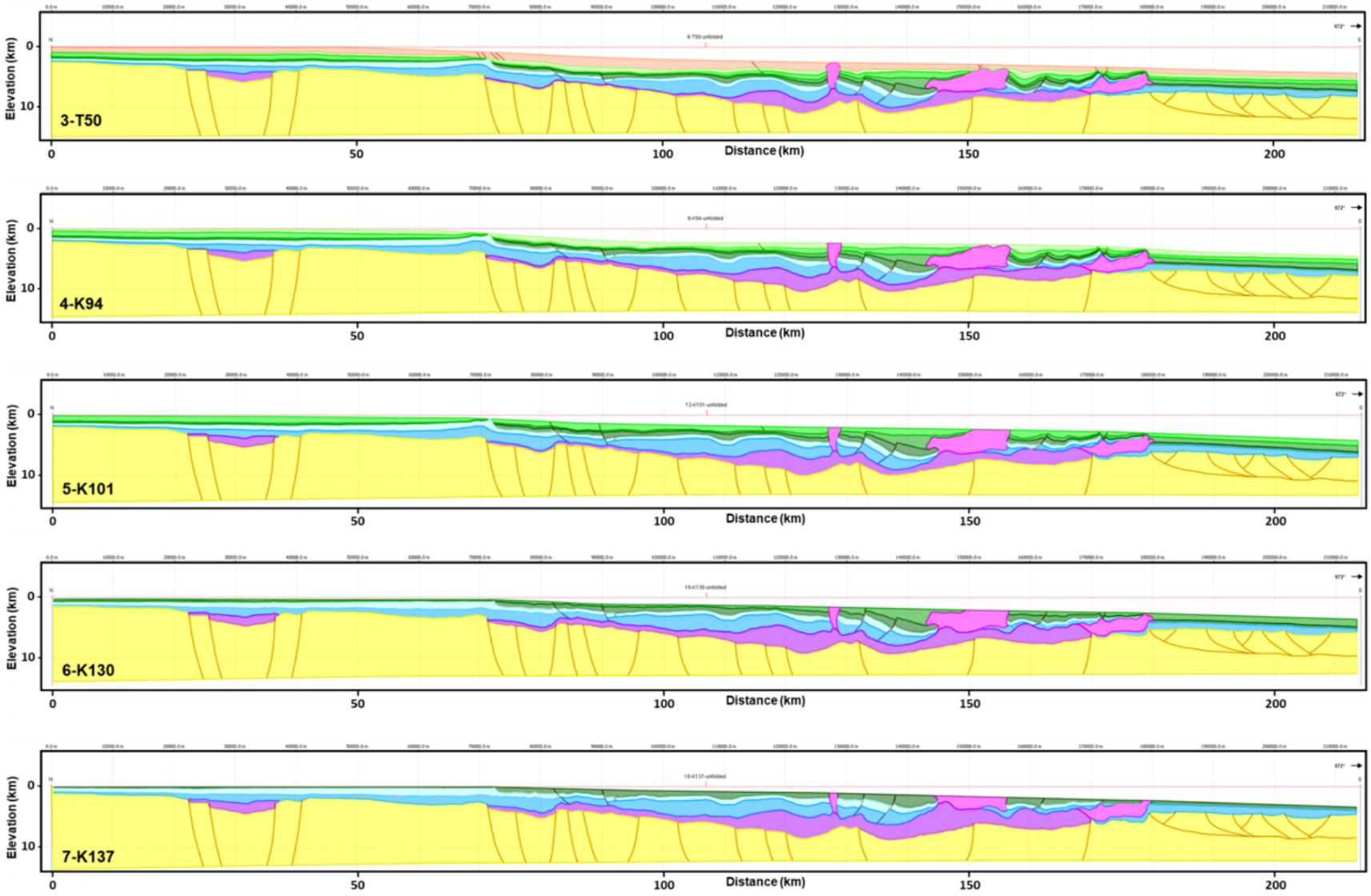
Elevation (km)
0
10
3-T50
0
50
100
Distance (km)
150
200
Elevation (km)
0
10
4-K94
0
50
100
Distance (km)
150
200
Elevation (km)
0
10
5-K101
0
50
100
Distance (km)
150
200
Elevation (km)
0
10
6-K130
0
50
100
Distance (km)
150
200
Elevation (km)
0
10
7-K137
0
50
100
Distance (km)
150
200

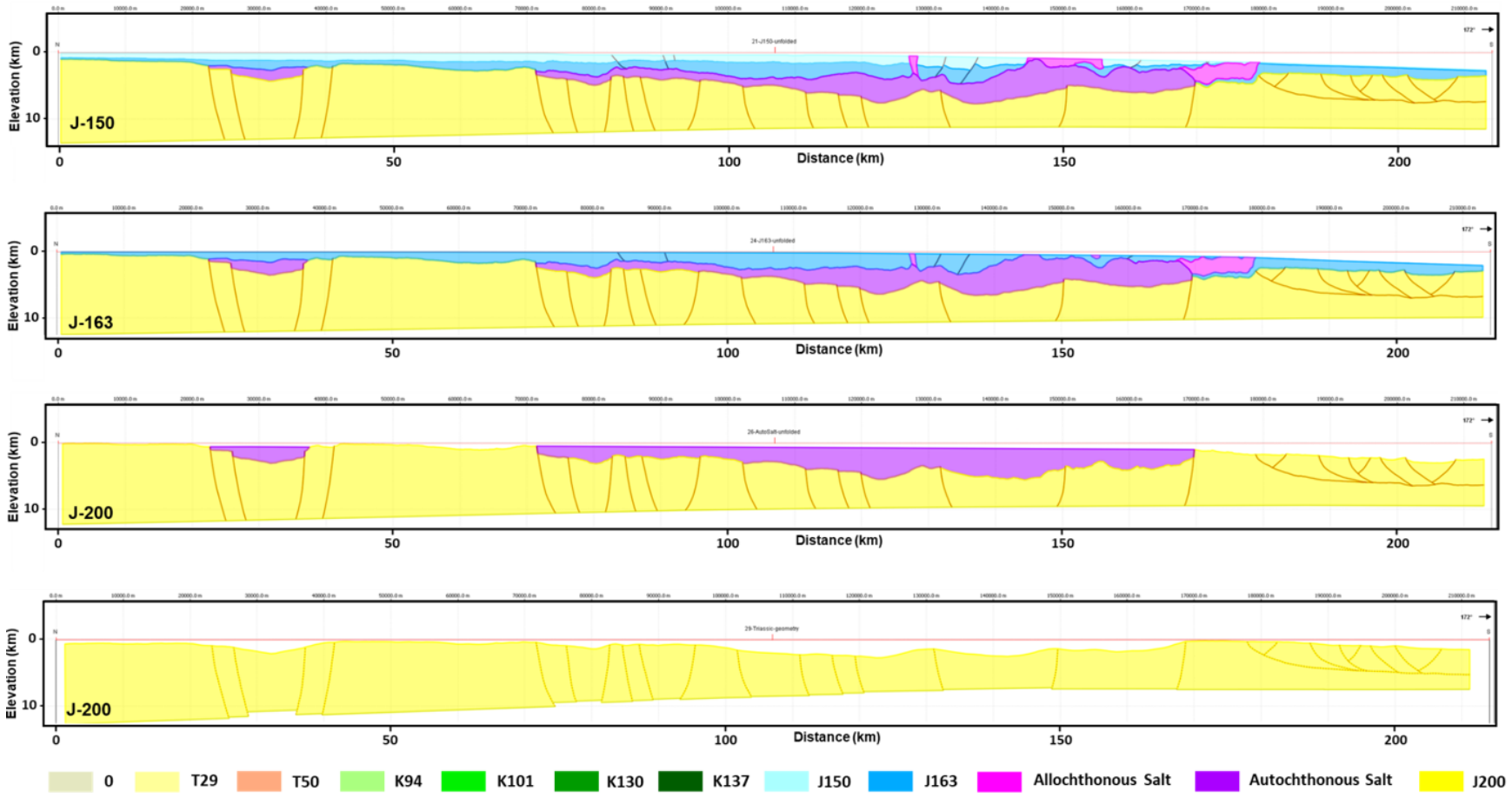

Figure 4.27: The 2D sequential restoration of the Novaspan PSDM 1400A line. Each cross-section is restored to the time step when the deposition of the top unit ended. The cross-sections are in depth domains, no vertical exaggeration.

The restored cross-section lengths and calculated extension amount for each time interval are given in Table 4.3. The NE-SW-striking syn-rift normal faults (sets I and II) accommodate a maximum extension amount (1.18%) along the profile. The SE-and NW-dipping growth faults in Lower Cretaceous to Jurassic units (sets III) below the continental slope that merge into the detachment along the top of the allochthonous salt contribute to the extension with an amount of 0.41%. The seaward-dipping normal faults in Cretaceous (set IV) and Tertiary units (set V) that are located below the present-day shelf edge and above salt diapirs accommodate only 0.41% of extension. The total extension amount of line 1400A is constructed as 1.99%. The maximum extension is associated with the syn-rift normal faulting (sets I and II) in the acoustic basement. The planar normal faults in the basement within the continental domain (set I) contributed 44% of extension, compared to the listric normal faults in the oceanic domain (set II) 56% of extension.

Table 4.3: The length of the restored cross-sections along line 1400A and extension amounts for each time step.

Time (Ma)	Restored Length (m)	Extension Amount (%)
0	214,032.9	0.00
T29	213,951.5	0.04
T50	213,714.1	0.11
K94	213,565.5	0.07
K101	213,523.4	0.02
K130	213,166.8	0.17
K137	212,911.9	0.12
J150	212,778.5	0.06
J163	212,298.6	0.23
J200	212,286.1	0.01
T225	209,824.9	1.17
Total extension amount		1.99

The total subsidence increases along line 1400A for each stratigraphic unit. The rapid subsidence during the rifting stage is followed by slow post-rift thermal subsidence with a gradual distribution (Fig. 4.11). The maximum thermal subsidence of 1190 m is reconstructed in the deep-water setting and 220 m in the shelf area by the end of rifting (J200). The subsidence for the post-rift units is ~20 m in the shelf, increasing in the deep basin. The subsidence of K101

(255 m), K137 (190 m), and J150 (230 m) is more significant than the subsidence of T29 (52 m) and K94 (36 m) in the deeper basin (See Chapter 2, Figs. 2.13-2.19).

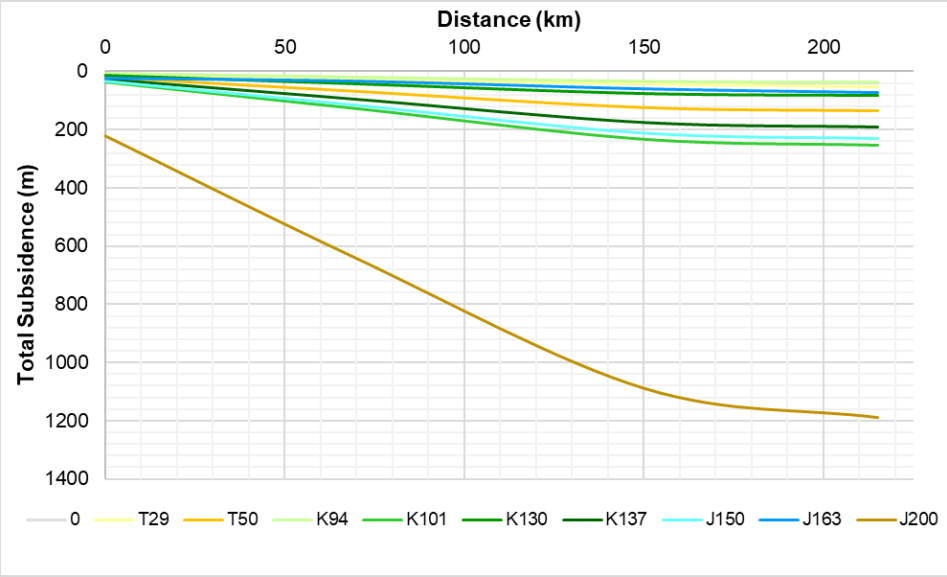

Figure 4.28: Reconstructed total subsidence of each horizon along line 1400A.

The maximum isostatic rebound of 920 m is reconstructed for Middle Jurassic (J163) unit and 500 m for Upper Jurassic (J150) below the continental slope as a result of subsidence and accommodation along the NW-dipping listric faults (set III) that merge into the detachment along the top of the autochthonous salt (Fig. 4.29, J150-J163). The maximum isostatic rebound of 420 m for K137, 445 m for K130, 350 m for K101, and 370 m for K94 is in the distal part of the Shelburne Subbasin, where isolated mini-basins developed between salt diapirs that create more accommodation (See Chapter 2, Figs. 2.13-2.19). The maximum isostatic rebound of Tertiary units is estimated at 340 m for T50 and 212 m for T29 on the slope setting (Fig. 4.29).

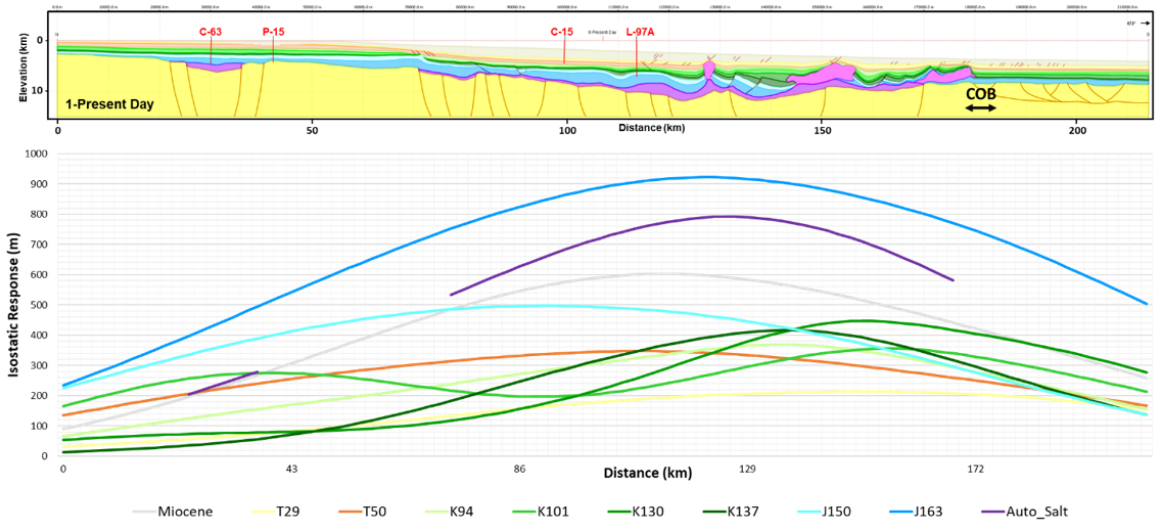

Figure 4.29: The present-day interpretation of the PSDM line 1400A (top figure) and the total isostatic response simulated for each horizon (bottom figure).

4.2.4. Novaspan PSDM Line 1100

The line is ~185 kilometres long (Fig. 4.30) and passes through the Mohawk Ridge and Shelburne Subbasin from the shelf to the deep-water settings in the southwestern part of the NS margin (Salt Diapir Province). The COB transition in this line is represented by the area of magmatic underplating ("volcanic ridge") located between 95 km and 150 km from the NW end of the line based on magnetic map (Fig. 2.6) (PFA, 2011; Miles & Oneschuk, 2016). This transition separates the continental crust domain in the NW from the oceanic domain in the SE. The maximum crustal thickness of ~36 km is at the northwestern end of the profile and decreases to the southeast, where it is around 5 km (See Chapter 2, Fig. 2.4) (Dehler & Welford, 2013). The depth interval of the PSDM seismic profile that was used in 2D restorations is 13 km (Fig. 4.31).

The 12-km-offset Bonnet P-23 was a reference well for rock properties of stratigraphic units and a compaction curve. The sequential restoration results for line 1100 are shown in Figure 4.31. The top surface of each cross-section displays the restored paleobathymetry of each time step annotated on the cross-sections.

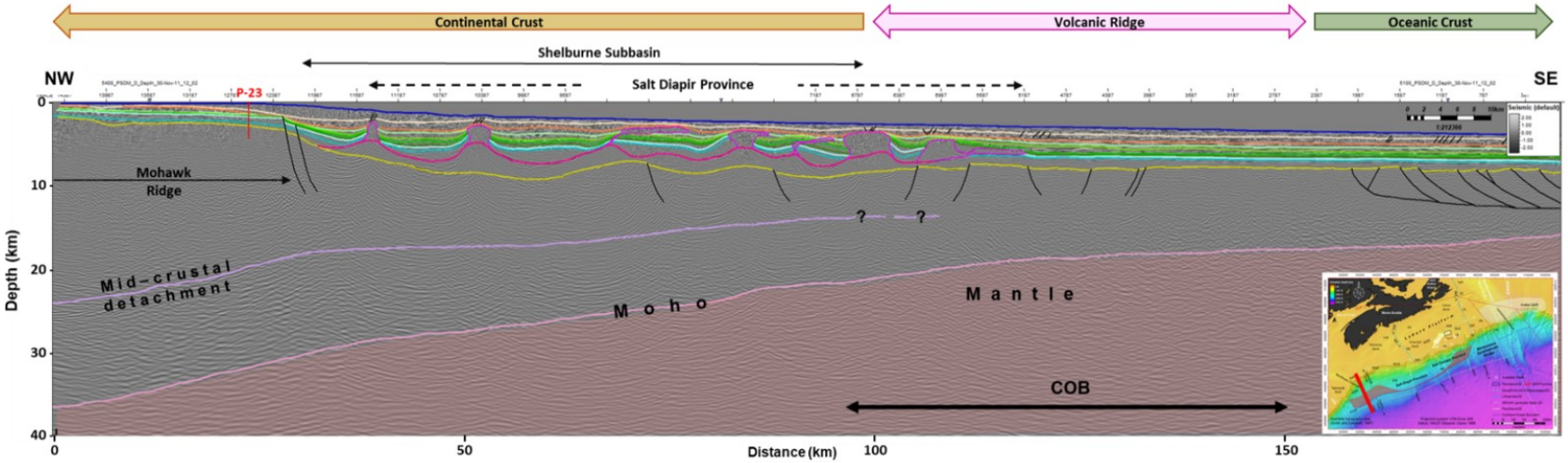

Figure 4.30: The structural interpretation of Novaspan PSDM line 1100. Lateral limits of the continental crust and COB, oceanic crust (PFA, 2011), the mid-crustal detachment (OETR, 2009; Dehler & Welford, 2013). No vertical exaggeration.

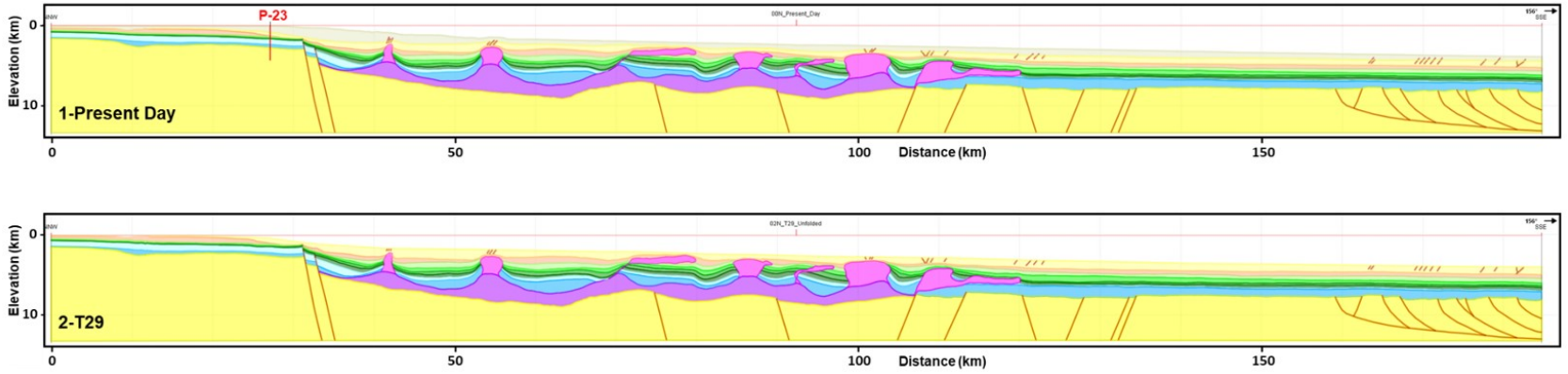

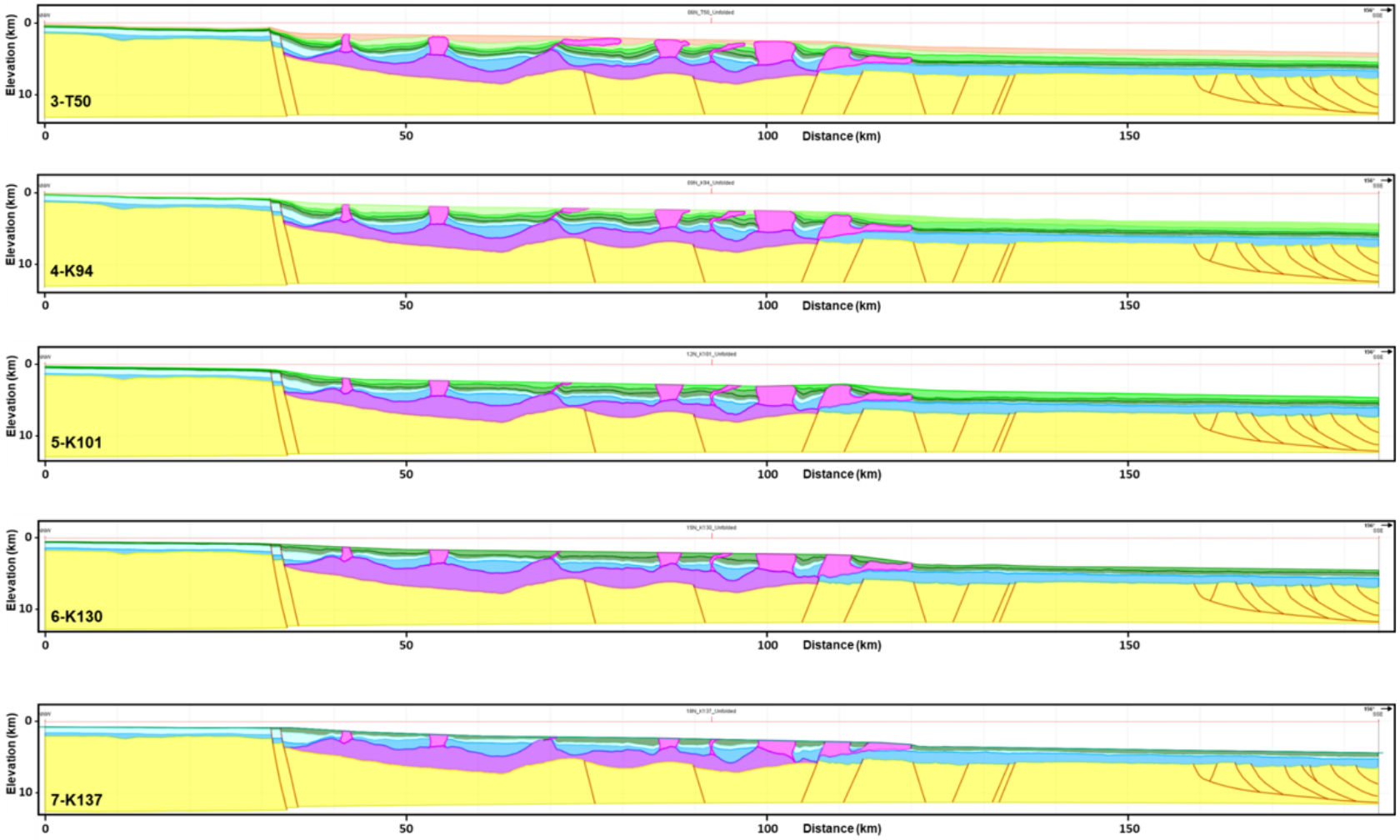
Elevation (km)
0
10
3-T50
0
50
100
Distance (km)
150
Elevation (km)
0
10
4-K94
0
50
100
Distance (km)
150
Elevation (km)
0
10
5-K101
0
50
100
Distance (km)
150
Elevation (km)
0
10
6-K130
0
50
100
Distance (km)
150
Elevation (km)
0
10
7-K137
0
50
100
Distance (km)
150

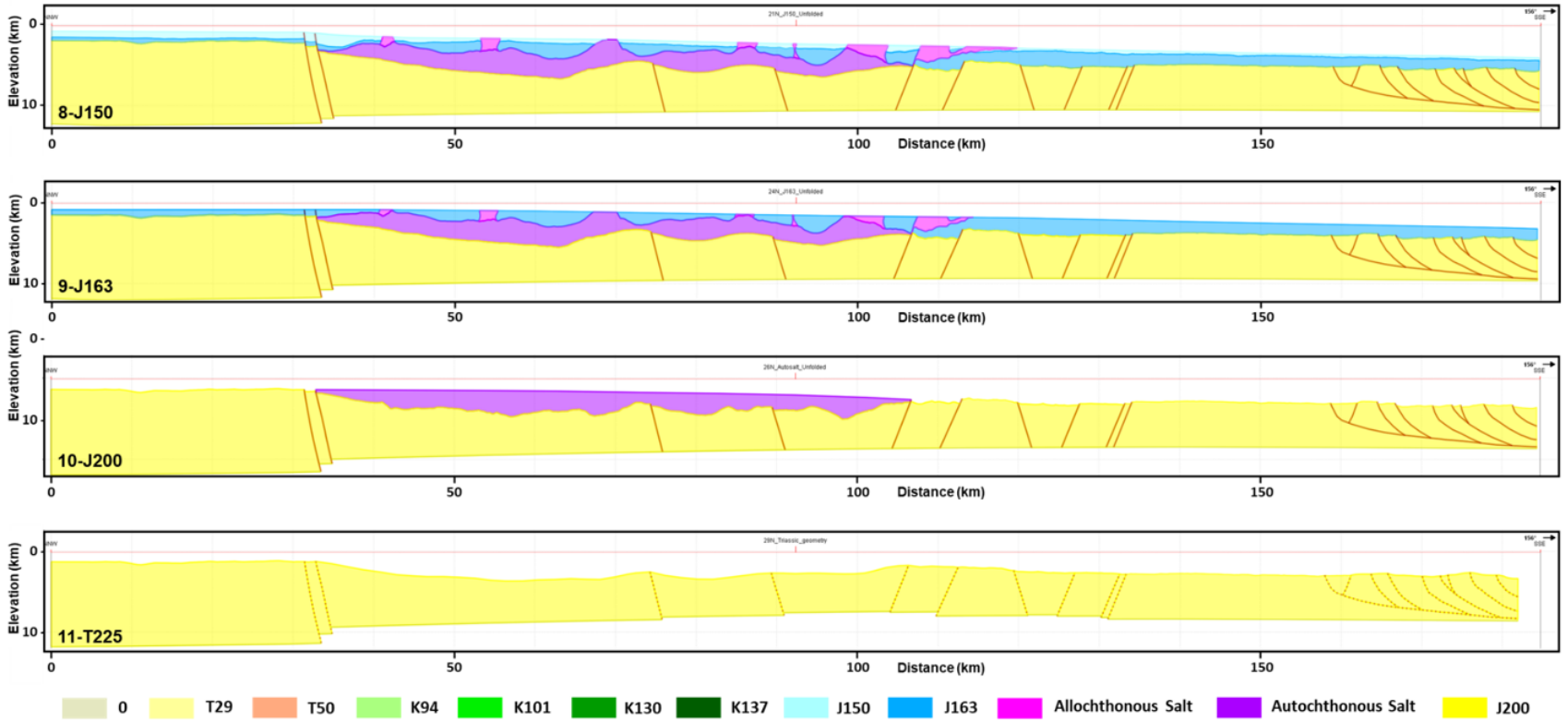

Figure 4.31: The 2D sequential restoration of the Novaspan PSDM 1100 line. Each cross-section is restored to the time step when the deposition of the top unit ended. The cross-sections are in depth domains, no vertical exaggeration.

The restored cross-section lengths and calculated extension amount for each time interval are given in Table 4.4. The NE-SW-striking syn-rift normal faults (sets I and II) accommodate a maximum extension amount (1.30%) along the profile. The SE-and NW-dipping faults in Tertiary units (set V) related to salt diapirism contribute 0.04% to the extension. The total extension amount of line 1100 is constructed as 1.55%, thus the maximum extension is associated with the syn-rift normal faulting (sets I and II) in the acoustic basement. The planar normal faults in the basement within the continental domain (set I) contributed 27% of extension compared to the listric normal faults in the oceanic domain (set II) 73% of extension.

Table 4.4: The length of the restored cross-sections along line 1100 and extension amounts for each time step.

Time (Ma)	Restored Length (m)	Extension Amount (%)
0	184,824.0	0.00
T29	184,824.0	0.00
T50	184,755.0	0.04
K94	184,745.0	0.01
K101	184,730.0	0.01
K130	184,701.0	0.02
K137	184,682.0	0.01
J150	184,600.0	0.04
J163	184,392.0	0.11
J200	184,373.0	0.01
T225	182,005.0	1.30
Total extension amount		1.55

The total subsidence increases along and across the line 1100 from the NW to the SE for each seismic marker. The maximum subsidence is reconstructed by the end of the rifting stage and it has been followed by slow post-rift thermal subsidence for each seismic marker along the line (Fig. 4.32). The maximum thermal subsidence of 775 m is reconstructed in the distal part of the basin and 220 m in the shelf area by the end of rifting (J200). The subsidence for the post-rift units is ~25 m in the shelf, increasing in the deep basin. The subsidence for of T50 (197 m), K101 (260 m), and K137 (184 m), and J150 (226 m) is more significant than the subsidence of T29 (55 m) and K94 (46 m) in the deeper basin (Fig. 4.32).

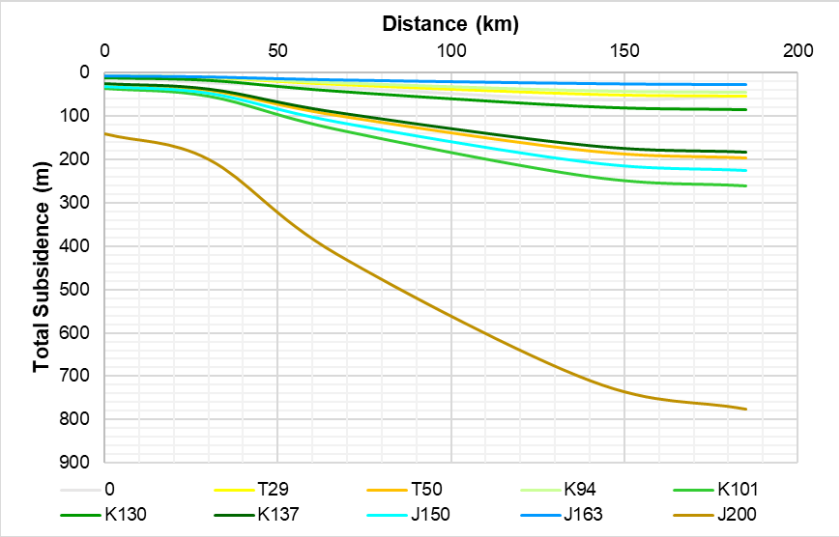

Figure 4.32: Reconstructed total subsidence of each horizon along line 1100.

Along this cross-section, the maximum isostatic rebound for each horizon is localized mainly in the area of the continent-oceanic transition (COB) (Fig. 4.33). The maximum isostatic rebound of 580 m is reconstructed for Middle Jurassic (J163) unit at the distal part of the Salt Diapir Province (Fig. 4.31, J163). The maximum isostatic rebound of 220 m for K137, 175 m for K130, 235 m for K101, and 230 m for K94 in the area of the COB. The maximum isostatic rebound of Tertiary units is reconstructed as 310 m for T29 on the slope setting, where the location of sedimentation was governed by the remobilization of salt diapirs and emplacement of mini-depocenters between them (See Chapter 2, Figs. 2.13-19).

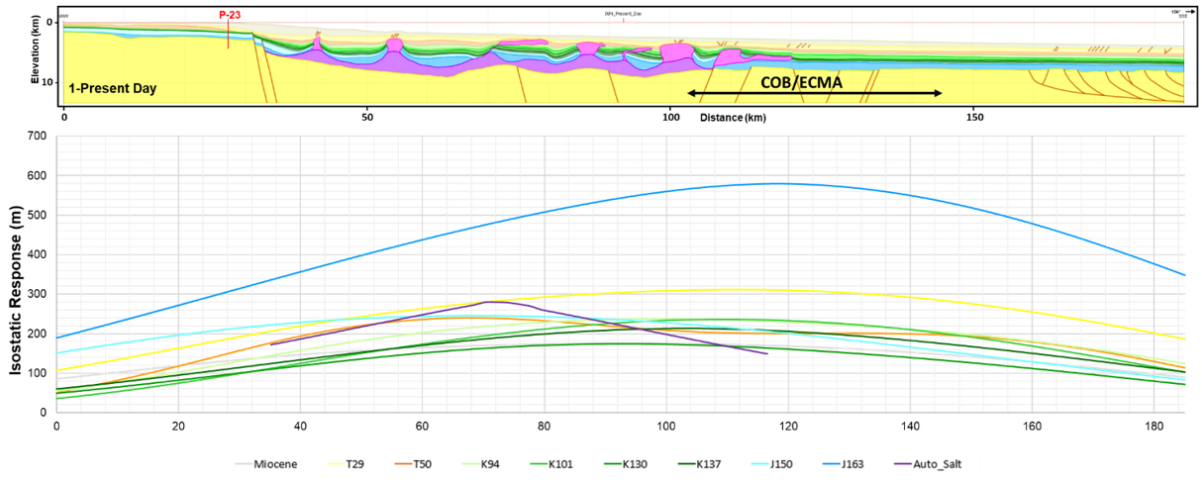

Figure 4.33: The present-day interpretation of the PSDM line 1100 (top figure) and the total isostatic response simulated for each horizon (bottom figure).

The maximum extension, subsidence, and isostatic response reconstructed for four lines summarized in Table 4.5.

Table 4.5: The summary of reconstructed parameters for four cross-sections.

Cross-section	Total Extension Amount, %	Maximum Subsidence (J200), m	Maximum Isostatic Response, m
Line 2000	3.72	1035	2610 (J163)
Line 1600	3.53	1200	1175 (K101)
Line 1400A	1.99	1190	920 (J163)
Line 1100	1.55	775	580 (J163)

4.2.5. Sensitivity Tests

Sensitivity tests were performed to analyze how the output of restoration modelling responds to the uncertainty in the input parameters. These uncertainties are associated with the assumed properties of crust and lithosphere (stretching factor, elastic thickness of the lithosphere) and their lateral variation along and across the Nova Scotia margin and with the restoration of missing intervals of bulk density logs. In this study, we run the sensitivity tests for three inputs related to different restoration steps: The crustal stretching factor (β), the elastic thickness of the lithosphere (T_e), and compaction curves.

Parameter of stretching factor, or beta value (β)

An estimated beta value (β) for the Nova Scotia passive margin (Fig. 2.5) is not uniform and varies from 0.2 within the continental domain in the NW to 2.0 in the oceanic domain in the SE of the margin (Dehler & Welford, 2013). The variation of the stretching factor reflects the higher extension in the oceanic domain during the rifting and opening of the Atlantic Ocean than on the continental shelf. Applying in the model a uniform beta value of 1.55, an average in Dehler & Welford (2013), results in a lower amount of subsidence compared to a non-uniform stretching factor. For example, the subsidence amount of K94 is 29.27 m and remains constant through the cross-section under the settings of a uniform stretching factor (Fig. 4.34a). The non-uniform stretching factor was applied with increasing values from 1.1 in the NW to 2.2 in the SE. As a result, the subsidence amount for the K94 increases from 8.2 m to 57.9 m toward the south along the profile, with an average of 37.12 meters (Fig. 4.34b).

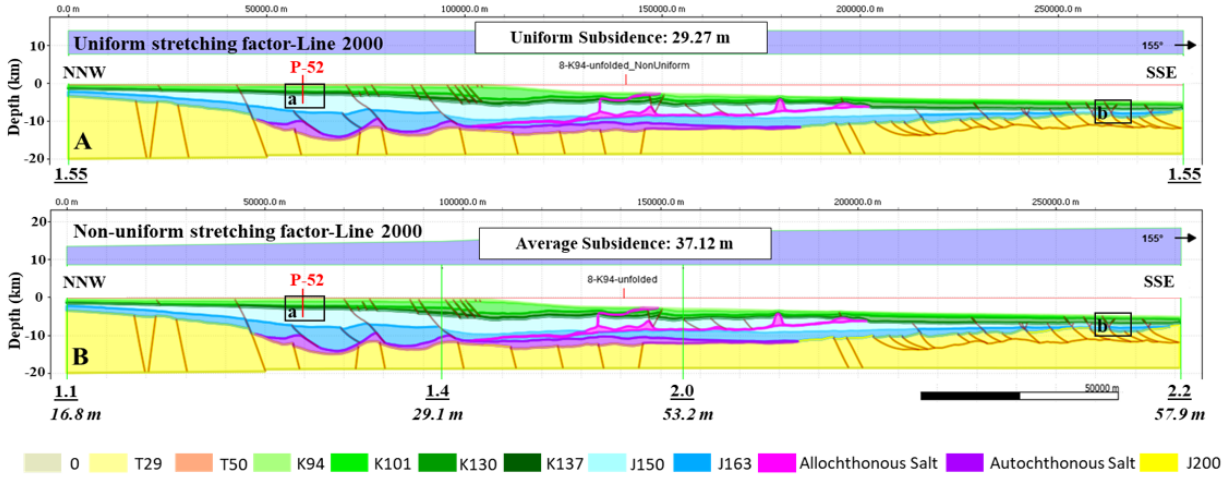

Figure 4.34: Reconstruction of thermal subsidence step for horizon K94 along line 2000 with a uniform (A) and a non-uniform (B) stretching factor (β). The underlined numbers show the beta values used in modelling in both cross-sections. The subsidence amounts of K94 are shown in italics at the reference points indicated by green lines. The black rectangles (a, b) depict the location of cross-sections shown in the Figure 4.35. The cross-section is in depth domain (PSDM), no vertical exaggeration.

The difference in resulting paleodepth at the shelf is ~10 m (Fig. 4.35a), but it reaches 80 m in the oceanic domain, where a higher beta value was applied (Fig. 4.35b). Therefore, a reconstruction model with a uniform beta value would result in under-restored subsidence of horizons and faults in the oceanic domain. Since the steps of sequential restoration were repeated for each time step, the differences would increase in every stage of the modelling.

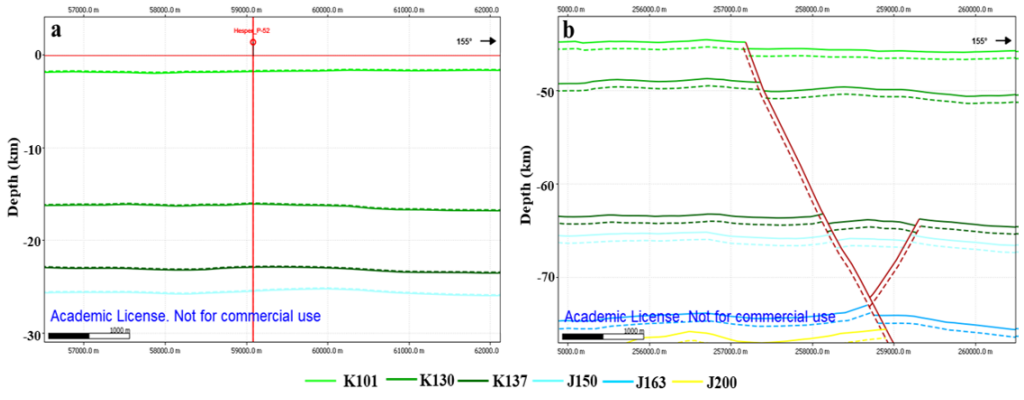

Figure 4.35: The example of thermal subsidence restoration for horizons in the shelf area (a) and in the deeper part (b) of line 2000. The results of modelling using uniform (solid lines) and a non-uniform (dashed lines) stretching factor β are compared. The location of the sections are shown in Figure 4.34. The cross-section is in depth domain (PSDM), no vertical exaggeration.

Elastic thickness of the lithosphere (T_e)

The elastic thickness of the lithosphere, T_e, is a key parameter in the flexural isostasy simulation (Watts, 1981; Watts, 2001; Audet, 2014). MOVE allows using only a uniform value of T_e along the cross-section. In this study, the flexural isostasy modelling was conducted by testing the constant elastic thickness that decreases from the SW to the NE along the margin that is compatible with the previous results supporting increasing crustal stretching and thinning from the SW to the NE (Funck et al., 2004; Wu et al., 2006; Dehler & Welford, 2013). T_e varies between 20 km and 30 km and it consists of 20 km for line 2000 in the NE segment of the margin, 22 km for line 1600 and 25 km for line 1400A in the central segment, and 30 km for line 1100 in the SW segment of the margin. The isostatic flexural response testing results are shown for line 2000 (Fig. 4.36) using two end-values of T_e (20 km and 30 km) assumed for the lithosphere of the Nova Scotia margin. In the first scenario of T_e equal 30 km, the paleowater depth of the K94 horizon at a given point (location of Hesper P-52 well) on the profile was reconstructed as equal -420 m or as an upper bathyal (Fig. 4.36a). In the second scenario of T_e equal 20 km, the paleowater depth of the K94 horizon was restored to be equal to -127 m, or an outer neritic (Fig. 4.36b). By decreasing T_e values from 30 km to 20 km, the reconstructed paleobathymetry of the K94 is ~300 meters shallower. As the paleodepth of K94 is middle neritic according to the biostratigraphy data (Weston et al., 2012), the lower T_e value of 20 km is more appropriate for the lithosphere along line 2000.

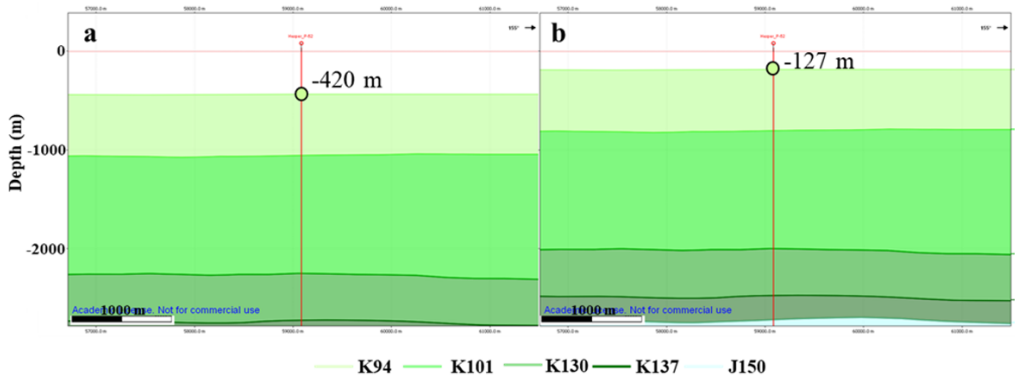

Figure 4.36: The results of flexural isostasy tests along line 2000 with Te of 30 km (a) and 20 km (b) and resulting changes of the paleobathymetry of the K94 horizon in the area of well Hesper P-52. The cross-section is in depth domain (PSDM), no vertical exaggeration. The location of the Line 2000 is shown in Figure 2.8.

The compaction curves

In this study, the porosity logs were derived from the bulk density (RHOB) logs for the wells located on or near the reconstructed cross-sections. The missing intervals of RHOB log recordings in the shallow intervals (0-1400 m) were completed by using the compaction curves of Sclater & Christie (1980) and Watts & Steckler (1979). The porosity in the shallow interval of the Sclater & Christie (1980) compaction curve is higher (0.56%-0.32%) than the porosity of the Watts & Steckler (1979) compaction curve (0.53%-0.24%).

In the example of Hesper P-52 well (Fig. 4.37), the first compaction curve was derived from the RHOB log well, and the Watts & Steckler (1979) curve was used to rebuild the shallow interval of the compaction curve (Fig. 4.37a). After the decompaction of T50 horizon, the paleo-depth of K94 in this case was reconstructed as -127 meters, outer neritic (Fig. 4.37a) that is deeper than paleodepth established from biostratigraphy. The second compaction curve was generated by using the curve of Sclater & Christie (1980) in the shallow part (0-1400 m). After the decompaction, the paleo-depth of K94 was restored as -78 meters (Fig. 4.37b), middle neritic that was compatible with the biostratigraphy report of the well (Weston et al., 2012). The higher porosity of sedimentary units in the shallow interval (0-1400 m) results in stronger decompaction and decreased modelled subsidence of young porous units (i.e. seabed, T29, T50) compared to the older, more compacted units.

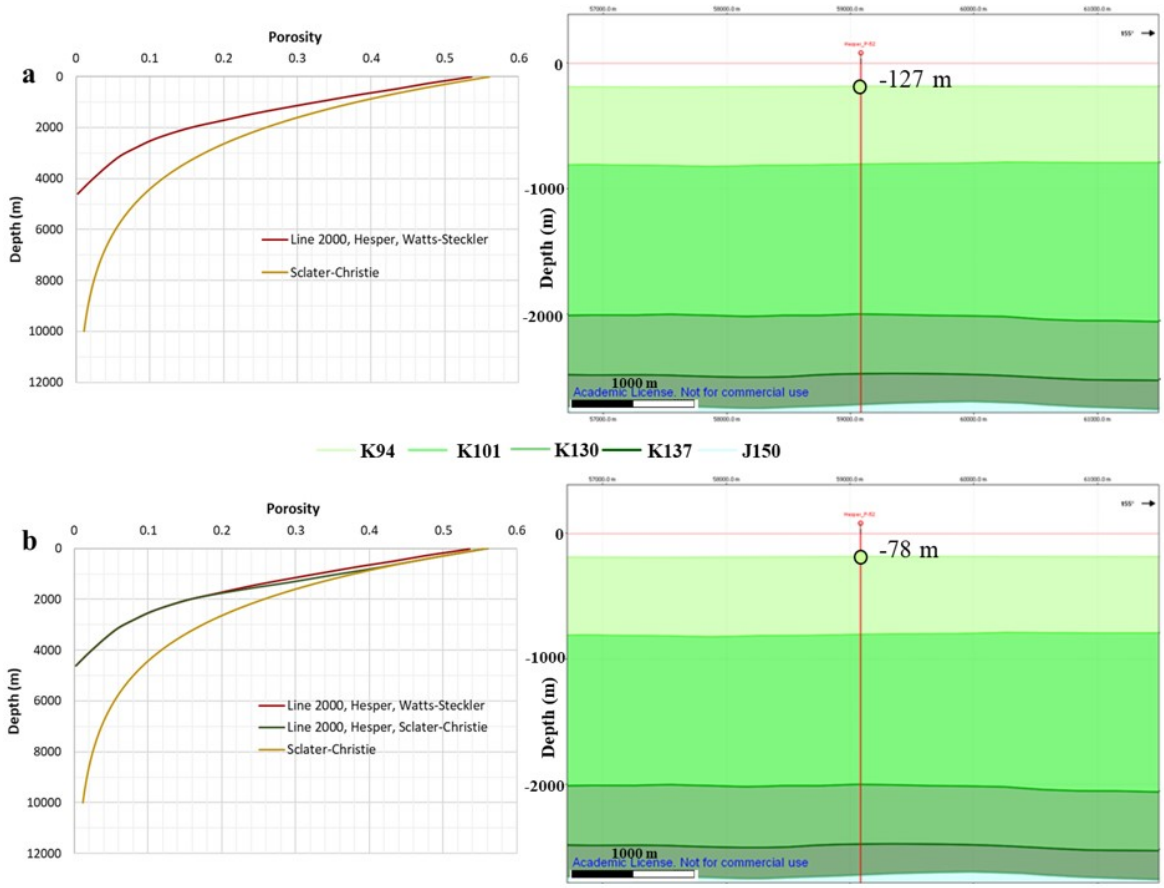

Figure 4.37: The compaction curves in well Hesper P-52 (left) and restored paleo-depth of K94 horizon after decompaction of the horizon T50 (right). The compaction curves from Watts & Steckler (1979) (a) and Sclater & Christie (1980) (b) are used in the shallow interval (0-1400 m), where RHOB log is missing. The lower porosity in shallow interval (a) results in deeper modeled paleo-depth of K94 (-127 m) compared to higher porosity case (-78 m).

In summary, all the sensitivity tests demonstrated that analyzing the impact of input parameters and then calibrating the results with the biostratigraphy data from the drilled wells were critical for the iterative steps of restoration modelling to improve the accuracy of 2D kinematic restorations. The weight of the input parameters on the simulation results varies with depth and laterally along and across the Nova Scotia margin. For instance, the compaction curves have a more significant effect on paleodepth restoration within the younger and porous units (seabed, T29, T50), and it is less pronounced in the older units. The increase of the stretching factor toward the deeper oceanic domain of the basin results in a more noticeable variation in simulated paleodepth in comparison with the shelf setting. The lower elastic thickness of the

lithosphere T_e (20 km) in the northeastern segment of the margin (Line 2000) results in a stronger isostatic flexural rebound compared to the higher T_e (30 km) in the southwestern segment of the margin (line 1100).

Chapter 5: Discussion

5.1. Volcanic- and Non-Volcanic Passive Continental Margins

Differences in the tectonic and magmatic evolution of the Atlantic volcanic and non-volcanic passive continental margins were recently reviewed by Biari et al. (2021). Volcanic-style passive margins (Fig. 5.1) are characterized by large amounts of extrusive lavas forming thick seaward dipping reflector sequences and intrusions in the form of magmatically overprinted high-velocity zones in the lower crust (Thybo et al., 2003). Volcanic margins show crustal thinning in a narrow (~20 km) area of continent-oceanic transition zone and the accretion of volcanic products and magmatic additions to the lower crust (Hinz et al., 1993; Eldholm & Grue, 1994; Geoffroy et al., 2015). Non-volcanic margins (Fig. 5.1) are characterized by the absence of significant mantle melting in their crustal section immediately before and throughout lithosphere extension. In such settings, the sub-crustal mantle can be exhumed and serpentinized in association with crustal stretching and thinning (Geoffroy et al., 2015).

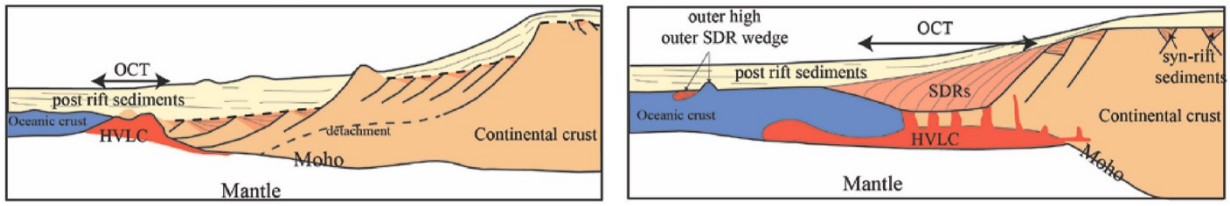

Figure 5.1: Architecture of slowly extended magma-poor (left) and rapidly-extended magma-rich (right) margins, after Biari et al. (2021).

In the Atlantic region, the non-volcanic margins are often transform margins, characterized by settings of oblique movement of the lithospheric plates (Briari et al., 2021). The length of a transform margin depends on three parameters: the obliquity between regional rift trend and extension orientation or relative plate motion, the width of the continental rift and the timing of the deformation partitioning (Basile et al., 2005; Agostini et al., 2009). The deformation partitioning along the transform rifted margin can accommodate a change in paleostress field and kinematic plate reorganization followed by the emplacement of transform faults, e.g., the Romanche and Saint Paul right-lateral transform faults between South and Central Atlantic during the rifting in Equatorial Atlantic at about 120 Ma (Basile et al., 2005).

The Nova Scotia passive continental margin is characterized by longitudinal variations in crustal structure from a volcanic-style margin in the southwest to a non-volcanic margin in the northeast (Keen & Potter, 1995a; Holbrook et al., 1994a; Kelemen & Holbrook, 1995; Keen & Potter, 1995b; PFA, 2011; Louden et al., 2012; Dehler, 2010; Sibuet et al., 2012). In previous studies, magnetic and gravity data integrated with the P-wave velocities of deep seismic refraction profiles (Figs. 2.3 and 2.4) have been modelled to interpret these variations across and along the margin (Funck et al., 2004; OETR, 2009; OERA, 2019; Dehler, 2012; Dehler & Welford, 2013). The Newfoundland Transform Zone (NFTZ) is a major crustal transform zone (Fig. 5.2) that separates the oceanic domain of the Nova Scotia margin from the Grand Banks continental block (OERA, 2019, chapter 3). The NFTZ seems to separate the "magma rich province" of Central Atlantic from the "magma poor province" of Grand Banks in the Northern Atlantic segment (McHone, 2000). As shown by kinematic reconstructions, the NFTZ was a left lateral strike-slip fault during the Jurassic drift of the future African plate with respect to the North American plate (Fig. 5.2). Additionally, possible secondary faults that "offset" continental blocks of the Scotian margin were reconstructed in the northern segment of the margin based on the distribution of autochthonous salt basins and discontinuity of the ECMA (OERA, 2019, chapter 3). These secondary faults likely represent minor replicas of the main NFTZ and also acted as early transforms faults (Fig. 5.2).

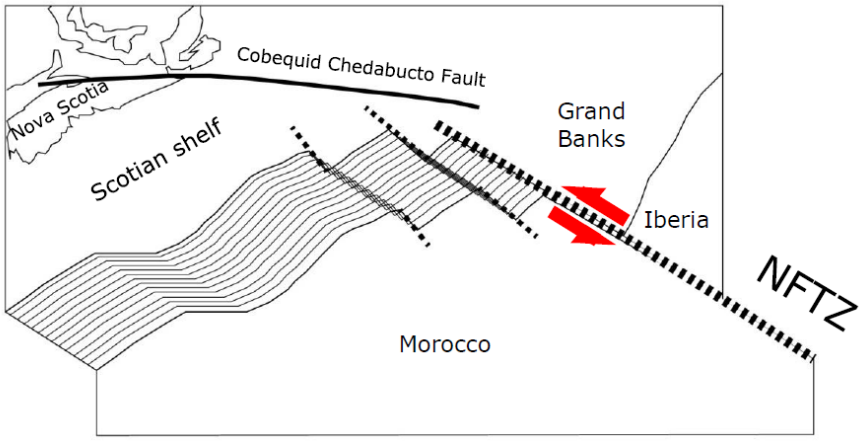

Figure 5.2: Schematic map of the plate boundary configuration on the first phases of drifting (Early Jurassic) of the future African plate with respect of the North American plate, after (OERA, 2019, chapter 3). During this early drift, Newfoundland Transform Zone (NFTZ) acted as a left lateral strike-slip fault.

The results of this study based on 2D structural interpretation and kinematic restoration have shown significant differences in tectonic structure and evolution of the northeastern and southwestern segments of the margin (Chapter 4). This chapter discusses how the variations in rifting styles (volcanic versus non-volcanic) and other factors, such as regional paleogeography and sediment supply, influence syn- and post-rift deformation of the margin, salt kinematics and sedimentation through time.

5.2. Syn-rift Deformation: Volcanic versus Non-volcanic Margin

The northeastern non-volcanic segment of the Nova Scotia margin experienced a higher degree of extension and faulting during the syn-rift deformation (Fig. 5.3; Table 5.1) than the southwestern volcanic segment. The structural map of the top of the basement (J200) and fault intensity is compared in Figure 5.4. The present-day shelf break is used as a pinning point to compare fault localizations along cross-sections. It is located at 105 km on line 2000, 80 km on line 1600, 55 km on line 1400A, and 28 km on line 1100 from the northwestern end of the cross-sections.

There is a strong correlation between fault intensity and extension amount, top basement geometry, and subsidence of the basement along the cross-sections. In the northeastern highly stretched segment of the margin (line 2000), the intensity of syn-rift normal faults (Fig. 5.4) is about 2 faults per 20 km in the continental domain (set I), increasing to about 4-5 faults per 20 km in the oceanic domain (set II). The present-day shelf area in this segment of the margin is much more extended than it is in the SW segment of the margin (line 1100), where high fault intensity (up to 7 faults per 20 km) mostly corresponds to the oceanic domain (set II).

The amount of extension during syn-rift deformation gradually increases along strike from 1.30% in the SW segment of the margin to 2.70% in the NE segment (Tables 5.1, 5.2). The intensity of listric normal faults in the oceanic domain (set II) contributes to a higher ratio of extension (56%-86%) compared to planar syn-rift normal faults (14%-44%) in the basement in the continental domain (set I) (Table 5.1).

The estimated total maximum subsidence amount for J200 is 1035 m along line 2000 in the Laurentian Subbasin and 1200 m along line 1600 in the Annapolis Subbasin in the northeastern segment of the margin (Figs. 4.20, 4.24, 5.3, and Tables 4.5, 5.2). It is lower in the

Shelburne Subbasin in the southwestern segment, where it consists of 1190 m along line 1400A and 775 m along line 1100 (Figs. 4.28, 4.32, 5.4 and Tables 4.5, 5.2).

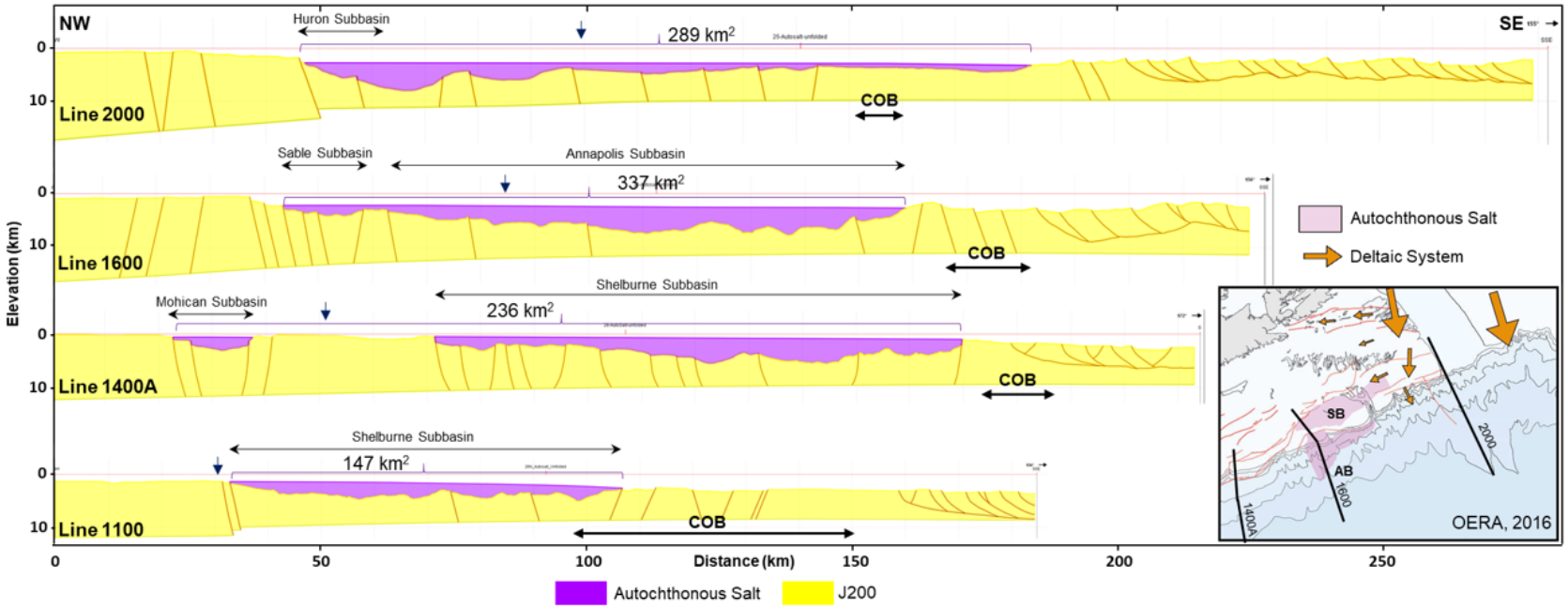

Figure 5.3: The cross-sections are restored to the time J200. The cross-sections are in depth domains, no vertical exaggeration. The estimated area (km^2) of restored autochthonous salt is shown above the cross-sections. Blue arrows show the location of present-day shelf breaks. The location of main Triassic salt basins and clastic transport during the early Jurassic are shown on the (J200-J163) paleogeography map (after OERA, 2016, chapter 2).

Table 5.1: Total extension amounts and the ratio of extension accommodated by syn-rift faults in the continental and oceanic domains.

Cross-section	Total Syn-rift (T225) Extension Amount, %	Extension in Continental Domain, %	Extension in Oceanic Domain, %
Line 2000	2.70	14	86
Line 1600	1.19	42	58
Line 1400A	1.17	44	56
Line 1100	1.30	27	73

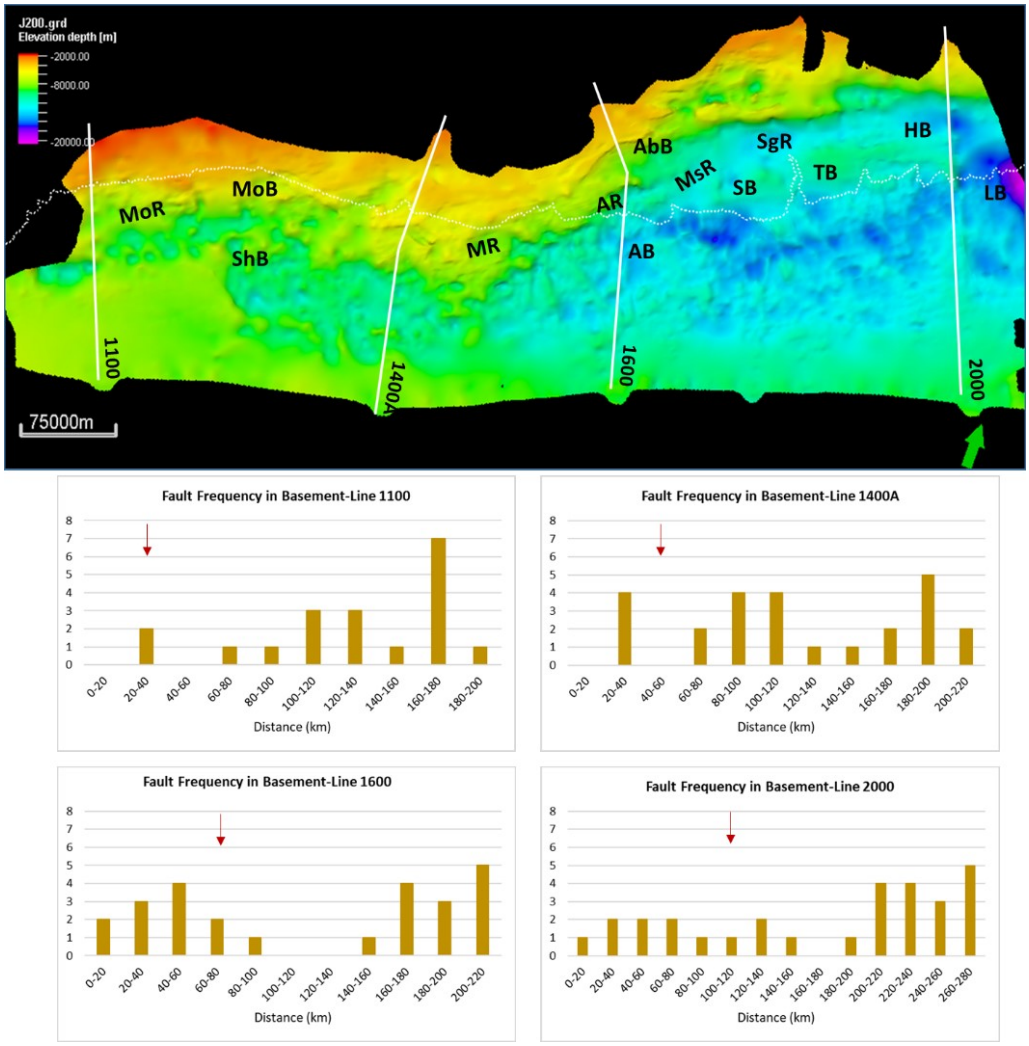

Figure 5.4: The depth structure map of the top of the basement (J200) of the Nova Scotia margin. The dashed line represents the present-day shelf edge. The graphs illustrate the fault intensity plotted along four NW-SE lines as a function of the distance from the NW end of the lines with a step of 20 km. Red arrows on graphs depict the location of the present-day shelf break. AbB: Abenaki Subbasin, AB: Annapolis Subbasin, AR: Alma Ridge, HB: Huron Subbasin, LB: Laurentian Subbasin, MoB: Mohican Subbasin, MoR: Mohawk Ridge, MR: Moheida Ridge, MsR: Missisauga Ridge, SB: Sable Subbasin, SgR: South Griffin Ridge, ShB: Shelburne Subbasin, TB: Tantallon Subbasin.

The greater syn-rift extension within the present-day shelf area in the NE segment of the margin (e.g. Huron Basin) results in the development of a more extended and steeper geometry of the reconstructed top-basement within this area, compared to a shorter and flatter top-basement geometry below the present-day shelf in the SW segment of the margin (Fig. 5.5).

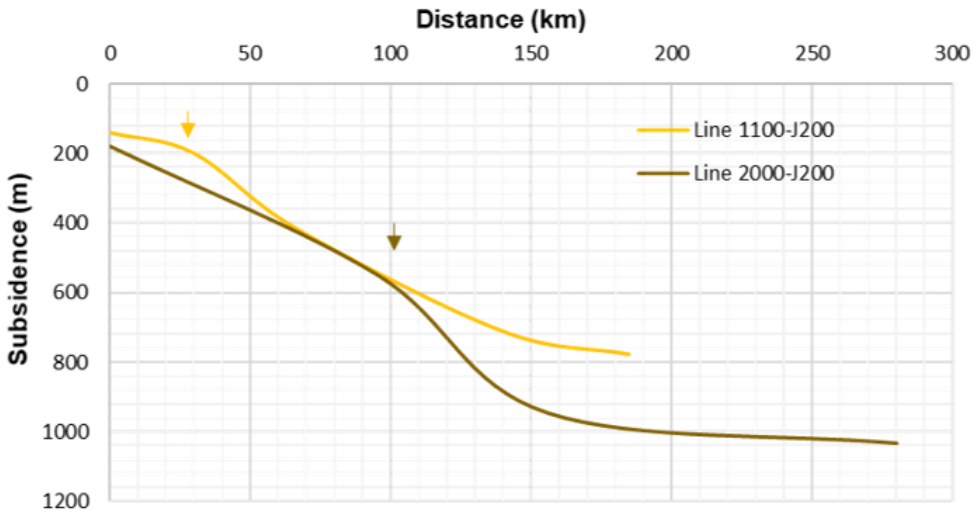

Figure 5.5: The subsidence curve of J200 (top basement) in northeastern (line 2000) and southwestern (line 1100) segments of the margin. The arrows show the location of present-day shelf breaks.

By the end of the rifting, 289 km^2 of autochthonous salt (estimated as a cross-sectional area) is reconstructed in the Huron Subbasin (line 2000) and 337 km^2 in the Sable and Annapolis Subbasins (line 1600) in the NE segment of the margin. It is 147 km^2 in the Shelburne Subbasin (line 1100) in the southwestern segment of the margin (Fig. 5.3; Table 5.2). According to the modelling results, the autochthonous salt accumulation is localized in the Huron Basin below the present-day continental slope in the NE segment of the margin (line 2000) with a maximum thickness of 5-6 km (Table 5.2). In contrast, it is likely more evenly distributed in the central and SW segments of the margin, with thickness reaching about 2-3 km in the SW of the margin (line 1100).

The difference in the top-basement geometry and thickness and distribution of autochthonous salt accumulation contributes to the variation of the depositional setting of the post-rift Jurassic and Cretaceous deposits and associated salt kinematics.

Table 5.2: The estimated parameters and characteristics of syn-rift tectonic deformation.

Syn-rift Phase								
		Syn-rift Extension		Autochthonous Salt			Normal Faulting	Maximum Subsidence (J200, m)
Segments	# Cross-sections	Total Extension (%)	Extended Area	Autochthonous Salt Paleobasin Geometry	2D Area (km^2)	Maximum Thickness (km)		
NE (Non-Volcanic)	2000	2.70	Highly strecthed shelf; highest extension in the oceanic domain	~140-km-wide basin (Huron and Laurentian Subbasins) below the present-day shelf and continental slope	289	5-6	SE-and NW-dipping planar normal faults (Set I) in continental domain (shelf, slope, and deep basin), SE-dipping listric normal faults (Set II) in oceanic domain	1035
Central (Volcanic)	1600	1.19	Highly strecthed shelf; high extension in the oceanic domain	~120-km-wide basin (Sable and Annapolis Subbasins) below the present-day shelf and continental slope	337	4-5	SE-and NW-dipping planar normal faults (Set I) in continental domain (mostly shelf and deep basin), SE-dipping listric normal faults (Set II) in oceanic domain	1200
	1400A	1.17	Localized strecthing on the shelf; high extension in the oceanic domain	~15-km-wide basin (Mohican Subbasin) on the shelf; ~100-km-wide basin (Shelburne Subbasin) in the deep basin	236	4	SE-and NW-dipping planar normal faults (Set I) in continental domain (locally at shelf and mostly at slope and in deep basin), SE-dipping listric normal faults (Set II) in oceanic domain	1190
SW (Volcanic)	1100	1.30	No strecthing on the shelf; high extension in the oceanic domain	~75-km-wide basin (Shelburne Subbasin) below the present-day continental slope	147	2-3	SE-and NW-dipping planar normal faults (Set I) at the shelf break and base of the slope in continental domain; SE-dipping listric normal faults (Set II) in oceanic domain	775

Note: 2D area (km^2) is a cross-section area estimation. See Table 5.1 for the amount of syn-rift extension in the continental and oceanic domains.

5.3. Post-rift Deformation: Controlling Factors

The difference in localization and amount of syn-rift deformation of the Nova Scotia margin and paleogeographic settings during the earliest stages of the post-rift evolution of the margin contributed to the variation of type and volume of sediment accumulation along the margin that, in turn, affected salt kinematics and post-rift fault emplacement.

The reconstructed amount and localization of extension and subsidence of post-rift deposits vary in the SW volcanic and NE non-volcanic segments of the Nova Scotia margin (Table 5.3). The higher extension localized below the present-day shelf in the NE segment of the margin during the syn-rift deformation contributed to thicker (maximum 5-6 km) salt accumulation in the Huron Subbasin (Fig. 5.3). Very limited stretching of the SW segment of the margin below the present-day shelf resulted in thinner (maximum 2-3 km) salt accumulation mostly below the continental slope and in a deep basin (Table 5.3 and Fig. 5.3). This difference in the upper crustal extension and salt accumulation below the present-day continental shelf reconstructed in the SW and NE segments of the margin contributed to variations in allochthonous salt tectonics and post-rift sedimentation (Table 5.3).

During the early post-rift stage of J163, the southward-directed deltaic systems provided sedimentary influx to the Scotian Basin (Figs. 5.3-5.6, orange arrows on maps). It resulted in the deposition of the predominantly clastic- or mixed clastic-carbonate deposits in the northeastern segment of the Nova Scotia margin (Fig. 5.6, line 2000). The top of the basement was extended beneath the present-day northeastern shelf and the reconstructed thickness of the J163 deposits reaches ~ 6200 m in the Huron Subbasin (Fig. 5.6). In the southwest and central segments of the margin, the J163 carbonate accumulation was predominant within the LaHave Platform with a maximum reconstructed thickness of ~2000 m (Fig. 5.6, line 1100).

The gravitational loading of a 5-6-km-thick J163 unit in the Huron Subbasin in the NE segment of the Nova Scotia margin triggered salt remobilization and expulsion of an extended (~40 km) thin (~550 m) canopy that progressed to the SE (Fig. 5.6, line 2000). The displacement of salt increased the accommodation for J163 clastic deposits resulting in the highest area of Jurassic J163 units of ~310 km^2 along line 2000 estimated from the NW end of the line to the root of the salt canopy. A similar thin and extended salt canopy started to develop at the SE edge of the Sable Subbasin, above the Alma Ridge (Fig. 5.6, line 1600). The predominantly shallow-

water carbonate sedimentation within the LaHave Platform in the SW segment of the margin (Fig. 5.7) was not favourable for salt remobilization close to the shore, thus isolated salt diapirs developed in the deeper part of the Shelburne Subbasin (Fig. 5.6, lines 1100 and 1400A). The area of the J163 deposits in the Abenaki and Sable Subbasins (line 1600) and Shelburne Subbasin is estimated along lines 1400A and 1100 from the NW end of the lines to the root of the first diapir. It gradually decreases along the margin from the NE to the SW from 86 km^2 (line 1600) to 75 km^2 (line 1400A) to ~28 km^2 (line 1100) (Fig. 5.6), likely reflecting the decreasing amount of the J163 sediment supply reaching the distal areas in the basins.

The expulsion of thin extended salt canopy rooted at the Alma Ridge, the J163 sediment loading and subsidence in the Huron (line 2000), Sable and Annapolis Subbasins (line 1600) in the NE segment of margin was accommodated by the emplacement of the post-rift listric normal faults (set III). The faults of set IIIa dip to the SE and NW, toward the root of the canopy (line 1600) and merge into the autochthonous basal detachment, and forming the Banquereau Synkinematic Wedge (Fig. 5.6, line 2000). The significantly lower volume of J163 deposits in the SW segment of the margin resulted in salt remobilization of isolated diapirs in the area of the present-day continental slope and small-scale canopies in more distal settings. No (line 1100) to very limited number of post-rift normal listric faults (set IIIa) developed in J163 in the Shelburne Subbasin (Fig. 5.6, line 1400A). These faults merge into the basal detachment along the autochthonous salt, accommodating the growth of isolated diapirs and associated deformation of the sedimentary deposits in the distal parts of the subbasin.

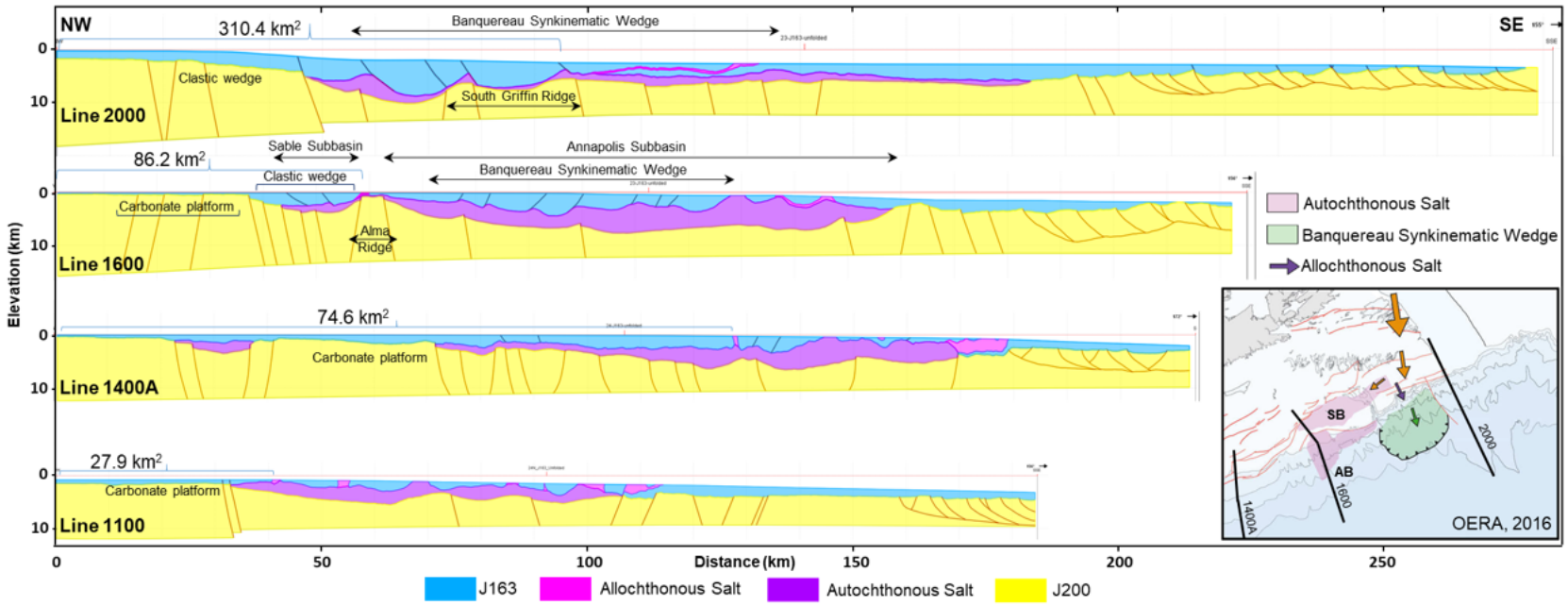

Figure 5.6: The distribution of Jurassic deposits (J163) and allochthonous salt canopy (Banquereau Synkinematic Wedge, BSW) restored along the NW-SE cross-sections. Estimated area of J163 sedimentary rocks (in km^2) accumulated from the NW end of cross-sections to the first mobilized salt bodies are shown by curly brackets. The location of main Triassic salt basins, clastic transport (orange arrows) during the early Jurassic and emplacement of the BSW are shown on the (J163-J150) paleogeography map (after OERA, 2016, chapter 2). The cross-sections are in depth domains, no vertical exaggeration.

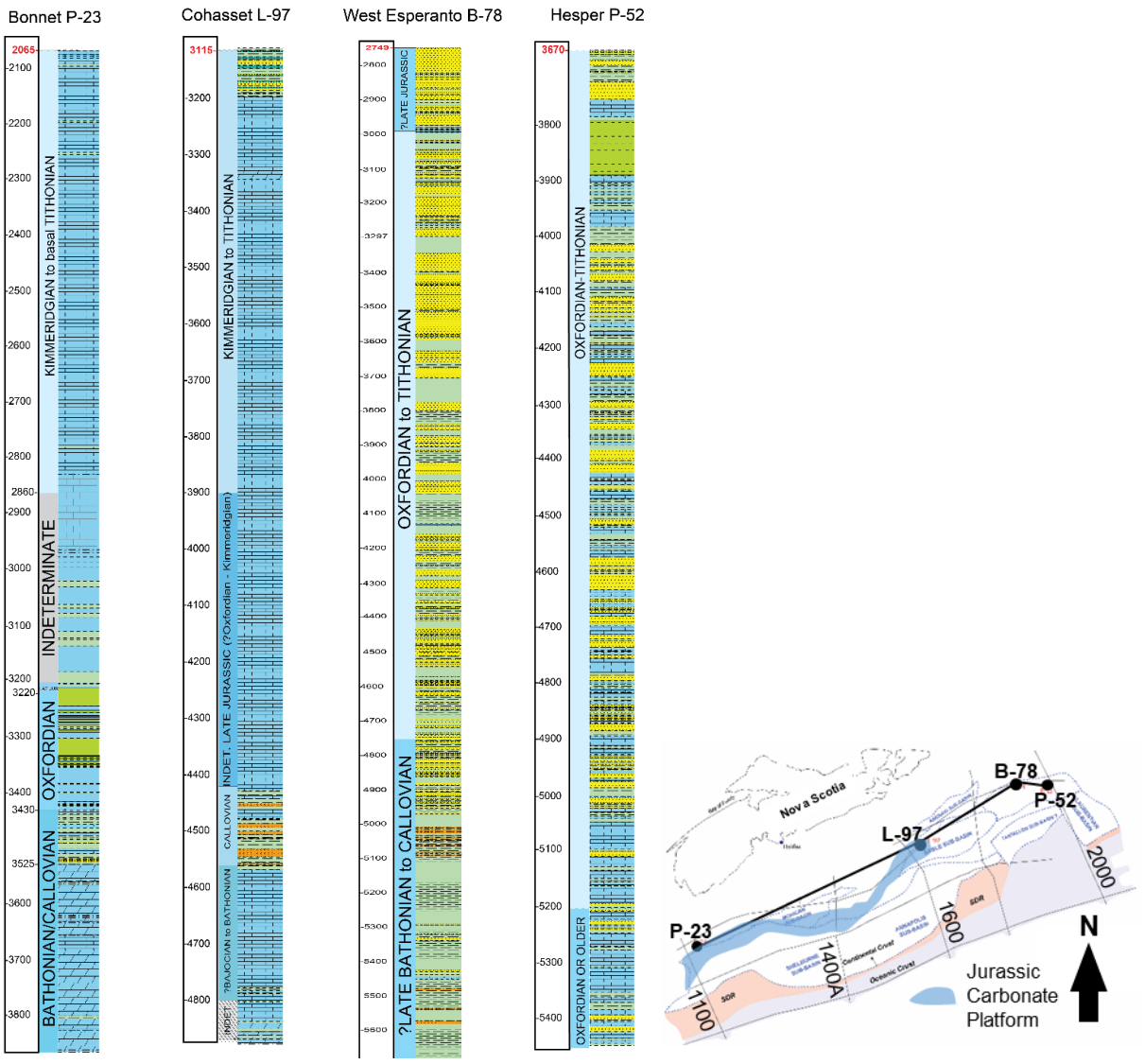

Figure 5.7: Correlation of Middle-Upper Jurassic units in four wells located (from SW to NE) within the present-day shelf along the Nova Scotia margin. The Jurassic units in the southwest are composed of carbonate-dominated deposits, while they consist of mixed clastic-carbonate or clastic-dominated deposits in the northeast. The paleogeography map shows the location of Jurassic LaHave carbonate platform, after (Rodrigues et al, 2022) and SDRs, after (PFA, 2011).

Similar interaction between sediment supply, salt expulsion and post-rift normal fault emplacement continued in J150 and during the Lower Cretaceous (Fig. 5.8). Higher volume of J150, K137 and K130 mostly clastic deposits supplied in the Huron Subbasin resulted in further progression of the thin salt canopy extended toward the SE for about 95 km and the emplacement of the post-rift SE-dipping normal listric faults (set IIIb) of the BSW merging into the basal detachment along the extended canopy (Fig. 5.8, line 2000).

The K137-K130 clastic sedimentary deposits were predominantly supplied at the NE segment of the Nova Scotia margin along the routes directed mostly to the south-southwest and southwest along the margin (Fig. 5.7, map) that resulted in the expulsion of the autochthonous salt from the Sable Subbasin in the form of salt canopy rooted at the Alma Ridge and extended to the SE for ~70 km (Fig. 5.8, line 1600). Post-rift SE-dipping listric normal faults (set IIIa) that merge into the basal detachment at the top of the autochthonous salt were emplaced in the Sable Subbasin (Balvenie Synkinematic Wedge, line 1600) to accommodate salt removal and K137-K130 sediment supply in the basin. Deeper in the basin, isolated salt diapirs started to grow vertically and later developed into the SE-propagating canopies of the Salt Canopy Province. The SE- and NW dipping faults merging in the detachment along the autochthonous salt (set IIIa) along Line 1400A continued to accommodating the growth of isolated diapirs in the deeper parts of the Shelburne Subbasin (Fig. 5.8).

Post-rift planar normal faults (set IV) were developed in the Cretaceous and Tertiary units below the present-day shelf edge along lines 1600 and 2000 (Fig. 5.8). Some of these faults represent the reactivated faults of set III that are merged into the basal detachment along the autochthonous salt and were developed above the South Griffin Ridge in response of salt remobilization and SE-propagation of the thin and extended salt canopy along the NE segment of the margin.

The estimated post-rift extension ranges between 0.25% in the SW segment to 1.02-2.34% in the central and NE segments of the margin (Table 5.4); it is mostly accommodated by post-rift listric normal faults of set III. The faults of set IV contribute to a lower extent, which is higher in the northeastern segment (0.15%) than in the southwestern segment (0.03%) of the margin.

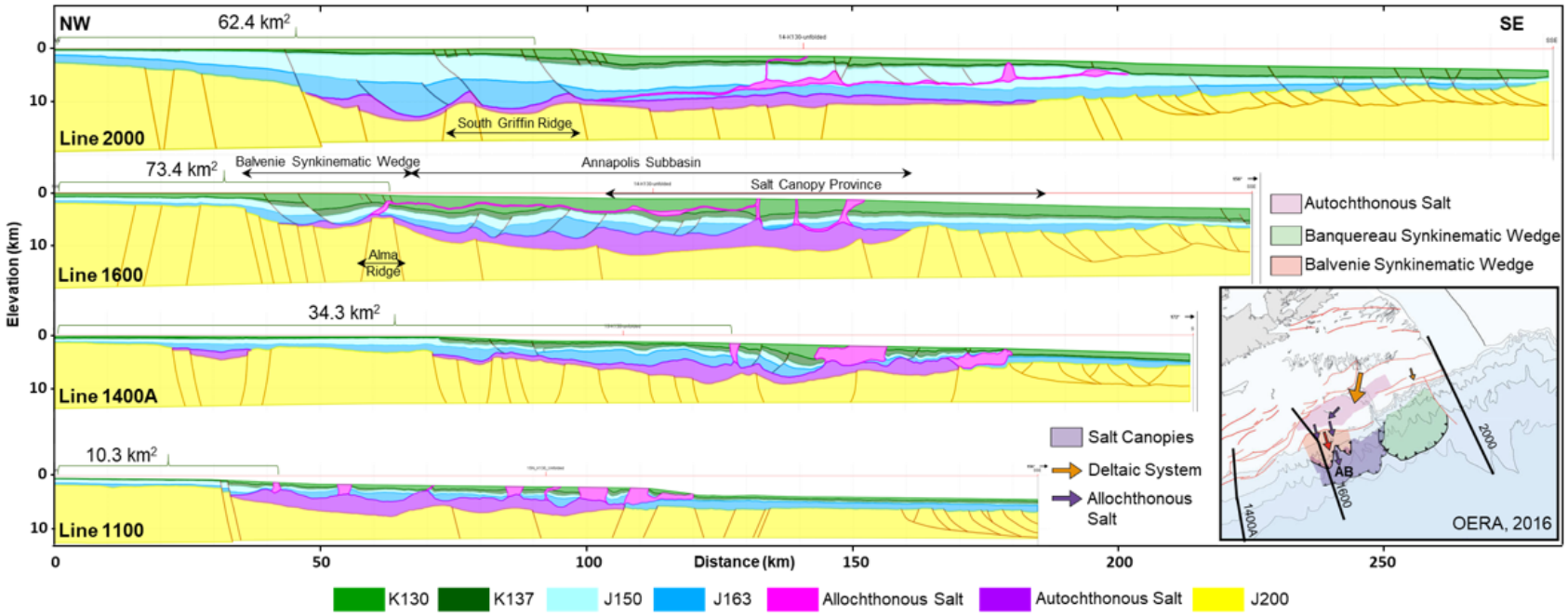

Figure 5.8: The distribution of Jurassic (J163-J150) and Early Cretaceous (K137-K130) deposits and allochthonous salt canopies (Banquereau and Balvenie Synkinematic Wedges) restored along the NW-SE cross-sections are restored to the time K130. Estimated areas of K137 and K130 sedimentary rocks (in km^2) accumulated from the NW end of cross-sections to the first mobilized by salt bodies are shown by curly brackets. The location of main Triassic salt basins, clastic transport during the Early Cretaceous and emplacement of the salt canopies are shown on the (K137-K94) paleogeography map, after (OERA, 2016, chapter 2).The cross-sections are in depth domains, no vertical exaggeration.

Table 5.3: The estimated parameters and characteristics of post-rift tectonic deformation.

Post-rift Phase									
		Extension associated with salt tectonics		Sedimentation			Type of Allochthonous Salt Kinematics	Normal Faulting	Maximum Subsidence (m)
Segments	#Cross-sections	Total Extension (%)	Area of Extension	Composition, Depositional Settings	2D Area (km^2)	Maximum Thickness (km)			
NE (Non-Volcanic)	2000	1.02	J163-T50 extension on the shelf (salt expulsion); J150-K137 extension above salt canopy below the present-day continental slope and in deep basin settings	Jurassic: Deltaic clastic deposits with limestone intercalation; Cretaceous: Deltaic clastic deposits with shale intercalation; Tertiary: Marine clastic deposits.	Jurassic: 310 Cretaceous: 188 Tertiary: 65	Jurassic: 6 Cretaceous: 12 Tertiary: 1	~95-km-wide extended canopies rooted to the autochthonous salt below the present-day shelf break, above the South Griffin Ridge	Set I: SE-dipping syn-sedimentary normal faults offsetting J163-T50 deposits below the shelf (salt expulsion); Set IIIb: SE-dipping normal faults offsetting J150-K137 deposits above salt canopy detachment in deep basin; Set II: reactivated syn-rift listric basement faults offsetting J163-K94 deposits in oceanic domain.	Jurassic: 375 Cretaceous: 630 Tertiary: 255
Central (Volcanic)	1600	2.34	J163-T50 extension below the present-day continental shelf and slope	Jurassic: Carbonate platform at inner shelf, mixture of carbonate and clastic sediments at outer shelf; Cretaceous: Deltaic clastic deposits with shale intercalation; Tertiary: Marine clastic deposits.	Jurassic: 86 Cretaceous: 130 Tertiary: 52	Jurassic: 5 Cretaceous: 6 Tertiary: 2	~155-km-wide extended canopies rooted to the autochthonous salt below the present-day shelf break, above the Alma Ridge	Set IIIa: SE-and NW-dipping syn-sedimentary normal faults offsetting J163-J150 deposits below the shelf and slope, convergent to the root of the salt canopy at the Alma Ridge (salt expulsion); Set IV: SE-dipping syn-sedimentary normal faults offsetting K137-K94 deposits above salt canopy detachment below continental slope; Set V: Small-scale conjugated normal faults offsetting T50-T29 deposits above salt canopies.	Jurassic: 620 Cretaceous: 540 Tertiary: 185
	1400A	0.82	No extension on the shelf, extension in beds (T50-T29) overlying diapirs in deep basin	Jurassic: Carbonate platform within the LaHave Platform; Cretaceous: Mini-basin sedimentation between salt canopies and diapirs in deep basin; Tertiary: Marine clastic deposits.	Jurassic: 75 Cretaceous: 70 Tertiary: 35	Jurassic: 4 Cretaceous: 4 Tertiary: 3	~2-17-km-wide salt diapirs and canopies	Set IIIa: SE-dipping normal faults offsetting J163-K101 deposits above autochthonous salt detachment below continental slope; Set V: Small scale conjugated normal faults offsetting T50-T29 deposits above salt canopies.	Jurassic: 300 Cretaceous: 565 Tertiary: 225
SW (Volcanic)	1100	0.25	No extension on the shelf, extension in beds (T50-T29) overlying diapirs in deep basin	Jurassic: Carbonate platform on the shelf; Jurassic-Cretaceous: Mini-basin sedimentation between salt diapirs; Tertiary: Marine clastic deposits.	Jurassic: 28 Cretaceous: 18 Tertiary: 83	Jurassic: 3 Cretaceous: 4 Tertiary: 3	~1-5-km-wide isolated salt diapirs	Set I: SE-dipping syn-sedimentary normal faults offsetting J163-K94 deposits below the shelf break; Set V: Small scale conjugated normal faults offsetting T50-T29 deposits above salt canopies.	Jurassic: 255 Cretaceous: 575 Tertiary: 305

Note: 2D area (km^2) is a cross-section area estimation. See Table 5.4 for the amount of post-rift extension in the continental and oceanic domains.

The amount and distribution of total subsidence along the restored four cross-sections vary across the margin, increasing basinward for each horizon (Fig. 5.9). Initial rapid thermal subsidence by the end of the rifting stage was followed by slow post-rift thermal subsidence. The subsidence rate ranges from 1.63-2.14 m/Ma on the shelf to 10.1-13.0 m/Ma in the deeper part of the basin (Fig. 5.9). The maximum subsidence rate (12.67-13 m/Ma) is estimated in the oceanic domain of the central segment of the margin. The increase of subsidence from the NW to the SE along the cross-sections is correlated with the applied non-uniform stretching factor (β value) that increases from 1.1 in the NW to 2.2 in the SE along the 2D cross-sections; higher β values result in higher values of subsidence (Chapter 4, sensitivity test).

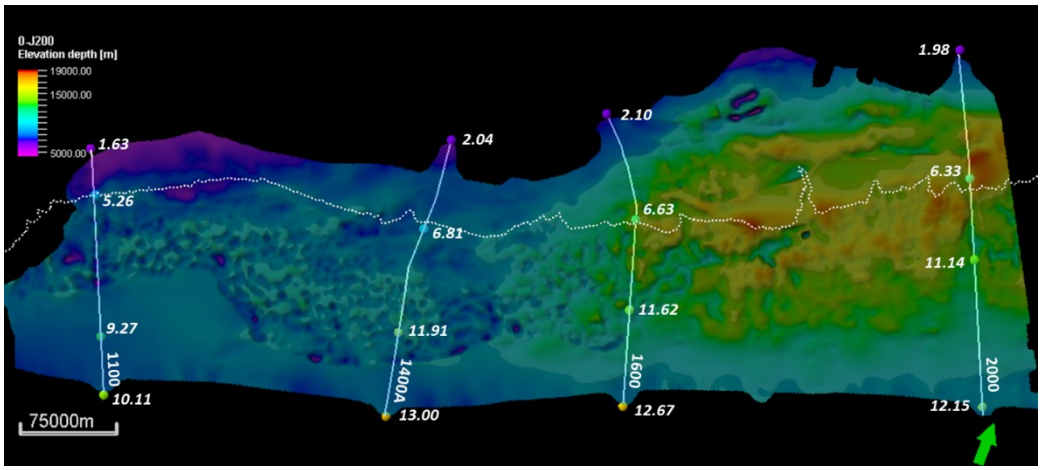

Figure 5.9: The subsidence rates (m/Ma) estimated along four NW-SE lines overlapped with the total thickness map of the Mesozoic-Cenozoic sedimentary cover of the Nova Scotia margin. The white dashed line represents the present-day shelf edge.

The post-rift fault intensity in Jurassic-Cretaceous units below the northeastern present-day shelf and slope reaches 4-6 faults per 20 km in the Huron Subbasin (Fig. 5.9, line 2000) and up to 8 faults per 20 km in the Sable Subbasin (Fig. 5.10, line 1600). Only a few faults are reconstructed in Jurassic-Cretaceous units below the present-day shelf break along lines 1400 and 1100 in the southwestern segment, with fault intensity varying from 1-4 faults per 20 km in the distal parts of the Shelburne Subbasin (Fig. 5.10).

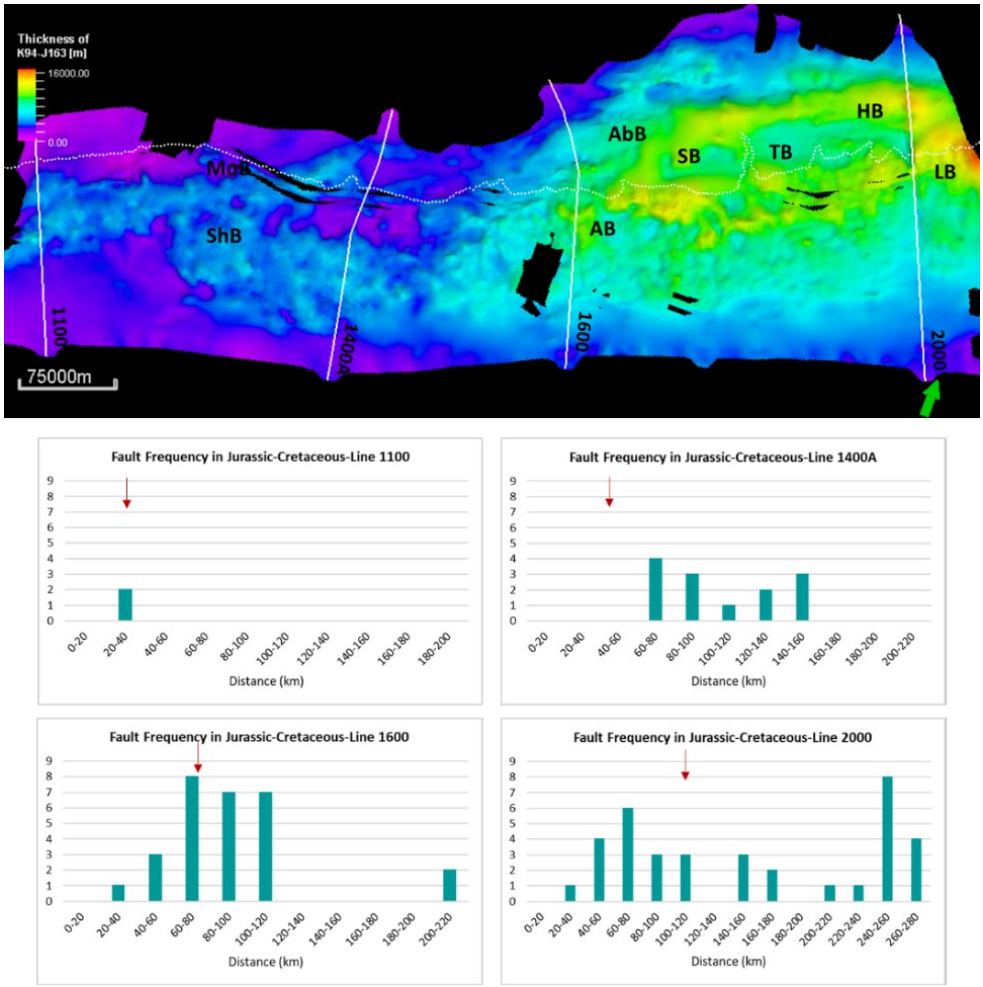

Figure 5.10: The map of the thickness (isopach) of Cretaceous-Jurassic units (K94-J163) of the Nova Scotia margin. The dashed line represents the present-day shelf edge. The graphs illustrate the fault intensity plotted as a function of the distance from the NW end of the lines along four NW-SE lines. Red arrows on graphs depict the location of the shelf break.

The faults in the Tertiary interval (set V) are mostly related to the crestal deformation above the salt diapirs (Figs. 4.14c and 4.14d). The fault intensity in Tertiary deposits is higher in the SW of the margin than it is in the NE (Fig. 5.11). However, as these faults (set V) have very low displacement and their contribution to the extension is low varying from 0.04% in the southwestern segment to 0.02% in the northeastern segment. Overall, the syn-rift faults accommodate a higher ratio of extension compared to the post-rift faults (Table 5.4).

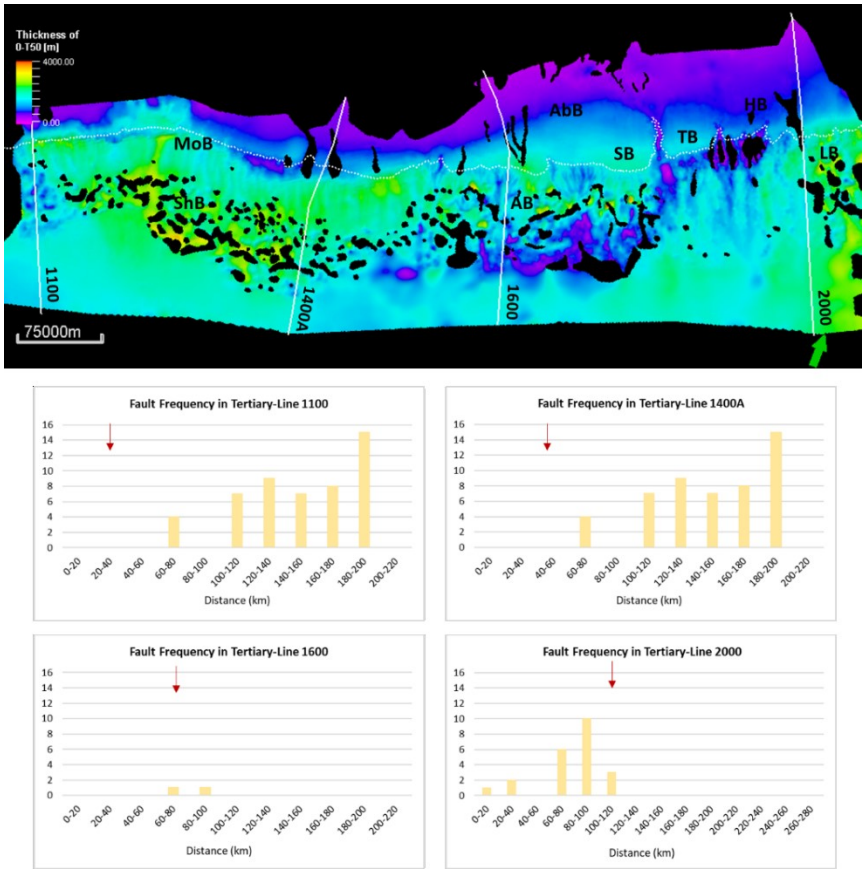

Figure 5.11: The map of the thickness (isopach) of Tertiary units (seabed to K94) of the Nova Scotia margin. The dashed line represents the present-day shelf edge. The graphs illustrate the fault intensity plotted as a function of the distance from the NW end of the lines along four NW-SE lines. Red arrows on graphs depict the location of the present-day shelf break.

Table 5.4: Total, syn- and post-rift extension estimated along four lines in the NE, central and SW segments of the Nova Scotia margin.

Cross-section	Syn-rift Extension Amount, %	Post-rift Extension Amount, %	Total Extension Amount, %
Line 2000	2.70	1.02	3.72
Line 1600	1.19	2.34	3.53
Line 1400A	1.17	0.82	1.99
Line 1100	1.3	0.25	1.55

The decompaction and isostatic rebound are estimated for each mapped stratigraphic unit along the four analyzed cross-sections of the Nova Scotia margin. The highest total isostatic rebound is reconstructed for the J163 strata that varies from 2610 m in the NE segment of the

margin (line 2000) to 580 m in the SW segment (line 1100) (Fig. 5.12, Table 4.5). The amount of isostatic rebound can be correlated with the thickness of the sedimentary cover in the NE segment of the margin (Fig. 5.12). It is highest below the Huron Subbasin along line 2000 and Annapolis Basin along Line 1600, where the thickness of the Jurassic and Cretaceous deposits is the highest.

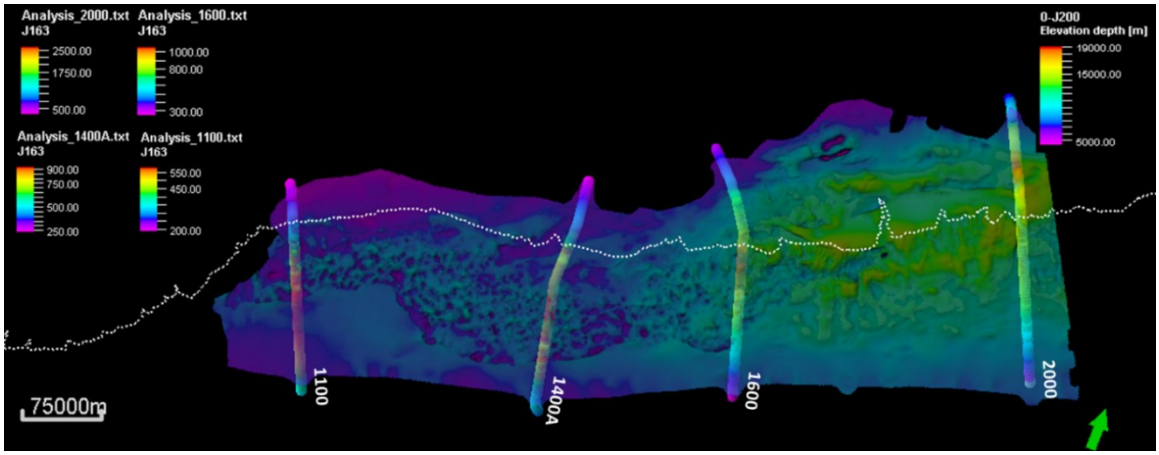

Figure 5.12: The maximum isostatic rebound of J163 reconstructed along four NW-SE lines overlapped with the map of the total thickness of the Mesozoic-Cenozoic sedimentary cover of the Nova Scotia margin. The white dashed line represents the present-day shelf edge.

In contrast, there is no direct correlation between the amount of isostatic rebound and thickness of the sedimentary cover in the SW segment of the margin. The maximum isostatic rebound there can be correlated with the location of the underplated magmatic bodies recognized by the presence of ECMA, which is prominent and wide (55 km) in the SW segment of the Nova Scotia margin (Fig. 5.13, lines 1100, 1400A, and 1600).

The decrease in isostatic rebound from the NE to the SW along the Nova Scotia margin is also correlated with the elastic thickness of the lithosphere (T_e) assumed in this study that consists of 20 km for line 2000 in the NE segment of the margin, 22 km for line 1600 and 25 km for line 1400A in the central segment, and 30 km for line 1100 in the SW segment of the margin. The increase of T_e from 20 km in the NE to 30 km in the SW along the margin is consistent with higher crustal stretching and thinning in the NE as compared to the SW established by the previous results (Funck et al., 2004; Wu et al., 2006; Dehler &Welford, 2013). Higher T_e results

in wider wavelength the lithospheric flexure and lower isostatic rebound (Chapter 4, sensitivity test).

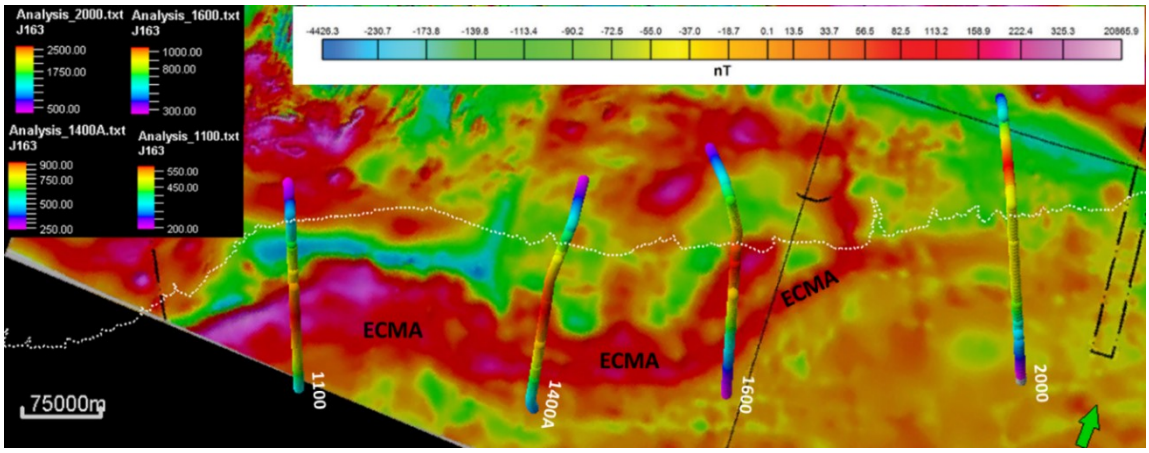

Figure 5.13: The maximum isostatic rebound of J163 reconstructed along four NW-SE lines overlapped with the map of magnetic anomaly data (Miles & Oneschuk, 2016) of the Nova Scotia margin. The white dashed line represents the present-day shelf edge.

5.4. Uncertainties in 2D Kinematic Restoration and Further Studies

The uncertainties in 2D kinematic restoration are related to the modelling parameters, such as compaction curves, value and type (uniform vs non-uniform) of stretching factors (β), and elastic thickness of lithosphere (T_e). The sensitivity tests described in Chapter 4 helped to determine how and in what proportion the selected parameters affect the 2D restoration results and reconstructed paleobathymetry constrained by biostratigraphy data from well reports. For instance, the compaction curves have more significant effects on paleodepth restoration within the younger and porous units (seabed, T29, T50), while it is less pronounced in the older units. The uncertainty in paleodepth estimation was addressed by the constraining of stretching factor as one of the 2D kinematic modeling parameter. The simulated paleodepth of different horizons in a given well location was compared to the paleodepth interpreted from the biostratigraphy data that helped to reduce the uncertainty in assumed values of the stretching factor. The basinward increase of the stretching factor results in more noticeable variations in reconstructed paleodepth in the deep-water settings in comparison with the shelf setting. Application of smaller stretching factors in the oceanic domain results in under-restored horizons and faults. The northeastward decrease of the elastic thickness of the lithosphere (from 30 km to 20 km) along the Nova Scotia margin results in a higher flexural rebound along line 2000 compared to line 1100 (Table 4.5).

The absence of biostratigraphy data in the deep basin settings increases uncertainty to paleodepth simulation results.

This study did not take into account the strike-slip component of the deformation along the Nova Scotia margin. The dextral strike-slip deformation along the margin was accommodated by the W-E 300-km long Late Paleozoic Cobequid-Chedabucto Fault System (Pe-Piper & Piper, 2003; Mawer & White, 1987) that separates the Avalon Terrain in the north from the Meguma Terrain in the south and can be traced in the offshore area (Figs. 2.2, 5.2). The fault was probably active for 150 million years, from about 350 to about 200 million years ago (White & Barr, 2004) and was reactivated during the opening of the Atlantic (Schlische & Withjack, 2003). The left-lateral strike-slip displacement in the northern segment of the Nova-Scotia margin was accommodated by the Newfoundland Transform Fault Zone (NFTZ) and possible secondary faults (Fig. 5.2). It was suggested that there is likely no direct connection of the NFTZ with the Cobequid-Chedabucto Fault (OERA, 2019, chapter 3). A 3D kinematic restoration would be required to consider oblique shear deformation along the passive margin.

Additionally, the 2D kinematic restoration conducted in this study along offshore seismic lines did not allow us to estimate the amount of the onshore uplift of the Nova Scotia margin. The analysis of the onshore uplift can contribute to the simulation of the volume of the eroded material transported to the Scotian Basin through time that is necessary to complete the multidisciplinary project with an objective of a source-to-sink analysis and the prediction of petroleum system elements in the Scotian Basin.

Further studies involving 2D lithosphere-scale numerical modelling using the SOPALE code could be helpful to simulate the geodynamic interaction of the North American lithospheric plate and asthenosphere mantle during the rifting and post-rifting extension along the Nova Scotia margin. The isostatic response of the lithospheric plate during extension and sediment accumulation modelled over the larger area can help to estimate the onshore uplift in addition to other parameters. The published onshore Apatite Fission Track (AFT) data, including Paleozoic samples from outcrop, onshore, and offshore wells, could be used to calibrate simulated results on tectonic uplift.

Chapter 6: Conclusions

This research aimed to interpret what is the connection between the different rifting styles (volcanic versus non-volcanic) and the nature of the post-rift deformation, whether the effects of the rift type persist into passive margin development or not, what factors contribute to the temporal change from one deformation style to another in different parts of the margin, and how much sediment load is required to mobilize salt. In this study, we analyzed how the syn- and post-rift deformation vary across and along the Nova Scotia continental margin through time, evaluated the variations in the amount of tectonic extension and sediment loading with time during the Atlantic opening, and estimated the subsidence, accommodation, isostatic response and decompaction across and along the Nova Scotia passive margin.

The horizon and fault interpretations along the Lithoprobe and Novaspan 2D seismic surveys in time and depth domains were carried out through Petrel Slb to characterize the tectonic structure of the margin.

Five sets of normal faults are identified on seismic profiles along the Nova Scotia continental margin.

- Two sets of the syn-rift faults are recognized in the acoustic basement: the NW- and SE-dipping planar faults merging into the mid-crustal detachment within the continental domain (set I) and SE-dipping listric normal faults that merge into a flat basal detachment at ~15 km of depth in the oceanic domain (set II).
- Three sets of post-rift faults involve the listric faults in the Jurassic and Cretaceous beds (set III) and in the Cretaceous-Triassic beds (sets IV and V).
- The post-rift faults of set IIIa developed in the Huron, Sable and Annapolis Subbasins below the present-day shelf and slope of the NE segment of the margin and in the distal parts of the Shelburne Subbasin in the central segment of the margin. These faults (set IIIa) merge into basal detachments along the top of the autochthonous salt and dip to the SE or NW. The post-rift faults of set IIIb merge into the top of the allochthonous thin extended canopy and dip to the SE, accommodating the SE-ward salt propagation.
- The post-rift SE-dipping growth faults of set IV offset the Cretaceous and Tertiary clastic units below the present-day shelf and/or continental slope in the NE and central segments

of the margin. These faults accommodate the accumulation of progradational clastic wedges and control their thickness.

- The post-rift faults of set V involve NE-SW-striking small-scale conjugated planar normal faults that resulted from crestal deformation of Tertiary deposits above the isolated salt diapirs in the southwestern segment of the margin.

The 2D kinematic restorations along four NW-SE-oriented cross-sections were conducted in MOVE Petroleum Experts Ltd. The emplacement of post-rift normal faults in the Nova Scotia margin was controlled by the interaction of several factors, including the amount and localization of extension and subsidence during the syn-rift deformation, volume, composition and direction routes of sediment supply and paleogeographic settings, and salt tectonics.

- The estimated amount of total extension varies across the margin, gradually increasing from 1.55% in the SW to 3.72% in the NE. The syn-rift extension ranges between 1.17-1.30% in the SW to 2.7% in the NE of the margin. The listric normal faults in the oceanic domain accommodate from 56% to 86% of total syn-rift extension. The post-rift extension ranges between 0.25% in the SW segment to 1.02-2.34% in the central and NE segments of the margin; it is mostly accommodated by listric normal faults of set III.
- The estimated maximum subsidence of J200 decreases from 1035-1200 m in the northeastern and central segments of the margin to 775 m in the southwestern segment of the margin. The higher amount of extension and subsidence localized below the present-day shelf in the NE segment of the Nova Scotia margin resulted in higher thickness of salt in the Huron Subbasin in the NE segment compared to the Sable, Annapolis, Mohican and Shelburne Subbasins in the central and SW segments of the margin.
- The supply of elevated amount of clastic material through the southward-directed deltaic fluvial systems into the NE segment of the Scotian Basin during the early post-rift stage of J163 resulted in accumulation of predominantly clastic- or mixed clastic-carbonate deposits of in the Huron, Sable and Annapolis Subbasins in the NE and central segments of the margin. The J163 carbonate accumulation was predominant within the LaHave platform in the southwest and central segments of the margin.
- The gravitational loading of the high-volume predominantly clastic Jurassic and Cretaceous units in the Huron and Sable Subbasins (NE and central segments of the

margin) triggered salt remobilization and expulsion of an extended (~100 km) thin salt canopy that progressed to the SE. The salt remobilization resulted in the associated emplacement of a series of post-rift normal faults of sets IIIa and IIIb merging into the top of the extended salt canopies forming the Banquereau and Balvenie Synkinematic Wedges in the NE and central segments of the Nova Scotia margin. The predominantly shallow-water carbonate sedimentation within the LaHave Platform in the SW segment of the margin was not favorable for salt remobilization close to the shore, thus isolated salt diapirs developed in the deeper part of the Shelburne Subbasin.

- The estimated values decompaction and isostatic rebound are the highest for the J163 strata and vary from 2610 m in the NE segment of the margin to 580 m in the SW segment. The amount of isostatic rebound can be correlated with the thickness of the sedimentary cover in the NE segment of the margin. The maximum isostatic rebound in the SW segment of the margin can likely be correlated with the location of the underplated magmatic bodies recognized by the presence of ECMA.

The input parameters of the modelling influence the 2D kinematic reconstruction results, therefore require validation. The porosity-versus-depth curve used to restore depositional thickness in shallow intervals affect the amount of decompaction of young deposits with an impact on restoration of older stratigraphic intervals. The applied non-uniform stretching factor (β) increases from 1.1 in the NW to 2.2 in the SE along the 2D cross-sections; higher β values result in higher values of subsidence. The decrease in isostatic rebound from the NE to the SW is correlated with the applied values of the elastic thickness of the lithosphere T_e that increase from 20 km in the NE highly stretched segment to 30 km in the SW less stretched segment of the margin. Higher T_e results in wider wavelength of lithospheric flexure and lower isostatic rebound. Comparing of the simulated paleodepths in the restoration models with the paleodepths interpreted from biostratigraphy helped to validate the 2D kinematic restoration results.

References

Agostini, A., Corti, G., Zeoli, A., & Mulugeta, G. (2009). Evolution, pattern and partitioning of deformation during oblique continental rifting: Inferences from lithospheric-scale centrifuge models. *Geochemistry, Geophysics, Geosystems*, *10*, Q11015. doi:10.1029/2009GC002676.

Albertz, M., Beaumont, C., Shimeld, J. W., Ings, S. J., & Gradmann, S. (2010). An investigation of salt tectonic structural styles in the Scotian Basin, offshore Atlantic Canada: 1. Comparison of observations with geometrically simple numerical models. *Tectonics*, *29*, TC4017. https://doi.org/10.1029/2009TC002539

Allen, P.A., & Allen, J.R. (2005) Basin Analysis, Principles and Applications. Blackwell Publishing, Hoboken.

Alsop, L.E., & Talwani, M. (1984). The east coast magnetic anomaly. *Science*, *226* (4679), 1189-1191.

Audet, P. (2014). Toward mapping the effective elastic thickness of planetary lithospheres from a spherical wavelet analysis of gravity and topography, *Physics of the Earth and Planetary Interiors*, *226*, 48-82.

Baldwin, B., & Butler, C.O. (1985). Compaction curves: *American Association of Petroleum Geologists Bulletin*, *69*, 622-626.

Barss, J. S., Bujak, J. P., Wade, J. A., & Williams, G. L. (1980). Age, stratigraphy, organic matter type and color, and hydrocarbon occurrences in forty-seven wells offshore eastern Canada. Geological Survey of Canada Open File Report No: 714.

Basile, C., Mascle, J., & Guiraud, R. (2005). Phanerozoic geological evolution of the Equatorial Atlantic domain. *Journal of African Earth Sciences*, *43*(1-3), 275-282.

Benson, R. H., & Doyle, R. G. (1988). Early Mesozoic rift basins and the development of the United States middle Atlantic continental margin (W., Manspeizer, Ed.). Triassic-Jurassic Rifting, Continental Breakup and the Origin of the Atlantic Ocean Passive Margins, Part A: New York, Elsevier, 99-127.

Benson, R.A. (2003). Age estimates of the seaward-dipping volcanic wedge, earliest oceanic crust, and earliest drift-stage sediments along the North American Atlantic Continental Margin (W.E., Hames, J.G, McHone, P., Renne, C., Ruppel, Eds.). The Central Atlantic Magmatic Province: Insights from Fragments of Pangea. *American Geophysical Union Monograph*, *136*, 61-75.

Biari, Y., Klingelhoefer, F., Franke, D., Funck, T., Loncke, L., Sibuet, J., Basile, C., Austin, J. A., Rigoti, C. A., Sahabi, M., Benabdellouahed, M., & Roest, W. R. (2021). Structure and evolution of the Atlantic passive margins: A review of existing rifting models from wide-angle seismic data and kinematic reconstruction. *Marine and Petroleum Geology*, *126*, 1-43.

Bodine, J. H., Steckler, M. S., & Watts, A.B. (1981). Observations of flexure and the rheology of the oceanic lithosphere. *Journal Geophysical Research*, *86*, 3695-3707.

Bowman, S., Pe-Piper, G., Piper, D., J.W., Fensome, R.A., & King, E.L. (2012). Early Cretaceous volcanism in the Scotian Basin. *Canadian Journal Earth Science*, *49*, 1523-1539.

Dehler, S. A. & Keen, C. E. (1993). Effects of rifting and subsidence on thermal evolution of sediments in Canada's east coast basins. *Canadian Journal of Earth Sciences*, *30*(9), 1782–1798. https://doi.org/10.1139/e93-158

Dehler, S. A. (2010). Initial rifting and break-up between Nova Scotia and Morocco: An examination of new geophysical data and models. In Central and North Atlantic Conjugate Margins Conference, Lisbon.

Dehler, S.A. (2012). Initial rifting and breakup between Nova Scotia and Morocco: insight from new magnetic models. *Canadian Journal of Earth Sciences*, *49*, 1385-1394. https://doi.org/10.1139/e2012-073

Dehler, S. A. & Welford, K. (2013). Variations in rifting style and structure of the Scotian margin, Atlantic Canada, from 3D gravity inversion. *Geological Society London Special Publications*, *369*, 289-300. DOI:10.1144/SP369.11

Deptuck, M. E. (2011). Proximal to distal postrift structural provinces of the western Scotian Margin, offshore Eastern Canada: Geological context and parcel prospectivity for Call for Bids NS11-1. CNSOPB Geoscience Open File Report, 42.

Deptuck, M. E., Kendell, K., Brown, D. E., & Smith, B. M. (2014). Seismic stratigraphic framework and structural evolution of the eastern Scotian Slope: Geological context for the NS14-1 Call for Bids area, offshore Nova Scotia Canada-Nova Scotia Offshore Petroleum Board, Geoscience Open File Report 2014-001MF, 58.

Deptuck, M. E., & Kendell, K. L. (2017). A review of Mesozoic-Cenozoic salt tectonics along the Scotian margin, eastern Canada (J.I. Soto, J. Flinch, G. Tari, Eds.). Permo-Triassic Salt

Provinces of Europe, North Africa and the Atlantic Margins: Tectonics and Hydrocarbon Potential, Elsevier, 287-312.

Dickinson, G. (1953). Geological aspects of abnormal reservoir pressures in Gulf Coast Louisiana: *The American Association of Petroleum Geologists Bulletin*, *37*, 410-432.

Egan, S.S., Buddin, T.S., Kane, S.J., & Williams, G.D. (1997). Three-dimensional modelling and visualisation in structural geology: new techniques for the restoration and balancing of volumes. Proceedings of the 1996 Geoscience Information Group Conference on Geological Visualisation, *Electronic Geology*, 67-82.

Eldholm, O., & Grue, K. (1994). North Atlantic volcanic margins: dimensions and production rates. *Journal of Geophysical Research: Solid Earth*, *99*, 2955-2968. https://doi.org/10.1029/93JB02879

Eliuk, L. S. (1978). The Abenaki Formation, Nova Scotia Shelf, Canada - A Depositional and Diagenetic Model for a Mesozoic Carbonate Platform. *Bulletin of Canadian Petroleum Geology*, *26*(4), 424–514.

Eliuk, L.S., & Levesque, R. (1989). Earliest Cretaceous sponge reef mound Nova Scotia shelf (Shell Demascota G-32) (H. H. J. Geldsetzer, N.P. James, and G.E. Tebbutt, Eds.). Reefs, Canada and Adjacent Areas. *Canadian Society of Petroleum Geologists Memoir*, *13*, 713-720.

Funck, T., Jackson, H. R., Louden, K. E., Dehler, S. A, & Wu, Y. (2004). Crustal structure of the northern Nova Scotia rifted continental margin (Eastern Canada). *Journal of Geophysical Research: Solid Earth*, *109* (B9), 1-19. https://doi.org/10.1029/2004JB003008

Geoffroy, L., Burov, E.B., & Werner, P. (2015). Volcanic passive margins: another way to break up continents, *Nature: Scientific Reports*, Number 14828.

Gibbs, A. (1983). Balanced cross section construction from seismic sections in areas of extensional tectonics, *Journal of Structural Geology*, *5*(2), 153-160.

Given, M. M. (1977). Mesozoic and early Cenozoic geology of Offshore Nova Scotia. *Bulletin of Canadian Petroleum Geology*, *25*(1), 63-91.

Gradstein, F. M., Oggs, J. G., & Smith, A. G. (2004). A geologic time scale 2004. Cambridge: Cambridge University Press. https://doi.org/10.1017/CBO9780511536045

Greenberg, M. L., & Castagna, J. P. (1992). Shear-Wave Velocity Estimation in Porous Rocks: Theoretical Formulation, Preliminary Verification and Applications. *Geophysical*

Prospecting, *40*, 195-209. https://doi.org/10.1111/j.1365-2478.1992.tb00371.x

Grist A.M., Reynolds P.H., Zentilli M., and Beaumont C. (1992). The Scotian Basin offshore Nova Scotia: thermal history and provenance of sandstones from apatite fission track and $^{40}Ar/^{39}Ar$ data. *Canadian Journal of Earth Sciences*, *29*(5), 909–924.

Groshong, R. H. (2006). Structural validation, restoration, and prediction. In: 3-D Structural Geology. Springer, Berlin, Heidelberg.

Hames, W. E, Renne, P. R., & Ruppel, C. (2000). New evidence for geologically instantaneous emplacement of earliest Jurassic Central Atlantic magmatic province basalts on the North American margin. *Geology*, *28*(9), 859-862. https://doi.org/10.1130/00917613(2000)28<859:NEFGIE>2.0.CO;2

Hellinger, S.J. & Sclater, J.G. (1983). Some comments on two-layer extensional models for the evolution of sedimentary basins. *Journal of Geophysical Research*, *88*, 8145-8349. https://doi.org/10.1029/JB088iB10p08251

Hinz K., Eldholm O., Block M., & Skogseid J., (1993). Evolution of N. Atlantic volcanic continental margins (J.R Parker, Ed.). Petroleum geology of Northwest Europe: Proceeding 4th Conference Geological Society of London, 901-913.

Holbrook, W. S., Purdy, G. M., Sheridan, R. E., Glover III, L., Talwani, M., & Hutchinson, D. (1994a), Seismic structure of the U.S. Mid-Atlantic continental margin, *Journal of Geophysical Research*, *99* (17), 871– 891.

Ings, S. J., & Shimeld, J. W. (2006). A new conceptual model for the structural evolution of a regional salt detachment on the northeast Scotian margin, offshore Eastern Canada, *AAPG Bulletin*, *90*, 1407-1423. DOI:10.1306/04050605159

Jansa, L. F., & Wade, J. A. (1975). Geology of the continental margin off Nova Scotia and Newfoundland (W. J. M. van der Linden, & J. A. Wade, Eds.). Offshore Geology of Eastern Canada, *Geological Survey of Canada*, 51-106.

Jansa, L. F., Pe-Piper, G., Robertson, P. B., and Friedenreich, O. (1989). Montagnais: A submarine meteorite impact structure on the Scotian Shelf, eastern Canada. *Bulletin of the Geological Society of America*, *101*, 450-463.

Kane, S.J., Williams, G.D., Buddin, T.S., Egan, S.S., & Hodgetts, D. (1997). Flexural-slip based restoration in 3D, a new approach. AAPG Annual Convention Official Program, A58.

Karner, G. D., and Watts, A. B. (1982). On isostasy at Atlantic-type continental margins, *Journal*

of Geophysical Research, *87*, 2923-2948.

Keen, C.E., & Dehler, S.A. (1993). Stretching and subsidence: Rifting of conjugate margins in the North Atlantic region. *Tectonics*, *12*, 1209- 1229.

Keen, C. E., & Potter, D. P. (1995a). The transition from a volcanic to nonvolcanic rifted margin off eastern Canada. *Tectonics*, *14* (2), 359-371.

Keen, C. E., & Potter, D. P. (1995b). Formation and evolution of the Nova Scotian rifted margin: Evidence from deep seismic reflection data. *Tectonics*, *14* (4), 918-932.

Kelemen, P. B., & Holbrook, S. (1995). Origin of thick, high-velocity igneous crust along the U.S. East Coast Margin. *Journal of Geophysical Research Atmospheres*, *1001*(B6), 10077-10094. DOI: 10.1029/95JB00924

Kidston, A. G., Brown, D. E., Smith, B. M., & Altheim, B. (2005). The Upper Jurassic Abenaki Formation offshore Nova Scotia: A Seismic and Geologic Perspective. Canada-Nova Scotia Offshore Petroleum Board, Halifax, 208.

Klein, F. (1962). Triassic sedimentation, Maritime Provinces, Canada. *Geological Society of America Bulletin*, *73*, 1127-1146.

Klitgord, K. D., & Schouten, H. (1986). Plate Kinematic of the Central Atlantic. In geology of the North Atlantic (P.R. Vogt and B. E. Tucholke, Eds.). Geological Society of America, 351-378.

Louden, K., Wu, Y., & Tari, G. (2012). Systematic variations in basement morphology and rifting geometry along the Nova Scotia and Morocco conjugate margins. *Geological Society London Special Publications*, *369* (1), 267-287. DOI: 10.1144/SP369.9

Macaulay, E. (2017). A new approach to backstripping and sequential restoration in subsalt sediments. *AAPG Bulletin*, *101*, 1385-1394.

MacLean, B. C., Edwards, A., McAlpine, K. D., & Wade, J. A. (1989). The enigmatic Avalon Unconformity, Geological Survey of Canada Open File 2099, 1-5.

MacLean, B.C., & Wade, J.A. (1992). Petroleum geology of the continental margin south of the islands of St. Pierre and Miquelon, offshore Eastern Canada. *Bulletin of Canadian Petroleum Geology*, *40*, 222 -253.

MacLean, B.C., & Wade, J.A. (1993). East Coast Basin Atlas Series: Seismic markers and stratigraphic picks in the Scotian Basin wells, *Geological Society of Canada*, East Coast Basin Atlas Series, 276. https://doi.org/10.4095/221116

Mawer, C. K., & White, J. C. (1987). Sense of displacement on the Cobequid–Chedabucto fault system, Nova Scotia, Canada. *Canadian Journal of Earth Sciences*, *24* (2), 217-223.

McHone, J. G. (2000). Non-plume magmatism and tectonics during the opening of the central Atlantic Ocean. *Tectonophysics*, *316*, 287-296.

McIver, N. L. (1972). Cenozoic and Mesozoic stratigraphy of the Nova Scotia Shelf. *Canadian Journal of Earth Sciences*, *9*, 54-70.

McKenzie, D. (1978). Some remarks on development of sedimentary basins. *Earth and Planetary Science Letters*, *40*, 25-32.

Miles, W., & Oneschuk, D. (2016). Magnetic anomaly map, Canada. Geological Survey of Canada, Open File 7799. https://doi.org/10.4095/297337

OERA (Offshore Energy Research Association) (2016). Central Scotian Slope Atlas.

OERA (Offshore Energy Research Association) (2019). Laurentian Subbasin Study, chapter 3: Regional Tectonic Context.

OETR (Offshore Energy Technical Research). (2009). Play Fairway Analysis.

Olsen, P. E., Kent, D.V., Cornet, B., Witte, W.K, & Schlische, R.W. (1996). High-resolution stratigraphy of the Newark rift basin (Early Mesozoic, Eastern North America). *Geological Society of America Bulletin*, *108*, 40-77.

Parthasarathy, R., Merker, A., Tremolada, F., & Gogin, I. (2017). Routine and wellsite biostratigraphic analysis of the Monterey Jack E-43/E-43A Wells, License EL 2424, Shelburne Basin, Offshore Nova Scotia, Canada. Completed by RPS Energy for Shell Canada Energy. Report No. ECB10941.3.

Parsons, M. G. (1975). The Geology of the Laurentian Fan and the Scotia Rise. *Canadian Society of Petroleum Geology Memoir*, 155-167.

Pascucci, V., Gibling, M. R., & Williamson, M. A. (2000). Late Paleozoic to Cenozoic history of the offshore Sydney Basin, Atlantic Canada. *Canadian Journal of Earth Science*, *37*, 1143–1165.

Pe-Piper, G., Jansa, L.F., & Lambert, R .S. J. (1992). Early Mesozoic magmatism on the eastern Canadian margin: Petrogenetic and tectonic significance, in Eastern North American Mesozoic Magmatism (J. H. Puffer and P. C. Ragland, Eds.). 13-36, *Geological Society of America Special*, 268.

Pe-Piper, G., & Jansa, L.F. (1999). Pre-Mesozoic basement rocks offshore Nova Scotia, Canada:

new constraints on the origin and Paleozoic accretionary history of the Meguma terrane. *Bulletin of the Geological Society of America*, *111*, 1773-1791.

Pe-Piper, G., & Piper, D. J. W. (2002). The Igneous Rocks of Greece. The Anatomy of an Orogen. Cambridge University Press, 357.

Pe-Piper, G., & Piper, D. J. (2003). A synopsis of the geology of the Cobequid Highlands, Nova Scotia. *Atlantic Geology*, *38* (2-3), 145–160.

PFA (Play Fairway Analysis) Offshore Nova Scotia, (2011). Nova Scotia Department of Natural Resources and Renewables, 88-11-0004-01, 349.

Roberts, A. M., Kusznir, N. J., Yielding, G., & Styles, P. (1998). 2D flexural backstripping of extensional basins; the need for a sideways glance. *Petroleum Geoscience*, *4*, 327-338.

Rodrigues, S., Deptuck, M.E., Kendell, K.L., Campbell, C., & Hernández-Molina, F.J. (2022). Cretaceous to Eocene mixed turbidite-contourite systems offshore Nova Scotia (Canada): Spatial and temporal variability of down- and along-slope processes. *Marine and Petroleum Geology*, *138*, 1-26.

Royden, L., & Keen, C. E. (1980). Rifting process and thermal evolution of the continental margin of Eastern Canada determined from subsidence curves. *Earth and Planetary Science Letters*, *51* (2), 343-361. https://doi.org/10.1016/0012-821X(80)90216-2

Sandwell, D. T., Müller, R. D., Smith, W. H. F., Garcia, E., & Francis, R. (2014). New global marine gravity model from CryoSat-2 and Jason-1 reveals buried tectonic structure. *Science*, *346* (6205), 65-67. DOI: 10.1126/science.1258213

Schlische, R.W., Withjack, M.O., & Olsen, P.E. (2003). Relative Timing of CAMP, Rifting, Continental Breakup, and Basin Inversion: Tectonic Significance (Hames, W.E.; McHone, J.G.; Renne, P.; Ruppel, C., Eds.). The Central Atlantic Magmatic Province: Insights from Fragments of Pangea, *American Geophysical Union Monograph*, *136*, 33-59.

Sclater, J. G., & Christie, P. A. F. (1980). Continental Stretching - an explanation of the Post-Mid-Cretaceous subsidence of the central North-Sea Basin. *Journal of Geophysical Research*, *85*, 3711-3739.

Shaw, J., Piper, D. J. W., Fader, G. B. J., King, E. L., Todd, B. J., Bell, T., Batterson, M. J., & Liverman, D. J. E. (2006). A conceptual model of the deglaciation of Atlantic Canada. *Quaternary Science Reviews*, *25*, 2059-2081.

Shimeld, J. (2004). A comparison of salt tectonic sub-provinces beneath the Scotian slope and

Laurentian Fan, in GCSSEPM Foundation Bob F. Perkins Research Conference: Annual. 24th 2004: Salt-Sediment Interactions and Hydrocarbon Prospectivity: Concepts, Applications and Case Studies for the 21st Century (P. J. Post, Ed.). Gulf Coast Section. SEPM, Houston, Texas.

Sibuet J. C., Rouzo, S., & Srivastava, S. (2012). Plate tectonic reconstructions and paleogeographic maps of the central and North Atlantic oceans. *Canadian Journal of Earth Sciences*, *49*, 1395–1415.

Simm, R., & Bacon, M. (2014). Seismic Amplitude: An Interpreter's Handbook, Cambridge University Press. https://doi.org/10.1017/CBO9780511984501

Smith, W. H. F., & Sandwell, D. T. (1997). Global seafloor topography from satellite altimetry and ship depth soundings. *Science*, *277*, 1957-1962.

Talwani, M., & Abreu, V. (2000). Inferences regarding initiation of oceanic crust formation from the US East Coast margin and conjugate South Atlantic margins. *Geophysical Monograph*, *115*, 211– 234.

Thybo, H.T., Janik, T., Omelchenko, V.D., Grad, M., Garetsky, R.G., Belinsky, A.A., Karatayev, G.I., Zlotski, G., Knudsen, M.E., Sand, R., Yliniemi, J., Tiira, T., Luosto, U., Komminaho, K., Giese, R., Guterch, A.,. Lund, C.-E.O., Kharitonov, M., Ilchenko, T., Lysynchuk, D.V., Skobelev, M., & Doody, J.J. (2003). Upper lithospheric seismic velocity structure across the Pripyat Trough and the Ukrainian Shield along the EUROBRIDGE'97 profile. *Tectonophysics*, *371*, 41-79.

Turcotte, D. L., & Schubert, G. (1982). Geodynamics, John Wiley, 450.

van Staal, C. R., Whalen, J. B., Valverde-Vaquero, P., Zagorevski, A., & Rogers, N. (2009). PreCarboniferous, episodic accretion-related, orogenesis along the Laurentian margin of the northern Appalachians (J. B, Murphy, J. D., Keppie, and A. J. Hynes, Eds.). Ancient Orogens and Modern Analogues. Geological Society of London Special Publications, 327, 271-316.

van Staal, C. R., & Barr, S. M. (2012). Lithospheric architecture and tectonic evolution of the Canadian Appalachians. In Tectonic Styles in Canada Revisited: The Lithoprobe perspective. Edited by J.A. Percival, F.A. Cook and R.M. Clowes. *Geological Association of Canada Special Paper*, *49*, 1-55.

Wade, J., & MacLean, B. (1990). The geology of the southeastern margin of Canada. In Geology

of the continental margin of eastern Canada (J. Keen & L. Williams, Eds.). Geological Survey of Canada, Geology of Canada. pp. 167–238. Ottawa, Geological Survey of Canada.

Wade, J.A., MacLean, B.C., & Williams, G.L. (1995). Mesozoic and Cenozoic stratigraphy, eastern Scotian Shelf: new interpretations. *Canadian Journal of Earth Sciences*, *32*, 1462-147.

Waldron, J. W. F., McCausland, P. J. A., Barr, S. M., Schofield, D. I., Reusch, D., & Wu, L. (2022). Terrane history of the Iapetus Ocean as preserved in the northern Appalachians and western Caledonides. *Earth-Science Reviews*, *233*, 1-75.

Watts, A.B., & Steckler, M.S. (1979). Subsidence and eustasy at the continental margin of Eastern North America. Maurice Ewing Symposium, Series 3, AGU, 218-234.

Watts, A. B. (1981). The US Atlantic continental margin: subsidence history, crustal structure, and thermal evolution. American Association Petroleum Geologists Education Series, 129, 1-75.

Watts, A. B. (2001). Isostasy and flexure of the lithosphere. Cambridge University Press, 265-280.

Weston, J. F., MacRae, R. A., Ascoli, P., Cooper, M. K. E., Fensome, R. A., Shaw, D., & Williams, G. L. (2012). A revised biostratigraphic and well-log sequence-stratigraphic framework for the Scotian Margin, offshore eastern Canada. *Canadian Journal of Earth Sciences*, *49* (12), 1417-1462. https://doi.org/10.1139/e2012-070

White, C. E., & Barr S. M. (2004). Age and petrochemistry of mafic sills in rocks of the northwestern margin of the Meguma Terrane, Bear River -Yarmouth area of southwestern Nova Scotia, In Mineral Resources Branch. Nova Scotia Department of Natural Resources, in Report of Activities 2003, 97-117.

Withjack, M. O., & Schlische, R. W. (2005). A Review of Tectonic Events on the Passive Margin of Eastern North America. Basins (Paul J. Post, Norman C. Rosen, Donald L. Olson, Stephen L. Palmes, Kevin T. Lyons, Geoffrey B. Newton, Eds.). Petroleum Systems of Divergent Continental Margin, SEPM Society for Sedimentary Geology, 25. https://doi.org/10.5724/gcs.05.25.0203

Wu, Y., Louden, K. E., Funck, T., Jackson, H. R., & Dehler, S. (2006). Crustal structure of the central Nova Scotia margin off Eastern Canada. *Geophysical Journal International*, *166*, 878-906. doi: 10.1111/j.1365-246X.2006.02991.x

Appendix A

	Well Name	MD (m)	Well Top	Checkshot	VSP	GR	DT	RHOB	Resistivity	Caliper
1	Acadia K-62*	5287	✓			✓	✓	✓	✓	✓
2	Albatross B-13*	4046	✓		✓	✓	✓	✓	✓	✓
3	Alma 1	4851				✓	✓		✓	
4	Alma 2	3790				✓	✓	✓	✓	✓
5	Alma 3	3380				✓	✓	✓	✓	✓
6	Alma 4	3985				✓			✓	✓
7	Alma 4A	4329				✓	✓	✓	✓	
8	Alma F-67*	5054	✓	✓	✓	✓	✓	✓	✓	✓
9	Annapolis B-24	3495				✓			✓	
10	Annapolis G-24*	6182	✓	✓		✓	✓	✓	✓	✓
11	Aspy D-11/D-11A	7400	✓			✓	✓	✓	✓	✓
12	Balvenie B-79*	4750	✓	✓		✓	✓	✓	✓	✓
13	Bandol 1	4046								
14	Banquerau C-21*	4985	✓			✓	✓	✓	✓	✓
15	Bonnet P-23*	4336	✓	✓		✓	✓	✓		
16	Chebucto K-90*	5233	✓	✓		✓	✓	✓	✓	✓
17	Cheshire L-97/L-97A*	7068	✓		✓	✓	✓	✓	✓	✓
18	Cohasset L-97*	4872	✓	✓		✓	✓	✓	✓	✓
19	Cree E-35	1920	✓			✓	✓	✓	✓	✓
20	Cree I-34	3945				✓	✓	✓	✓	✓
21	Crimson F-81	6676	✓	✓		✓	✓	✓	✓	✓
22	Crow F-52*	1493	✓		✓	✓	✓	✓	✓	✓
23	Dauntless D-35*	4741	✓	✓		✓	✓	✓	✓	✓
24	Dominion J-14	3700				✓		✓	✓	✓
25	Dominion J-14A	4440				✓	✓	✓	✓	✓
26	East Wolverine G-37	6857								
27	Emma N-03	3352	✓			✓		✓	✓	✓
28	Evangeline H-98*	5035	✓	✓		✓	✓	✓	✓	✓
29	Fox I-22*	822	✓			✓	✓	✓	✓	✓
30	Glenelg H-59	4116	✓			✓	✓	✓	✓	✓
31	Glenelg J-48*	5140	✓	✓		✓	✓	✓	✓	✓
32	Glooscap C-63*	4541	✓	✓		✓	✓	✓	✓	✓
33	Hesper P-52*	5679	✓	✓		✓	✓	✓	✓	✓
34	MarCoh D-41	3625				✓	✓	✓	✓	✓
35	Margaree E-70	2539				✓				✓
36	Margaree F-70	3677	✓			✓	✓	✓	✓	✓
37	Mariner I-85	5408	✓			✓	✓	✓	✓	✓
38	Marquis L-35/L-35A	4552	✓			✓	✓	✓	✓	✓
39	Mohawk B-93*	2126	✓			✓	✓	✓	✓	✓
40	Moheida P-15*	4298	✓		✓	✓	✓	✓	✓	✓
41	Mohican I-100*	4393				✓	✓	✓	✓	✓
42	Musquodoboit E-23	3818	✓			✓	✓	✓	✓	✓
43	Naskapi N-30*	2204	✓		✓	✓	✓	✓	✓	✓
44	Newburn H-23*	6070	✓	✓		✓	✓	✓	✓	✓
45	North Sydney F-24*	1707				✓	✓	✓	✓	✓
46	North Sydney P-05*	5426				✓	✓	✓	✓	
47	North Triumph 1	3805				✓	✓	✓	✓	✓
48	North Triumph 2	3937				✓	✓	✓	✓	✓

49	Oneida O-25*	4120				✓	✓	✓	✓	✓
50	Onondaga B-84	5019	✓			✓	✓	✓	✓	✓
51	Panuke F-09	3815	✓			✓	✓	✓	✓	✓
52	Panuke H-08	3682	✓			✓	✓	✓	✓	✓
53	Panuke M-79	4598	✓			✓	✓	✓	✓	✓
54	Panuke PI1B_J-99	4046	✓			✓	✓	✓	✓	✓
55	Panuke PIA1 J-99	4033	✓			✓	✓	✓	✓	✓
56	Panuke PP3C J-99	4163	✓			✓		✓	✓	✓
57	Queensland M-88	4443	✓			✓	✓		✓	✓
58	Sambro I-29*	3054	✓			✓	✓	✓		✓
59	Sauk A-57*	4575	✓		✓	✓	✓	✓	✓	
60	Shelburne G-29*	4005	✓	✓		✓	✓	✓	✓	✓
61	Shubenacadie H-100*	4200	✓	✓		✓	✓	✓		
62	South Griffin J-13*	5911	✓			✓	✓	✓	✓	✓
63	South Venture 1-P-60	4439				✓	✓	✓	✓	✓
64	South Venture 2-P-60	5315				✓	✓	✓	✓	✓
65	South Venture 3-P-60	4666				✓	✓	✓	✓	✓
66	Southampton A-25	5058	✓			✓	✓	✓	✓	✓
67	St Paul P-91*	2885				✓	✓	✓	✓	
68	Tantallon M-41*	5596	✓	✓		✓	✓	✓	✓	✓
69	Thebaud 3E-74	4011	✓			✓	✓	✓	✓	✓
70	Thebaud 5E-74	5015	✓			✓	✓	✓	✓	✓
71	Thebaud 6E-74	4011				✓	✓	✓	✓	✓
72	Torbrook C-15	3600	✓		✓	✓	✓	✓	✓	✓
73	Tuscarora C-61*	3939	✓		✓	✓	✓	✓	✓	✓
74	Venture 6-O-32	6025				✓	✓	✓	✓	✓
75	Venture 7-O-32	6455				✓	✓	✓	✓	✓
76	West Esperanto B-78*	5703	✓			✓	✓	✓	✓	✓
77	Weymouth A-45*	6520	✓	✓		✓	✓	✓	✓	✓

Appendix B

Lithoprobe 2D lines in the time domain were downloaded from the website below, while the lines in the depth domain were provided by Nova Scotia Department of Natural Resources and Renewables.

https://ftp.maps.canada.ca/pub/nrcan_rncan/vector/lithoprobe/web_gis/ec_fgp/index.html#5/54.519/-42.649

Survey Name	Line Name	Domain
Lithoprobe 2D PSTM	865_m	Time
	865a_m	Time
	881_m	Time
	881a_m	Time
	891_mrg	Time
	892	Time
Lithoprobe 2D PSDM	881_m	Depth
	881a_m	Depth
	891_mrg	Depth

Penobscot 2D lines in the time domain and Penobscot 3D survey in time domain were downloaded from the website below.

https://terranubis.com/datainfo/Penobscot

Survey Name	Line Name	Domain	Line Name	Domain
Penobscot 2D	1A_Sable Island	Time	19_Sable Island	Time
	1B_Sable Island	Time	20_Sable Island	Time
	2A_Sable Island	Time	21_Sable Island	Time
	2B_Sable Island	Time	23_Sable Island	Time
	2C_Sable Island	Time	24_Sable Island	Time
	4A_Sable Island	Time	25_Sable Island	Time
	4B_Sable Island	Time	26_Sable Island	Time
	4C_Sable Island	Time	27_Sable Island	Time
	5A_Sable Island	Time	28_Sable Island	Time
	5B_Sable Island	Time	29_Sable Island	Time
	5C_Sable Island	Time	30_Sable Island	Time
	6B_Sable Island	Time	31_Sable Island	Time
	7A_Sable Island	Time	32_Sable Island	Time
	7B_Sable Island	Time	34_Sable Island	Time
	7C_Sable Island	Time	35_Sable Island	Time
	8B_Sable Island	Time	36_Sable Island	Time
	8C_Sable Island	Time	37_Sable Island	Time
	9_Sable Island	Time	38_Sable Island	Time
	10A_Sable Island	Time	39_Sable Island	Time
	11_Sable Island	Time	40_Sable Island	Time
	12_Sable Island	Time	41_Sable Island	Time
	13_Sable Island	Time	42_Sable Island	Time
	14_Sable Island	Time	43_Sable Island	Time
	15_Sable Island	Time	44_Sable Island	Time
	16_Sable Island	Time	45_Sable Island	Time
	17_Sable Island	Time	47_Sable Island	Time
	18_Sable Island	Time	49_Sable Island	Time

Laurentian Basin 2D lines in the time domain were downloaded from the website below.

https://terranubis.com/datainfo/Laurentian-Basin-Complete

Survey Name	Line Name	Domain	Line Name	Domain
Laurentian 2D	01_Seis	Time	15_Seis	Time
	02_Seis	Time	16_Seis	Time
	03_Seis	Time	17_Seis	Time
	04_Seis	Time	18_Seis	Time
	05_Seis	Time	19_Seis	Time
	06_Seis	Time	20_Seis	Time
	07a_Seis	Time	21_Seis	Time
	07b_Seis	Time	22_Seis	Time
	08_Seis	Time	23_Seis	Time
	09_Seis	Time	24_Seis	Time
	10_Seis	Time	25_Seis	Time
	11_Seis	Time	26_Seis	Time
	12_Seis	Time	27_Seis	Time
	13_Seis	Time	28_Seis	Time
	14_Seis	Time	29_Seis	Time